A Novel Approach for Cuff-less and Continuous Blood Pressure Monitoring Using Deep Learning Networks

Solmaz Rastegar Moghaddam Mansouri

Supervisors:
Associate Professor Hamid GholamHosseini
Professor Andrew Lowe

A thesis submitted to
Auckland University of Technology
in fulfilment of the requirements for the degree of

Doctor of Philosophy (PhD)

2020

School of Engineering, Computer and Mathematical Sciences

Table of Contents

List of Tables

List of Figures

List of Abbreviations

AAMI	Association for the Advancement of Medical Instrumentation
ABP	Arterial Blood Pressure
ADL	Activities of Daily Life
AI	Augmentation Index
APG	Acceleration Plethysmogram
ARMA	Autoregressive Moving Average
BBB	Beat-By-Beat
BCG	Ballistocardiography
BP	Blood Pressure
CART	Classification and Regression Tree
CC	Correlation Coefficient
CNN	Convolutional Neural Network
CVD	Cardiovascular Diseases
DBN	Deep Belief Network
DBP	Diastolic Blood Pressure
DNN	Deep Neural Network
DT	Diastolic Time
ECG	Electrocardiogram
EI	Elasticity Index
EMD	Empirical Mode Decomposition
FdBV	Face Blood Volume Pulse Wave
FFNN	Feed-Forward Network
FFT	Fast Fourier Transform
FIR	Finite Impulse Response
GA	Genetic Algorithm
GPR	Gaussian Process Regression
HD	Heart Diseases
HdBV	Hand Palm Blood Volume Pulse Wave
HF	High Frequency
HR	Heart Rate

ICG	Impedance Cardiography
ICU	Intensive Care Unit
IIR	Infinite Impulse Response
ILC	Iterative Learning Controller
IPG	Impedance Plethysmography
JSQI	Joint Signal Quality Index
LCF	Level Crossing Features
LF	Low Frequency
LSTM	Long Short-Term Memory
MAE	Mean Absolute Error
MAP	Mean Arterial Pressure
MD	Mean Difference
MIMIC	Multiparameter Intelligent Monitoring in Intensive Care
M-K	Moens-Korteweg
MLR	Multivariate Linear Regression
MPG	Magnetic Plethysmograph
NIBP	Non-Invasive BP Systems
OWE	Oscillometric Waveform Envelope
PAT	Pulse Arrival Time
PEP	Pre-Ejection Period
PIR	Photoplethysmogram Intensity Ratio
PLS	Partial Least-Square
PPG	Photoplethysmography
PTT	Pulse Transit Time
PWV	Pulse Wave Velocity
RBF	Gaussian Radial Basis Function
RBM	Restricted Boltzmann Machine
RF	Random Forest
RGB	Red-Green-Blue
RMSE	Root Mean Square Error
RNN	Recurrent Neural Network
SBP	Systolic Blood Pressure
SCG	Seismocardiogram

SQI	Signal Quality Index
ST	Systolic Time
STD	Standard Deviation
STT	Slope Transit Time
SVM	Support Vector Machines
SVR	Support Vector Regression
VI	Viscosity Index
WFDB	Wave Form Data Base
WHO	World Health Organization
WT	Wavelet Transform

Attestation of Authorship

"I hereby declare that this submission is my own work and that, to the best of my knowledge and belief, it contains no material previously published or written by another person (except where explicitly defined in the acknowledgements), nor material which to a substantial extent has been submitted for the award of any other degree or diploma of a university or other institution of higher learning."

Signed:

Date: 09/10/2020

Acknowledgements

I would like to thank the following people, without whom I would not have been able to complete this research, and without whom I would not have made it through my PhD study.

I would like to express my sincere gratitude to my primary supervisor Associated Professor Hamid GholamHosseini, for his tremendous academic support during my PhD study and research. I appreciate his patience, motivation, and advice, which gave me the opportunity to do this research and providing valuable guidance throughout this study. His guidance helped me in all the time of research, different research activities and writing of this thesis as well as publications.

I would also like to express my deepest thanks to my second supervisor Associated Professor Andrew Lowe, for being dedicated to his role and for his continuous support and advice to this research and publications.

I would also like to thank Auckland University of Technology and the School of Engineering, Computer and Mathematical Sciences for their collaborative research support and funding.

Last but not least, thanks go to my beloved husband and son, Arash and Arshan for their unbelievable support. They have been extremely supportive throughout the entire process and have made countless sacrifices to help me get to this point. I would also like to thank all my friends and colleagues who supported me through this long journey of study and my life in general.

List of Publications

1. S. Rastegar, H. GholamHosseini, A. Lowe, “A Novel Approach for Cuff-less and Continuous Blood Pressure Monitoring”, in 11th Annual Postgraduate Research Symposium, AUT University, Auckland, New Zealand, 2017

2. H. GholamHosseini, M. M. Baig, S. Rastegar, and M. Lindén, "Cuffless Blood Pressure Estimation Using Pulse Transit Time and Photoplethysmogram Intensity Ratio," in *pHealth*, 2018, pp. 77-83.

3. S. R. Mansouri, A. Lowe, H. GholamHosseini, and M. M. Baig, "Blood Pressure Estimation from Electrocardiogram and Photoplethysmography Signals Using Continuous Wavelet Transform and Convolutional Neural Network," In International Conference on Information Resources Management (*CONF-IRM)*, 2019, p. 28.

4. S. Rastegar, H. GholamHosseini, A. Lowe, F. Mehdipour, and M. Lindén, "Estimating Systolic Blood Pressure Using Convolutional Neural Networks," in *pHealth*, 2019, pp. 143-149.

5. S. Rastegar, H. GholamHosseini, A. Lowe, “A novel method for continuous systolic blood pressure monitoring using convolutional neural network”, In Queenstown Research Week, September 2019

6. S. Rastegar, H. GholamHosseini, and A. Lowe, "Non-invasive continuous blood pressure monitoring systems: current and proposed technology issues and challenges," Australasian Physical & Engineering Sciences in Medicine Journal, pp. 1-18, 2019.

7. S. Moghaddam Mansouri, H. GholamHosseini, A. Lowe, and M. Lindén, "Systolic Blood Pressure Estimation from Electrocardiogram and Photoplethysmogram Signals Using Convolutional Neural Networks," European Journal for Biomedical Informatics (EJBI), vol. 16, no. 2, pp. 2-34, 2020.

8. S. Rastegar, H. GholamHosseini, A. Lowe, “A Novel Convolutional Neural Network for Continuous Blood Pressure Estimation”, in 8th European Medical and Biological Engineering Conference (EMBEC), October 2020

9. S. Rastegar, H. GholamHosseini, A. Lowe, “Cuff-less Blood Pressure Measurement Using ECG and PPG Signals and Deep Learning Networks”, Submitted to Computer Methods in Biomechanics and Biomedical Engineering, February 2021

10. S. Rastegar, H. GholamHosseini, A. Lowe, “Machine Learning Techniques for Non-invasive Cuff-less and Continuous Blood Pressure Measurement”, Submitted to Heath and Technology Journal, February 2021

Abstract

Blood pressure (BP) is one of the most important and meaningful vital signs of the human body that can be assessed as a critical risk factor for severe health conditions, especially cardiovascular diseases (CVD) and hypertension. An accurate, continuous and cuff-less BP monitoring technique could help clinicians to improve the rate of prevention, detection, and diagnosis of hypertension and manage related treatment plans.

BP is influenced by many factors such as various abnormalities in cardiac output, blood vessel wall elasticity, circulation blood volume, peripheral resistance, respiration, and emotional behaviour. Importantly, the complex and dynamic nature of the cardiovascular system necessitates that any BP monitoring system should benefit from an intelligent technology that can extract and analyze compelling BP features. However, employing handcrafted feature-engineering before estimating the BP is a cumbersome and compute-intensive task.

Deep learning techniques could be applied to BP feature extraction and classifying other physiological signals. Moreover, these techniques could be employed for estimating BP as a potential approach for achieving continuous BP measurement. This study aims to develop an optimized convolutional neural network (CNN)-based model to estimate BP using the fundamental capability of CNN algorithms to perform automatic feature extraction, which then precludes the necessity of handcrafted feature engineering.

In order to resolve the issue of engineered feature extraction, several techniques are proposed and discussed in this study, which aims to find the best approach to measuring BP. A CNN regression model designed from scratch is proposed to estimate systolic blood pressure (SBP) and diastolic blood pressure (DBP). Scalograms of electrocardiogram (ECG) and photoplethysmography (PPG) signals were created using continuous wavelet transform and were used to train and test the proposed CNN model. The CNN model was also trained and tested with time series of ECG and PPG signals with the intention of finding the best approach to train a CNN network.

Furthermore, to enhance and optimize the model design and to estimate the BP value through the relationship between the pulse transit time (PTT) and BP, signal pre-processing and R-peak detection for ECG signals were utilized. The main idea was to ensure that all parameters related to PTT were included in each cardiac sample.

The performance of the proposed CNN was compared with an optimized long short-term memory (LSTM)-based model and validated with a pre-processed dataset. A low root mean square error was achieved, which indicated the proposed CNN-based outperformed an LSTM-based model.

The study was further extended by proposing a novel hybrid system that combines the CNN model with a support vector regression (SVR) model. The CNN used as a trainable feature extractor, and the SVR performed as the regression operator. Moreover, a set of features were computed and extracted from the same dataset to train the SVR model, and the result was compared to the proposed novel hybrid CNN-SVR. The experimental results demonstrated that the proposed hybrid CNN-SVR model could effectively extract features from ECG and PPG signals and their corresponding SBP and DBP, while achieving higher accuracy and less errors.

The hybrid CNN-SVR framework, with its less-complex solution, was selected as an ideal framework for measuring BP among other proposed methods and related studies discussed in the literature. Results of this study showed that the estimated SBP and DBP from the hybrid CNN-SVR framework were highly correlated with the actual SBP and DBP. The proposed model is the first hybrid CNN-SVR BP model for predicting BP to be found in the known literature and offers a significant contribution towards the management of BP and effectiveness of CVD treatments.

1 CHAPTER 1 Introduction

1.1 Background

Blood pressure (BP) is a vital physiological parameter of the human body that can provide insight into a person's risk factor for hypertension and heart disease [1]. BP can vary over time due to physical condition, physiological rhythm, environmental conditions, and so many other factors. Since hypertension is preventable, and its effective management is a key component of any healthcare strategy in the ambulatory setting, a reliable continuous BP monitoring system would increase the rate of awareness, treatment, and control of hypertension. By collecting activities of daily life (ADL) and BP variations in individuals at risk of developing cardiovascular diseases (CVD), there is a possibility of improving the assessment of a patient's hypertension state.

As a result, the risk factors could be minimized, clinicians can encourage patients to adopt lifestyle modifications, and patients can receive early medical intervention [2]. Recent studies have been conducted that indicate the non-invasive and continuous BP monitoring could create an opportunity for clinicians to measure patients' BP variation during their daily activity and predict BP-related risks [3, 4]. Therefore, continuous BP monitoring is vital in order to improve the diagnosis of hypertension in health care and provide better data for making decisions regarding treatment plans [5-7]. Furthermore, early detection and treatment of hypertension can reduce the economic and social costs associated with heart disease [8].

1.2 Research Motivation

CVD are dysfunctions of the heart and blood vessels and include hypertension, cardiac arrhythmia, cardiac ischemia, and stroke. CVD is the primary cause of universal death and is the leading cause of damage to arteries in organs such as the heart, brain, eyes, and kidneys [9]. High BP or hypertension is the single most crucial adjustable risk factor for CVD, and arterial blood pressure (ABP) is an efficient way to detect and control CVD [10-12]. The World Health Organization (WHO) has reported that around 17.7 million people die from CVD every year, representing 31% of all deaths worldwide, and this number is likely to rise in the coming years as the world's population ages [13, 14]. Heart diseases are the primary cause of death in the US, where the total number of people who died from CVD, heart diseases (HD), and stroke is on the rise. In 2017, almost 92.1 million Americans were

diagnosed with CVD, and an average of about 2,200 Americans die from CVD each day. Additionally, the estimated cost of CVD-related treatments in the US is more than $316 billion annually [15, 16].

According to 2018 mortality data from the New Zealand Ministry of Health, more New Zealanders are dying from CVD than cancer, diabetes, and infectious diseases. The statistics show one in seven New Zealanders has high BP, and every 90 minutes, a New Zealander dies from CVD, which comprises 40% of deaths annually [17-19]. The need for daily monitoring of hypertension for those with heart diseases is increasing significantly. At the same time, there is a universal interest in changing from hospital-centred care to individual-centred healthcare [20].

Fortunately, most of the problems caused by CVD are preventable and treatable. Continuous and cuff-less BP monitoring techniques would help reduce CVD risk through early detection and maintaining control at earlier stages of the disease. Moreover, early detection of hypertension could dramatically decrease the likelihood of disability and mortality and reduce treatment costs.

High BP results from multiple parameters, including various abnormalities in cardiac output, blood vessel wall elasticity, circulation blood volume, peripheral resistance, respiration, and emotional behaviour [21]. Monitoring the long-term continuous changes in systolic, diastolic, mean, and the waveform shape of BP can significantly increase the ability of clinicians to manage the evaluation of arterial alterations and therefore determine CVD risk. Many studies have indicated that continuous, cuff-less, ambulatory and self-managing BP monitoring systems can measure patients' BP variations during their ADLs, which can then be used for predicting BP-related risks [3, 4]. Several studies propose a novel continuous and cuff-less BP monitoring method; however, meeting the universal standard for clinical validation of BP measuring devices is very challenging.

Nowadays, the auscultatory or oscillometric method is the most common non-invasive BP measuring method. It can only monitor BP intermittently and may cause discomfort for the patients due to the use of an inflatable cuff. The other available methods, such as tonometry and volume clamping, are either bulky or more intrusive and are not suitable for continuous and cuff-less BP monitoring.

With recent revolutionary developments in signal processing and the computational power of machine learning, researchers have recognized the remarkable potential of such a method in the healthcare industry to improve people wellbeing towards cuff-less BP measurement [22-26]. The machine learning approach has been explored by several past studies which verified the feasibility of

the solution. There are so many established regression methods, such as support vector machines (SVM), linear regression, regression trees, model trees, ensemble of trees, and random forest [27, 28]. Considering the ability of machine learning to learn the function of the complex system makes it a promising method for BP estimation. A well-trained model can address the latent affecting parameters that cannot be measured in an analytical model. The main idea is to use machine learning to extract surrogate cardiovascular features from time-domain or frequency-domain of physiological signals, then train the data with a machine learning-based model, and finally estimate the BP through the developed model [29].

The most common method for cuff-less BP measurement utilizing machine learning algorithms is based on manual examination of pulse wave velocity (PWV) features. PWV is the velocity of the pressure wave owing through the blood vessels. This PWV based method can predict the blood pressure value by using the relationship between the time required for the blood to move between two points and the distance between them. However, the PWV-based method requires recognizing features from the biomedical signal waveforms, and thus additional effort. Furthermore, the PWV-based method usually requires an elaborate individual cuff-based calibration process because the correlation between PWV features and BP varies from person to person.

Recent times have seen the development of a new generation of healthcare technology based on deep learning. Deep learning as a subfield of machine learning has a powerful ability to handle supervised and unsupervised learning and solve different type of classification and regression problems. Deep learning has shown promising results in object detection [30], speech recognition [31], and image recognition [32]. This technique has also been used in biomedical technologies such as risk assessment for hypertension [33, 34] and echocardiography images analysis [35, 36]. Researchers apply deep neural networks because they allow them to have large amounts of labelled input data and be capable of modelling extremely complex and non-linear relationships between inputs and outputs. Due to the availability of a vast amount of medical data, deep learning is considered to be a powerful tool in the mining of medical data collected from BP monitoring wearable devices.

This research study aims to develop an optimized deep learning algorithm to meet the BP monitoring clinical standard. Different machine learning and deep learning-based architectures were developed and compared to estimate the systolic blood pressure (SBP) and diastolic blood pressure (DBP) from electrocardiogram (ECG) and photoplethysmogram (PPG) signals. In addition, the robustness

performance of each method was evaluated by comparing the results with results from previous studies in this field.

1.3 Problem Statements and Research Questions

According to the census on the New Zealand Ministry of Health website, CVD is one of the leading morbidities and cause of mortality for New Zealanders. It is estimated that approximately one in seven New Zealanders has high BP, and every 90 minutes a New Zealander dies from CVD. This equates to 40 percent of deaths in New Zealand annually [37]. According to the WHO, the number of adults with CVD globally increased from 594 million in 1975 to 1.13 billion in 2015 [38].

An accurate, cuff-less, continuous, and non-invasive BP estimation method is required for enhancing early detection of CVD, where the demand is strong in New Zealand and worldwide to decrease the disability and mortality rate. Developing such a BP estimation model that overcome the drawbacks of hand-engineered feature extraction of the machine learning-based methods and the low BP prediction accuracy of other methods in literature is very challenging.

This research investigates the following main questions:

- Which features could be considered for increasing the accuracy of BP estimation? How can the acceptable accuracy be achieved by using an automated feature extraction method?
- How will deep learning contribute to the measurement of BP considering a trade-off between accuracy and process efficiency? What is the optimum deep learning architecture to improve the accuracy of the continuous and cuff-less BP estimation?
- What is the best deep learning-based BP model that can meet the clinical standard criteria? Is the implemented BP model feasible to be integrated efficiently into wearable devices?

1.4 Objectives and Goals

Managing and predicting hypertension combined with deep learning technology and wearable devices could provide an opportunity for cardiovascular disease treatment.

The ***main objective*** of this research is to propose a continuous and cuff-less BP estimation model that can measure SBP and DBP by utilizing the advantage of a deep learning algorithm that

automatically extracts features. This research aims to develop a BP estimation framework to eliminate the process of training the model for each new user and predict relatively accurate BP without individual calibration. Moreover, it is desired to achieve an efficient BP estimation with a high accuracy rate and optimum solution. In addition, the ***ultimate goal*** of this study is to develop an optimized cuff-less and continuous BP model that meets the universal standard for BP measurement devices and could be integrated into wearable devices.

1.5 Original Contributions

The main contribution of this research work will be:

- To implement the proposed system and evaluate its robustness using data collected from Multiparameter Intelligent Monitoring in Intensive Care (MIMIC) III database.

- For the first time, the proposed CNN-based model was trained with scalograms from ECG and PPG signals while achieving acceptable accuracy and eliminating the cumbersome and time-consuming feature extraction step.

- A novel hybrid CNN-SVR method for continuous and cuff-less BP measurement is proposed, which is trained and tested with ECG and PPG signals. The proposed method can effectively reduce the CNN's model complexity and estimation time. Moreover, it can effectively improve the accuracy of the BP estimation.

- This novel hybrid model fills the research gap by utilizing CNN to extract features automatically. Due to its calibration-free and unsupervised feature learning ability, the proposed method has high prospects for application in wearable BP monitoring device.

- The proposed hybrid model can predict SBP and DBP simultaneously, with a minimum number of sensors using only ECG and PPG signals, offering a convenient approach for health monitoring.

- The development of a hybrid BP estimation framework eliminates the necessity for training the model for each new user or calibration to maintain the measurement accuracy.

- The proposed hybrid method can be easily utilized in a wearable application by taking benefit of the CNN architecture flexibility in dealing with various inputs such as ECG and PPG signals.

- The proposed hybrid BP model satisfies the Association for the Advancement of Medical Instrumentation (AAMI) standard protocol.

1.6 Thesis Outline

The thesis is structured into six chapters, as follows:

Chapter 2 presents an overview of classical non-continuous BP measurement techniques. Then a comprehensive survey of current literature for advanced continuous BP measurement techniques is presented. It includes a critical analysis and comparison of existing works with in-depth discussions around limitations, challenges, and research gaps.

Chapter 3 introduces the database that was used to evaluate the proposed BP models in this study. Then the architecture of the proposed CNN-based BP model is presented in detail. The proposed model was trained and tested with the scalograms of ECG and PPG signals. The continuous wavelet transform (CWT) was used to create the scalograms from the ECG and PPG signals.

Chapter 4 compares two different optimized deep learning-based BP models, aiming to find the best model based on the correlation between PTT and BP. Both models trained and tested with time series of ECG and PPG signals after a series of pre-processing steps were performed to ensure that all critical points of the ECG and PPG signals were included in each sample.

Chapter 5 compares machine learning-based BP regression models with manual features extraction with the proposed novel hybrid CNN-SVR BP model. The performance of the proposed hybrid method is evaluated based on medical instrumentation standards.

Chapter 6 gives an overall conclusion of the thesis and highlighting the original and significant outcomes of the study. Finally, some key future research directions are suggested.

2 CHAPTER 2 Literature Review

2.1 Introduction

In this chapter, an overview of the cardiovascular system and blood pressure is introduced. Then classical non-invasive, non-continuous BP measurement methods are briefly presented as background information. This is followed by a comprehensive review of the current continuous BP monitoring techniques, along with their strengths and limitations. This review focuses on the descriptions and analyzes of the latest continuous and cuff-less methods, along with their key challenges and barriers. Particularly, most advanced and standard technologies, including Pulse Transit Time (PTT), ultrasound, Pulse Arrival Time (PAT), machine learning, and deep learning are investigated. The impact of machine learning and deep learning on BP monitoring is also reviewed and analyzed in detail. Moreover, the tools and environment that were used in this research are introduced. In addition, a comparison of existing works with in-depth discussions around limitations, challenges, and research gaps are presented. Material discussed in this chapter that was written by the author of this thesis has been previously published [39].

2.2 Heart and Cardiovascular System

To design an algorithm that can measure BP, it is important to have a clear and accurate understanding of the functional anatomy of the heart structures, as well as the definition of BP. In this manner, the first part of this literature review will focus on the information about the anatomy of the heart, associated cardiac structures, and a definition of BP.

The heart is one of the key organs of the body. It constantly supplies nutrition to body tissue through the pumping of blood to the organs. The heart has four chambers, divided into two sets: the upper atria and the lower ventricles. They are working together to circulate blood through the pulmonary and systemic pathways. Deoxygenated blood is pumped from the systemic circulation to the pulmonary circulation through the right atrium and ventricle, and from pulmonary circulation to the systemic circulation through the left atrium and ventricle [40].

The heart pump functionality includes systole (contracting phase) and a diastole phase (the time that the heart fills up with blood). As shown in Figure 2-1(a), during the diastole phase, the atrioventricular valves are open, and the blood flows from the atria into the respective ventricles while the ventricles are relaxed. By the end of this phase, as shown in Figure 2-1(b), the left and right atria start to contract

and fill the ventricles. The systole phase appears when the atrioventricular valves close and the ventricular pressure increases. Once this phase begins, the aortic valves open and the blood is pumped out into the arterial system, as shown in Figure 2-1(c)

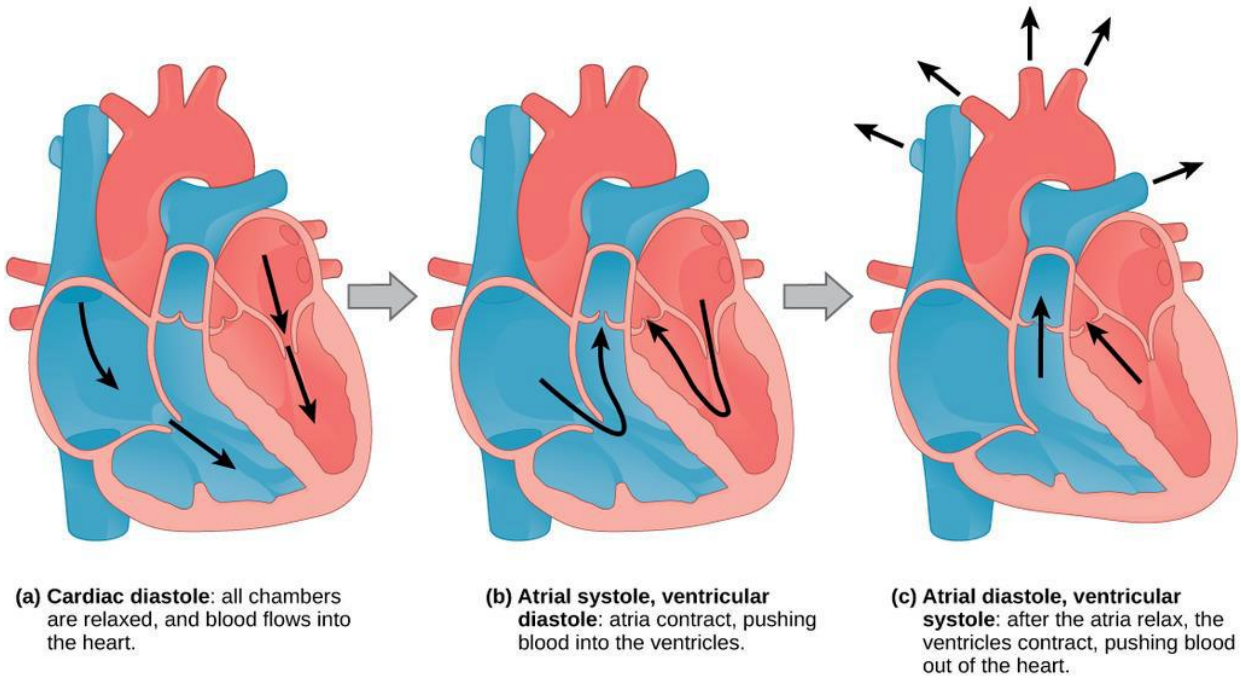

Figure 2-1: Cardiac cycle [41]

Left ventricular and atrial pressure for two normal cardiac cycles is presented in Figure 2-2. The first three curves denote the variations in the left side of the heart, including pressure in the left ventricle and the left atrium. The next curve illustrates the volume changes in the left ventricle. The fifth curve presents the ECG curve and the last one shows the phonocardiogram (PCG).

BP is the pressure of the blood within the arteries as it circulates through the body. BP is generally expressed in terms of systolic pressure and diastolic pressure and measured in millimetres of mercury (*mmHg*). As shown in Table 2-1, systolic blood pressure (SBP) ranges less than 120 and diastolic blood pressure (DBP) less than 80 are considered as a normal range. Prehypertension range is when the SBP consistently ranges from 120 to 139 mm Hg or DBP ranges within 80 to 90 mmHg. A value higher than 140 systolic or 90 diastolic implies a state of hypertension and is divided into three ranges of value related to the risk of cardiovascular diseases [42-44]. BP is generally described as a ratio of SBP and DBP; the upper number is the maximum pressure applied through the ventricular systole and the lower number is the minimum pressure measured while the ventricles are filled with blood.

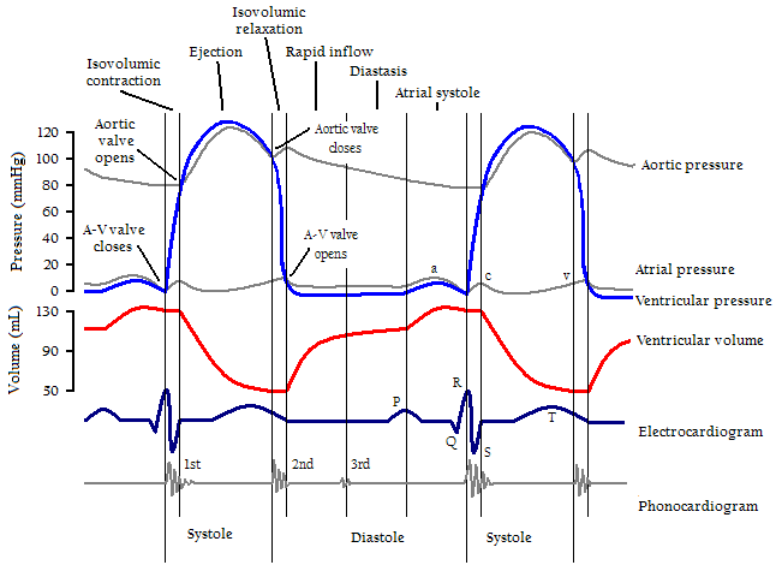

Figure 2-2: Trends of aortic pressure, left ventricular pressure and left atrial pressure, ventricular volume and electrocardiogram during the cardiac cycle [45]

High BP or hypertension can damage the vessel's cells and limit the blood flow through the organs. Constant high BP can cause the expansion of the arteries' walls, which could cause internal bleeding. High BP forces the heart to work harder to properly deliver blood throughout the body, causing an expansion of the left part of the heart with ventricular hypertrophy. This could lead to heart failure, heart attack, or sudden death. It also can affect the brain due to the inconsistent or absent supply of blood in the brain, which causes strokes or cognitive impairments [44].

Table 2-1: Blood pressure categories defined by the American Heart Association [44]

Blood Pressure Category	Systolic (mmHg)		Diastolic (mmHg)
Normal	Less than 120	and	Less than 80
Prehypertension	120-139	Or	80-90
High Blood Pressure (Hypertension) Stage 1	140-159	Or	90-99
High Blood Pressure (Hypertension) Stage 2	160 or higher	Or	100 or higher
Hypertensive Crisis	Higher than 180	Or	Higher than 110

2.3 Existing Classical BP Measurement Techniques

BP can be measured by invasive and non-invasive ways. Invasive arterial BP (ABP) is considered to be the gold standard for BP monitoring[46, 47]. The advantage of automated non-invasive BP systems (NIBP) over invasive method is to avoid bleeding and the risk of infection as there is no need for catheter insertion into the skin. Following, we briefly discuss the current continuous invasive and non-invasive BP measurements and their challenges.

2.3.1 Invasive Method

William Harvey first described arterial pulse and circulation physiology in the 16th century [48]. He also introduced hemodynamic parameters, such as cardiac output, stroke volume, and ejection fraction [48-50]. In 1733, Reverend Stephen Hales noted that the presence of blood pressure and pulse pressure could be used to observe the pulsatile rise and fall of an animal's BP [51]. In the same century, John Floyer measured pulse rate. The Kymograph ("wave writer" in Greek) was developed by Carl Ludwig in 1847 to record arterial pressure graphically; this involved inserting a brass pipe cannula into the artery and the use of a mercury manometer. Vierordt in 1855 used the sphygmograph to develop a non-invasive BP technique.

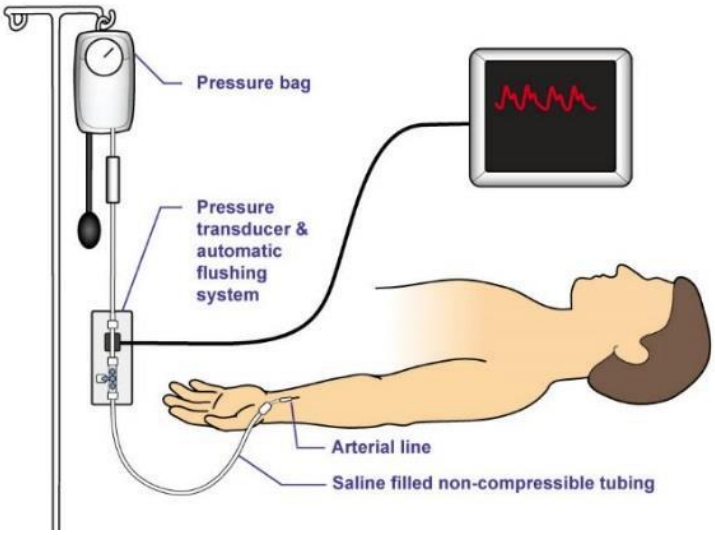

Figure 2-3: Gold standard method for BP measurement in ICU

Currently, the most clinically adopted continuous BP monitoring method is the intra-arterial catheter that can be used only in the intensive care unit (ICU). Even though this method is considered the gold standard for BP measurement, it is invasive [52]. It is typically performed using a high-pressure plastic

tube and catheter that connects to the peripheral artery of the patient. The most common site for cannulation is the radial artery, as this is associated with a low rate of complications. Although this technique has high accuracy and high precision, this intra-arterial method is associated with bleeding, infection risk, and nerve damage [53, 54] (Figure 2-3).

2.3.2 Non-invasive Methods

2.3.2.1 Auscultatory and Oscillometric Methods

In 1985, Scipione Riva-Rocci developed the inflatable cuff armband [55], and a Russian surgeon named Korotkoff introduced the auscultatory method in 1905. This method involves an inflatable BP cuff and stethoscope that has become the clinical standard for measuring BP [55, 56]. In general, the most commonly used methods for measuring BP during standard examinations at a medical facility are auscultatory and oscillometric. Both methods use an inflatable cuff to measure SBP and DBP, the auscultatory method (Figure 2-4) is based on hearing Korotkoff's sounds which equates to the SBP when first heard and the DBP when barely audible, and the oscillometric method is based on observing pressure oscillations. SBP is indicated when the oscillation pressure appears, mean BP when the pressure is at its maximum, and DBP when the oscillations disappear [57].

Figure 2-4: Auscultatory method for BP measurement

Both of these methods are not suitable for continuous BP monitoring as a minimum of three minutes' gap is required between each successive measurement. When long-term monitoring is required, clinicians use the auscultatory method and the patient leaves the clinical facility with a cuff around the

arm. During 24 hours, a device records the value of BP every 20 minutes to create a hypertensive profile of patients to help plan the ideal treatment. However, the accuracy of measurement is reduced after a couple of hours; furthermore, this type of measurement is uncomfortable and painful and is too noisy for the patients, especially during sleep [58].

2.3.2.2 Tonometry Method

Tonometry can be a suitable method for continuous BP monitoring. As shown in Figure 2-5, a controlled force is applied vertically to the wall of a superficial artery against a bone, and the pressure at contact measured by utilising a force sensor. As a result, local occlusion has appeared around the superficial artery. In this manner, a cuff may not be required, but a pushing force device is essential. Consequently, the applied force adjusts and pursues the pressure wave. Another aspect that plays an important role in accurate measurement is the positioning of the tonometer. It needs to be placed exactly in the middle of the artery because even one millimetre is enough to distinguish between correct measurements. Generally, this method is motion-sensitive, and the correct position of the sensor and regular monitoring is a crucial part of the measurement, so having the patient in a rest position is considered as the best position for this method. Consequently, this technique is not convenient for daily use. The result is that despite its accuracy, this method still is not the most common method used for BP measurement [59].

Figure 2-5: Tonometric method for measuring BP

2.3.2.3 Volume Clamp Method

One of the first version of a continuous non-invasive BP monitoring device was presented in 1969 by Jan Penaz, a Czech medical doctor [60]. An inflatable finger cuff with a built-in PPG sensor is utilised in this device and a pressure control unit is positioned on the wrist. This method is partially occlusive of the blood flow under the cuff due to the usage of the cuff around the finger [61]. The Finapres (Medical Systems, Netherlands), introduced in the 1980s, was the first widely accessible device in the market which applied volume clamp methodology [62]. Blood pressure can be measured continually by Finapres; however, the finger- cuff is not a pleasant method for patients (Figure 2-6).

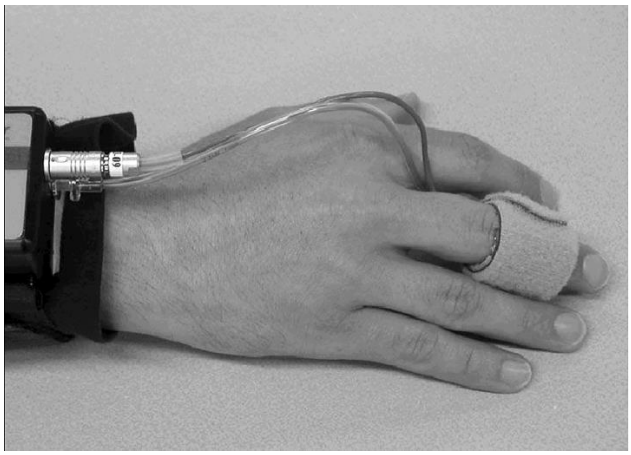

Figure 2-6: Volume-clamp method for measuring blood pressure

2.3.3 Summary of Current Methods

None of these existing BP measuring methods is suitable for ambulatory, continuous, and cuff-less BP monitoring due to their lack of accuracy during repetitive and long-term monitoring. From the patient's perspective, the ideal method should be convenient, non-occlusive, painless, and no risk during BP measurement. None of the aforementioned methods can satisfy all of these criteria. A comparison of the existing BP measurement techniques in terms of advantages and limitations is summarized in Table 2-2.

Table 2-2: Comparison of existing BP measurement techniques

Method	Periodicity	Long-time monitoring	Advantages	Disadvantages
Auscultatory [63, 64]	Discrete-time	No	• Clinical "Gold standard" • No risk to the patient • Inexpensive • Non-invasive	• Cannot measure continuously • Needs medical supervision • Cuff-based • Uncomfortable for long-time of time monitoring
Oscillometric [58, 65]	Discrete-time	Yes	• The most automatic measurement used for long-time monitoring • Non-invasive	• Cannot measure continuously • Cuff-based • The automatic measurement is noisy and painful because of inflation and deflation • Uncomfortable for long-time of time monitoring • Sensitive to the stiffness of the arteries and at the site of measurement
Tonometry [55]	Beat-to-beat	Yes	• Beat-to-beat measurement Continuous BP measurement • Non-invasive	• Continuous control of the positioning of tonometer over the radial artery needed • The subjects need to be in a supine position during monitoring • In long-term monitoring the accuracy and comfort decrease • Sensitive to anatomical skin abnormalities

				• In practice, needs calibration via the cuff whenever a BP changes
Volume clamp [66]	Continuous	Yes	• Continuous BP measurement Non-invasive	• Oxygen decreases in the tissue under the cuff • Affected by blood circulation • Affects patient comfort in long-time monitoring • Bulky • Limited only to bedside uses

2.4 Advanced Continuous and Non-invasive Techniques for BP Measurement

Given the increasing prevalence of non-communicable diseases (like heart attacks and stroke) and an increasingly aged population [67], a growing interest exists for providing a continuous and ubiquitous BP monitoring method with cuff-free calibration that minimizes any discomfort for patients. The number of people diagnosed with hypertension is increasing thanks in part to a system that does not promote continuous monitoring and the possibility of early diagnosis of any BP abnormalities [68].

Currently, the most clinically adopted continuous BP monitoring method is the intra-arterial catheter that is used only in the ICU. Even though this method is considered the gold standard for BP measurement, it is invasive [52]. It is typically performed using a high-pressure plastic tube that connects to the peripheral artery of the patient with a catheter. The most common site for cannulation is the radial artery as this is associated with a low rate of complications. Nevertheless, this intra-arterial method has been associated with bleeding, infection risk, and nerve damage [53, 54].

2.4.1 Ultrasound-based Methods

The ultrasound can track the diameter waveforms and vessel wall thickness accurately [69]. Any artery which is visible for ultrasound can be monitored with this technique. Most ultrasound-based

techniques do not require cuffs for measurements. Furthermore, this user-friendly method can indirectly measure PWV and estimate BP for long-time monitoring. Some of the well-established study based on ultrasound technique is discussed below.

A new non-invasive continuous BP monitoring has been presented by Weber et al. [70] using ultrasound to detect the blood velocity in the wrist vessel. A polyurethane balloon was placed over the wrist radial artery to measure the blood velocity. The BP was controlled by an ultrasound sensor and voice coil actuator placed on the lower arm. A microcontroller Arduino DUE R3 board, including an iterative learning controller (ILC) and a proportional-integral-derivative controller, was implemented to control the balloon pressure and adjust the collected ultrasound signals. This method can provide BP monitoring for over 24 hours and does not require a cuff. However, the balloon attached to the wrist is compulsory and the patient's position change will affect the measurements. Moreover, further analysis of the controller is required and reducing the size of the voice coil actuator power amplifier should be considered.

Joohyun et al. [71] estimated ABP by employing a two-channel ultrasound system. PWV was calculated based on a combination of arterial vessel cross-sectional area and elasticity of the vessel. A flow phantom including a diaphragm pump, a soft latex rubber, and a reservoir was designed for the experimented setup. The pre-processing of signals was done by a bandpass filter to remove all the RF signal noise on both channels. The feasibility of ABP waveform calculation was shown in this research and the effect of PWV reflection on ABP was discussed. The measured PWV, using 16 cardiac cycles of data was 8.47 ± 0.63 m/s with an associated scaling error of $-1.56 \pm 14.0\%$ in a direct pressure waveform comparison, showing minimum error on average. To meet the standard accuracy, the feasibility of this technique in vivo needs to be further validated.

A calibration-free technique using a dual magnetic plethysmograph (MPG) transducer and a single-element ultrasound transducer has been presented by Jayaraj et al. [72]. The measurement of arterial dimensions, along with local PWV, was needed for calibration-free evaluation. Therefore, an arterial compliance probe from the carotid artery was designed and validated for pulse pressure measurement on superficial arteries. The results of this study validated with ten volunteers highlights the value in tracking local PWV changes and carotid pulse pressure. Although the measured local PWV obtained a large correlation with brachial BP, the absolute value of local PWV and calculated carotid pulse pressure correlated at lower than the previously reported value.

Aaron et al. [73] placed an ultrasound probe with force measuring capability, on the carotid artery and then the contact force between the probe and the patient skin was slowly increased. Meanwhile, the ultrasound images and contact forced data video were recorded. An optimization Matlab algorithm was used to calculate the BP from the video segmentation done by a Star-Kalman filter. Each time the pressure was reported, an algorithm calculated the patient-specific artery stiffness making it suitable for the patients with atherosclerosis. Moreover, the pressure measurement can apply to any artery and does not require medical supervision. Nevertheless, obtaining BP through this method takes a long time, and the result did not validate with any clinically approved technique.

In sum, the ultrasound approach does not need the inflatable cuff, so it does not affect patient comfort. Nevertheless, the ultrasound device is large and requires calibration to estimate absolute BP value. In addition, this method depends on reliable detection of the foot of the diameter waveforms and an appropriately high sampling frequency.

2.4.2 Pulse Arrival Time (PAT)-based Methods

The pulse arrival time (PAT) is defined as the sum of PTT and the time taken for the opening of the aortic valve, which is known as the pre-ejection period (PEP). In this method, an ECG represents the proximal arterial waveform and a PPG at the finger a surrogate of the distal waveform, in which case PTT is known as PAT. A great number of studies focus on PAT-based techniques and some of them achieved accurate results compared with actual BP. This section reviews some of the highlighted studies carried out using the PAT-based method.

Braiam et al. [74] calculated the PAT as difference time between R-peak of ECG and two points of PPG waveform. First is the maximum amplitude of PPG and second is the sharpest slope of the rising edge of PPG. After initial filtering, eight subjects from the MIMIC database were selected for the experiment. A linear regression model was used to show the relationship between the PAT and the systolic, diastolic and mean BP. While the results showed a strong correlation between BP and PAT, but the sample size was not large enough to meet the clinical standards.

A chair-based method using PAT-based technique has been presented by Zunyi et al. [75]. This system consists of an ECG with four electrodes, a PPG sensor with green lighting LED and a photodetector. Additionally, a control circuit with a Bluetooth module and a high capacity battery was mounted on a common armchair. The ECG and PPG signals were collected from users while they are

in a sitting position. All the collected data transfer to a PC to calculate the beat-to-beat PAT. A cuff-based method was considered as a reference and the results were validated on 12 subjects with no CVD histories. In spite of the acceptable results of this method, elderly subjects and hypertensive people need to be involved in further validation and a cuff-less calibration method needs to be considered.

The motion artifacts and daily activities reduce the accuracy of the PAT-based technique. Qiang et al. [76] used a Kalman filter to improve signal quality and overcome this issue. The MIMIC II database was used to evaluate the method and the twenty signals, including the ECG, ABP, and PPG were selected. An FIR band-pass filter was employed to filter all signals during the process and the Pan-Tompkins algorithm was considered to select the R-peak of ECG. The PAT was then calculated as the time difference between the R wave and the synchronized PPG signal. The least square algorithm was used to calibrate the PAT to BP every 30 minutes. A joint signal quality index (JSQI) was used to adjust the Kalman filter and reduce the effect of noise and artifacts on the PPG and ECG signals. The simple computation of the proposed algorithm makes it very suitable for wearable devices. Nevertheless, the MIMIC II database has small BP variation, and a different database needs to be used for validation of such a technique.

A study has been conducted by Yali et al. [77] to validate the accuracy of the PAT method on 24 subjects, including 15 hypertensive patients. A PAT-based cuff-less armband wearable device including one PPG sensor and two pieces of e-textile ECG patch was used every 15 to 30 minutes to monitor the BP during daily activities. At the same time, an experienced nurse measured the BP with an oscillometric BP device attached to the upper arm of the subjects. The Bland-Altman plots were employed to estimate mean SBP and DBP during the day and night-time activities. The results showed that the PAT-based method could replace the traditional BP monitoring for night-time ABP monitoring via cuff-less and convenient monitoring methods. However, the accuracy of this method on day-time is not accurate as nigh-time.

Satu et al. [78] used an arm ECG and finger PPG to measure the PAT in four different methods. The PAT was estimated as the time interval between the ECG R peak and four different points in the PPG. 10 subjects in a seated position were involved for measurements and the signal processing was completed by using the Matlab program. The results of different measurement techniques were compared, and the first PPG signal derivative was considered as the most promising method. To enhance the accuracy and increase the reliability of the measurement, the signal quality in noisy environments needs to be further investigated and improved.

In summary, the PAT correlates with BP and it can be used as an indicator of big trends changes such as hypertensive or hypotensive episodes. However, the ability of PAT for continuous and non-invasive BP estimation is not confirmed due to the limited experimental setup.

2.4.3 PTT-based Modelling Approach

PTT is a non-invasive and continuous BP monitoring technology. PTT is defined as the required time for the PWV to propagate between two arterial points within the cardiovascular system. The mathematical relation between PWV and the elasticity of the arterial vessel is described by the Moens-Korteweg (M-K) Equation (2-1):

$$PWV = \sqrt{\frac{Eh}{\rho D}} \qquad (2\text{-}1)$$

where E is the elasticity of the artery, h is the wall thickness of artery, ρ is the blood density, and D is the artery diameter [79]. Concerning using PWV technique, in recent year, the researchers have extracted more features based on time and frequency domain from PWV signals to accomplish multivariate regression models [80, 81]. The pulse wave transit time (PTT) is one of the features that has shown a high correlation with BP [82]. PTT is related to PWV, and both were shown a relationship with BP [8] inversely. The PTT is the time takes for an artery pulse to propagate between two arterial sites. The definition of PTT can be shortened as the time difference between the R-wave peak in the ECG and the specific point in PPG signals, as shown in Figure 2-7 [83, 84]. Blood pressure can be estimated based on PTT and Equation (2-2), and Equation (2-3) [85, 86] :

$$SBP = SBP_0 - \frac{2}{\gamma PTT_0}(PTT - PTT_0) \qquad (2\text{-}2)$$

$$DBP = SBP_0 - \frac{2}{\gamma PTT_0}(PTT - PTT_0) - (SBP_0 - DBP_0).\left(\frac{PTT_0}{PTT}\right)^2 \qquad (2\text{-}3)$$

where SBP_0 and DBP_0 is the first value of SBP and DBP which can be measured at the start of estimation, PTT_0 is the first value of the PTT depending to the SBP_0 and DBP_0. Therefore, with the initial calibration of PTT to BP, beat-to beat BP can be estimated from beat-to-beat PTT that calculated from each cardiac cycle. PTT is usually measured as the time difference between the R wave of an ECG and the specific points of the PPG Figure 2-7 [83].

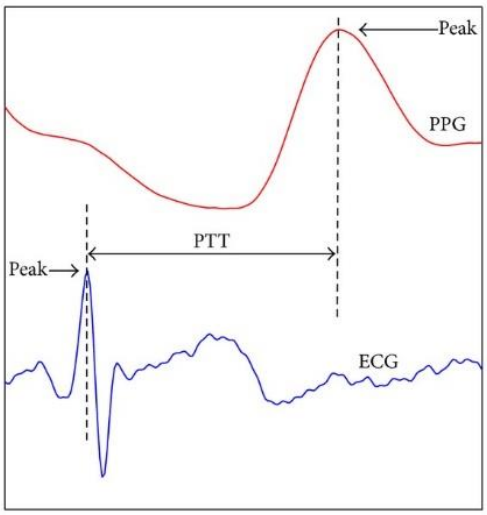

Figure 2-7: Graphical explanation of PTT

A new indicator, the photoplethysmogram intensity ratio (PIR) has been presented by Xiao et al. [87-89]. The PIR was defined as the ratio of PPG peak intensity to valley intensity which contributes to the change in arterial diameter and is capable of tracing low frequency (LF) variations in BP. The ratio of the PPG peak intensity to the PPG valley intensity of one cardiac cycle was determined by the PIR [88, 89]. The author combined both PIR and PTT methods to develop a new BP measurement algorithm. PTT is advanced to track the BP in the high frequency (HF) range and PIR in the LF range. To validate the results, a total of 27 subjects were selected for this experiment. The results of BP measurement using the proposed technique compared with Finapres measurements as a reference method to confirm the influence of vasomotor tone on LF components and accurate results [90]. However, the results needed to be validated with a gold standard that involved adequately powered studies with a sufficient number of patients with CVD and who are monitored over the long term.

Following the PIR study [89], a new feature related to BP named the intensity ratio of the first derivative wave of the PPG (1th dPIR) has been proposed by Wan-Hua et al. [91]. Where 1th dPIR was calculated by differentiating the original PPG wave and likely to remove the low frequency and bassline noise to improve the accuracy. Twenty-two healthy volunteers participated in mental arithmetic stress and Valsalva's manoeuver tests. The Finapres device was used as a reference, and the result showed standard deviation errors of 3.22±8.02 mmHg and 3.13±4.82 mmHg for SBP and DBP estimation, respectively. The proposed method is linear and makes the character points of the waveform more visible so it could improve the accuracy of BP estimation. Regarding the sample size of the subjects, this study didn't meet the requirement of standards.

Jing Liu et al. [92, 93] used a four-channel PPG signal system to collect the PPG waveform of the different blood vessels to estimate PTT. A simple infrared (IR) at only one body location was used to measure the time interval between the PPG signals at different skin depths as a PTT. Six signals, including ECG, continuous BP measured by Finapres, Blue PPG, green PPG, yellow PPG, and IR PPG signals were collected and analyzed through an algorithm. Eventually, the peak amplitude of continuous BP was identified as a SBP measurement. This technique eases the integration of the system and the architecture, which makes it also suitable for wearable cuff-less BP monitoring. Although MW-PPG produced better results compared to previous methods, the size of PPG sensor need to be miniaturized, and the effect of motion artifacts should be considered for BP estimation.

A combination of contactless image-based PTT (iPTT) and image-based PPG (iPPG) using a high-speed camera has been introduced by Cheol et al. [94, 95]. The interval time between the arrivals of the pulse wave at two body locations is measured with iPPG using an analysis of sequential images. The images were obtained using a high-speed video camera with the subject in the seated position. The potential feasibility result of this research was validated in a small preliminary 'in vivo' assessment with seven healthy volunteers. The iPPT data was calculated as the time interval between the derivative of the face blood volume pulse wave (FdBV) and a derivate of the right-hand palm blood volume pulse wave (HdBV). The iPTT and SBP had a high correlation in each subject compared to the high-precision clinical automated oscillometric method results. However, individualized calibration is needed for this method as iPPT versus the SBP slope will be different in each subject depending on the light reflection, skin penetration, and pulse wave propagation.

In [96] the author employed a linear regression algorithm to estimate the PTT. The correlation between the ECG and the PPG in five different positions (recumbent, seated, standing, walking, and cycling) in 14 healthy subjects have been estimated. The main concern of this research was considering the effect of patient's activities on PTT-based estimation. For this purpose, a wearable biomedical device was used to capture and record three channels of ECG and one channel of PPG by the local pod. A customized MATLAB algorithm was designed to compute the PTT automatically from the PPG and the ECG signals. The results were compared to the reference standard and the root-mean-squared-error was within 1% of the standard measurement. However, this technique has shown accurate result in the seated or standing positions, but not during other positions. Moreover, this approach needs a cuff-based method for calibration.

An affordable, simple, and portable BP estimation method has been proposed by Aishwarya et al. [97] to monitor the SBP and DBP. This technique required a smartphone camera to capture only the PPG signal by placing a finger over the camera lens of an iPhone 4. A total of 17 features, including the time domain features of the PPG signals and the height, weight, and age of each subject were used to train the system. To detect and remove the noise of the PPG signal, a finite state machine (FSM) was applied as a pre-processing system. Two different training model was used for estimation and the result of both models has been compared. The results showed that the support vector machine (SVM) model had a better performance in comparison with the linear regression model. Besides, to evaluate the proposed method, the University Queensland Vital Sign dataset and outcomes from 17 healthy subjects have been used in the experiments. Although the results approved the ability to use this technique in BP estimation, this study involved only an iOS, and so an Android device capability should be considered in future work. Moreover, the feature selection method needs to be improved in order to capture more parameters related to BP.

A PTT-based technique using a wearable BP device controlled by a smartphone has used to estimate the BP continously[98]. Both ECG and PPG signals were captured via the PPG and ECG sensors. A peak detection algorithm from previous studies was employed to extract the BP features from the PPG signal. Eventually, MATLAB software was used for testing, calibrating and estimating the BP. An Android application was developed to allow users to monitor their ECG, PPG, SBP, DBP and heart rate indexes. Moreover, a new PPG sensor with four LEDs which can detect different blood vessels and different blood volume has been introduced. The result showed that the new sensor provided a 30% current saving compared to a one LED case. The adaptive threshold algorithm was used to test ten recordings from the MIT-BIH database. The results showed a reduction in both power consumption.

Aliar et al. [99] also used a smartphone camera and microphone to measure PTT and then estimate the BP. PTT was calculated as the time difference between blood leaves the heart and the time it reaches the finger. For measuring these two values, the heart sound recorded using a smartphone's microphone and its camera as a PPG sensor to measure the pulse wave, respectively. To achieve a reliable heart rate, a combination of autocorrelation and a fast Fourier transform (FFT)-based algorithm was used to detect the exact moment the pressure pulse reached the distal point. The proposed method involved processing the PPG and PCG signals to estimate the PTT using inexpensive sensors. Although the results were within the acceptable range and could detect the beat-t-beat variations of

PTT, the sample size was relatively small. The results need to be validated with the gold standard and during motion. Moreover, positioning the smartphone correctly is very difficult for users.

A dual-modality arterial pulse monitoring system was proposed to overcome the limitation of the PTT-based technique. [100]. In this method, a pressure-volume cure was created by recording the pressure wave and PPG signals related to the radial artery. Then the elasticity index (EI), and viscosity index (VI) was extracted to calculate the PTT. The pressure wave and PPG signals were collected from seven healthy subjects, and at the same time, ECG and BP signals were monitored by the Finapres device as a reference. The average correlation of EI, VI, and PTT was compared, and the results showed that both EI and VI have a high correlation with SBP and DBP compared to PTT. Even the combination of EI and VI had a significantly higher correlation coefficient than PTT. However, this method could not track the BP in low-frequency due to the vasomotor tone.

A novel method to estimate the PTT using a seismocardiogram (SCG) was proposed by Chenxi Yang and Tavassolian [101]. A three-axis MEMS accelerometer was strapped to the chest wall of a subject to record the SCG signal. A customized microphone sensor and pre-amplifying circuit were placed inside the ear to record the distal arterial location data [101]. At the same time, a cuff-based BP monitor recorded DBP and SBP every 30-40 seconds as a reference. All high-frequency SCG signals were removed by an infinite impulse response (IIR) filter. Likewise, all the PPG signals underwent a finite impulse response (FIR) filtering. All the synchronized data were then fed to the Matlab so that PTT could be calculated. Although a high correlation coefficient was obtained in this study, the age and a small number of subjects (ten only), limited the generalisability of these results to daily life.

As PTT mostly calculated from ECG and PPG signal and very related to pulse wave (PW) shape, an algorithm was proposed to remove the effect of artifacts and movement of subject on PW signal [102]. A “Seven Step PW-Filter” algorithm was proposed to remove the inappropriate PW characteristics which not related to PTT calculation to improve the accuracy of the measurement. Compared to previous studies on manual/visual filtering, the proposed algorithm achieved 99.3 % accuracy in detecting any unwanted PW. Moreover, elimination using the seven-step PW-Filter was much faster compared with manual elimination. Further experiments need to be considered, including CVD subjects in a different position.

Bassem et al. [103] used a combination of synchronized ECG, PPG, and bio-potential based impedance (Bio-Z) to estimate the PTT. All the signals were filtered by a low pass filter in order to

remove high frequency and noise. After filtering, the ECG, Bio-Z and PPG signals were analyzed to determine the points of R peaks in ECG, the points of maximum negative slope of the Bio-Z and maximum positive slope of the PPG in order to calculate the corresponding PTT values. To evaluate the results of this method, the outcomes were compared with PPT measured using only ECG and PPG signals. The result of an *in vivo* experiments presented a high correlation coefficient of 0.92 with previous measurements. These outcomes suggest that this method could be used as an alternative to establishing a PTT measurement technique for ambulatory and cuff-less monitoring. However, a reliable calibration for long-time monitoring needs to be investigated.

A watch-based system (SeismoWatch) to estimate the PTT using SCG and PPG signals were presented by Andrew et al. [104]. A prototype watch included an accelerometer to measure the SCG, and photodiodes and LEDs were designed to measure PTT and estimate the BP without the need for a cuff. The watch is pressed against the sternum to measure the micro-vibrations of the chest wall associated with the heartbeat. The time that a pulse wave travels from the heart to wrist calculated with an accelerometer and optical sensor mounted on the watch as PTT. This technique was used for the first time in an at-home setting rather than a clinic environment and supine position. To validate this study, three different sections were considered for 13 healthy subjects who participated in the experiment; one minute of rest, one minute of exercise, and five minutes of recovery. The results were indicated that the accuracy of this watch-based method improved significantly compared to a conventional BP monitoring method. However, this technique needs cuff-based calibration, and only young and healthy subjects were selected for validation. Moreover, PTT was calculated through the brachial arteries rather than the larger arteries.

Less computation makes any technique more suitable for use as a wearable BP monitoring device. Hence, a single PPG signal feature has been proposed by Yang et al. [105] The mean slope transit time (MSTT) as a new and only feature with more stability compared to the slope transit time (STT) was introduced in this study. Ten subjects with no CVD history participated in validating the method. All subjects were in the supine position, and all signals were recorded for five minutes. The results showed the mean error of -0.90 ± 3.84 mmHg and - 0.31 ± 3.36 mmHg for the SBP and DBP estimation, respectively, which determined a better performance compared to the conventional PTT method. An obvious limitation of this study is that only healthy and young people participated in the experiment.

In order to estimate PTT and pulse arrival time (PAT) at the centre of arteries, an electrical bio-impedance (BImp) ECG across the shoulder and continuous wave radar antennas on the sternum were

used by Buxi et al. [106]. The Pan-Tompkins algorithm was employed to detect the ECG R-peak and a tangent hyperbole function was used to calculate the arrival of the BImp pulse wave, and finally, the radar signal was used to estimate the PTT. The result was validated with six healthy male subjects during exercise. The proposed architecture can be utilized while completely hidden under patients' clothes, making it suitable for ambulatory BP, sleeping time and during exercise. However, this method only has the potential to estimate SBP, a method for positioning the antenna in terms of the electrical axis, size, and female anatomy need to be studied.

According to the clinical demand for cuff-less ambulatory BP monitoring, Sola et al. [107] introduced a method to estimate mean arterial pressure (MAP) using the chest-BP sensor. The proposed method required two measurements. First, impedance cardiography (ICG) technology was used to estimate the opening time of the aortic valve. Then a multichannel PPG was employed to measure the arrival time at the sternum. Finally, PTT determined the time difference between the PAT and a pre-ejection period (PEP). The results were validated with 15 healthy subjects, and overall baseline MAP values were 80 ± 6 mmHg and maximum MAP values of 107 ± 9 mmHg during handgrip manoeuvres. Also, the method was tested with six different calibration strategies for each subject. It has been proven that this method can provide continuous BP monitoring in a clinical environment. However, the subjects involved were all healthy, and only the single stress maneuver was considered. Also, the results were compared with a single brachial oscillometric device and not with the gold standard.

Authors of [108] proposed a system to integrate both electrocardiography and BP measurement by adopting transit pulse time. PTT was defined as the systematic time lay off between oscillometric pulses and R- peaks of ECG waveform. The major advantage of the system is to exhibit non-zero crossing and gives a more accurate result. They evaluated their method only for thirty seconds and didn't mention the number of subjects involved in the experiments. Although the proposed method increased the accuracy of BP measurement, further evaluation needs to be done in an extended period.

A new feature related to BP named the intensity ratio of the first derivative wave of the PPG (1^{th} dPIR) has been proposed by Wan-Hua et al. [91, 109]. Twenty-two healthy volunteers participated in mental arithmetic stress and Valsalva's manoeuver tests. The Finapres device was used as a reference and the result showed standard deviation errors of 3.22 ± 8.02 mmHg and 3.13 ± 4.82 mmHg for SBP and DBP estimation, respectively. Considering both subjects with CVD history and a bigger group was proposed as a future work for this study.

2.4.3.1 Challenges of PTT Techniques

Although the PTT method for cuffless BP monitoring has already shown remarkable development, there are still several issues and challenges that exist for non-invasive and continuous BP measurement. In particular, the existing cuff-less non-invasive continuous PTT-based methods don't have adequate accuracy to replace direct invasive measurement of arterial BP. Following is a summary of the key issues and challenges of PTT-based BP monitoring.

Most of the studies attempted to measure only SBP through the PTT-based methods, rather than DBP as well. Although SBP has a higher correlation with PTT than DBP, in some studies, PTT-based DBP estimation showed lower error rates than SBP. The reason behind this can be due to the unique physiological mechanisms of SBP and DBP. Compared to SBP, DBP varies more slowly under the regulation of peripheral arteries.

Secondly, most studies use PTT as the only variable targeting for BP with linear or non-linear regression models. On the one hand, PTT on its own cannot fully represent dynamic BP, as PTT is determined by factors other than just the arterial BP, and vice versa. On the other hand, PWV is a function of the elasticity of the vessel, where the function would vary among individuals and even within the same individual in different situations. Because of this, the PWV changes in a given segment of the artery can be determined almost entirely by changes in the local BP and/or the activity of the smooth musculature of the segment.

Third, frequent calibration is required for most of the studies to provide accurate results. The reason lies in the assumption and simplification of the M–K equation since the arterial dimensions, such as the arterial diameter, is not a constant but a variable changing with the arterial pressure cycle by cycle under the regulation of vascular vasomotion.

Although it is difficult to compare the results of all previously discussed methods as they are using different evaluation techniques, a comparative analysis of PPT-based techniques is presented in Table 2-3. This comparison was conducted in terms of the number of extracted features, experimental tools, sample size, and type of calibration.

Table 2-3: Comparison of PTT-based BP monitoring techniques in terms of PTT definition, features, tool, calibration, and experiment time

Ref.	Definition of PTT	Key Feature	Experiment Tools	Calibration	Number of Subjects	Experiment Time	Important Results
[87, 88, 90, 110]	Time interval between the R wave peak of ECG and the peak of the first derivative of PPG	PTT, PIR	ECG and PPG logger	One point	27/Healthy/ Seated	5 minutes	• Proposing new indicator (PIR) • Measuring DBP at LF • Cuff-less • Non-invasive • Finapres was the reference
[111, 112]	Time arrival between the arrival of pulse wave at two peripheral sites	Multi-Wavelength PPG	ECG, PPG	Not specified	10/Healthy/ Seated	30 seconds	• Simple sensor implementation at one body site • Suitable for wearable device • The size of the sensor should be reduced • Effect of motion artefacts not considered
[94, 95]	Time lag between pulse wave peak at two body locations	iPTT, iPPG	High-speed Camera, Light source	No	7/Healthy/ Seated	13 minutes	• Contactless monitoring • High correlation between PTT and iPTT • Cuff-less • Uncomfortable for the patient • Calibration of each subject required

							• Pulse oximeters sensitive to motion artifacts
[106]	The time take for the PW to travel from the aortic arch to the common carotid arteries	PTT, PAT	ECG, Bimp, CW radar antenna	No	6/ Exercise	5 minutes	• The method architecture is suitable for wearable device • Only systolic and mean BP measured • Cuff-less and convenient
[107]	The time difference between the PAT and a pre-ejection period	MAP	PWV chest sensor, ICG, PPG, ECG	Six different cuff-based techniques	15/Healthy/ Supine	On days D, D+3, and D+14 for 20Seconds	• Only MAP is estimated • Oscillometric device used as calibration reference • ICG on CVD doesn't have signal quality • The implementation is suitable for wearable BP monitoring device
[96]	Correlation between ECG and PPG	PTT, Age, Height, Weight	Bio-Radio, local pod	Cuff-based	14/Healthy/ recumbent, seated, standing, walking, cycling	20 heartbeat	• Oscillometric method used as reference • Validate in posture and activity. • Not suitable for ambulatory BP monitoring • Acceptable accuracy for seated and standing position • Inaccurate during activity

[99]	The time blood leaves the heart and reach to finger	PPG, PCG	Smartphone	No	Not specified	Not specified	• Tracking beat to beat BP • More robust technique for filtering system • Cost effective system • Telehealth system • Not validated with any standard method or in vivo
[113]	Peak of PW	PPG	PPG, ECG, Smartphone, MCU	No need	10/MIT-BIH database	200ms	• less power consumption • Unobtrusive and cuff-less • Calibration needed
[114]	Not specified	14 features from time domain of PPG, Weight, Height, and age	PPG	No	1-32/University vital sign dataset/ ICU	-	• Telehealth system • Only use one signal • Multi-parameters
[115]	-	Pressure of radial artery, PPG	PPG, Photodetector, Pressure sensor	No	7/Healthy/ Seated	3 minutes	• Cannot track BP in low frequency • Convenient and continuous • Need to be validated for gold standard and larger group
[101]	6 type of measurements	PAT	SCG, Acoustic sensor, PPG	No	10/Healthy/ Seated	20 minutes	• First SCG-based system • Cuff-less • Cost-effective • Not beat to beat measurement

							• Detection move rate needs to be improved
[102]	PW foot	PPG, PW	PPG, ECG	-	10/ Healthy	-	• Eliminating inappropriate signal • Fast system
[116]	Time difference between the max negative slope of Bio-Z and max positive slope of the PPG	PTT	PPG, Bio-Z	-	3/Healthy/ Seated	16 seconds	• Suitable for ambulatory and cuff-less monitoring • Continuous • Cuff-less
[104]	Travelling time of blood from the heart to wrist		Wristwatch	Cuff-based	13/ Healthy/ Rest, exercise, and recovery	7 minutes	• Estimation of the brachial artery • Convenient
[117]	Max slope of upslope of PPG	Mean slope transit time	ECG, PPG	-	10/Healthy/ seated	5 minutes	• The measure of one typical point • Suitable for wearable device
[109]	The first derivative of PW	1^{th} dPIR	ECG, PPG	•	22/ Healthy		• New indicator proposed • Eliminating the baseline and LF noise • Linear

2.4.4 Machine Learning and Deep Learning Techniques

Considering the fact that BP is the result of multiple parameters and is highly influenced by various factors, multiple features extraction BP monitoring methods could significantly improve the accuracy of BP monitoring. Moreover, there is a growing demand for automated BP monitoring to perform efficient daily regular home BP monitoring to improve remote healthcare. Automated BP monitoring produces a significant amount of digital data, which increases the rate of diagnosis and the likelihood of identifying ideal treatments. However, the predictive analytics model of such big data is very challenging. Many recent studies have adopted machine learning and deep learning as an effective method in managing big data and predicting the risk factors of hypertension. By taking advantage of such algorithms' computational power and their ability to develop big data, the accuracy of these techniques has improved. Thus, the main idea of using these techniques is to extract multiple features related to BP from time and frequency domains of physiological signals and then use these techniques to eliminate unwanted features and calculate the BP from extracted data. In this section, a variety of different machine learning and deep learning techniques are reviewed.

2.4.4.1 Common Design Steps of Machine Learning-based BP Estimation Methods

The overall flow diagram and design steps of most machine learning-based BP estimation methods are shown in

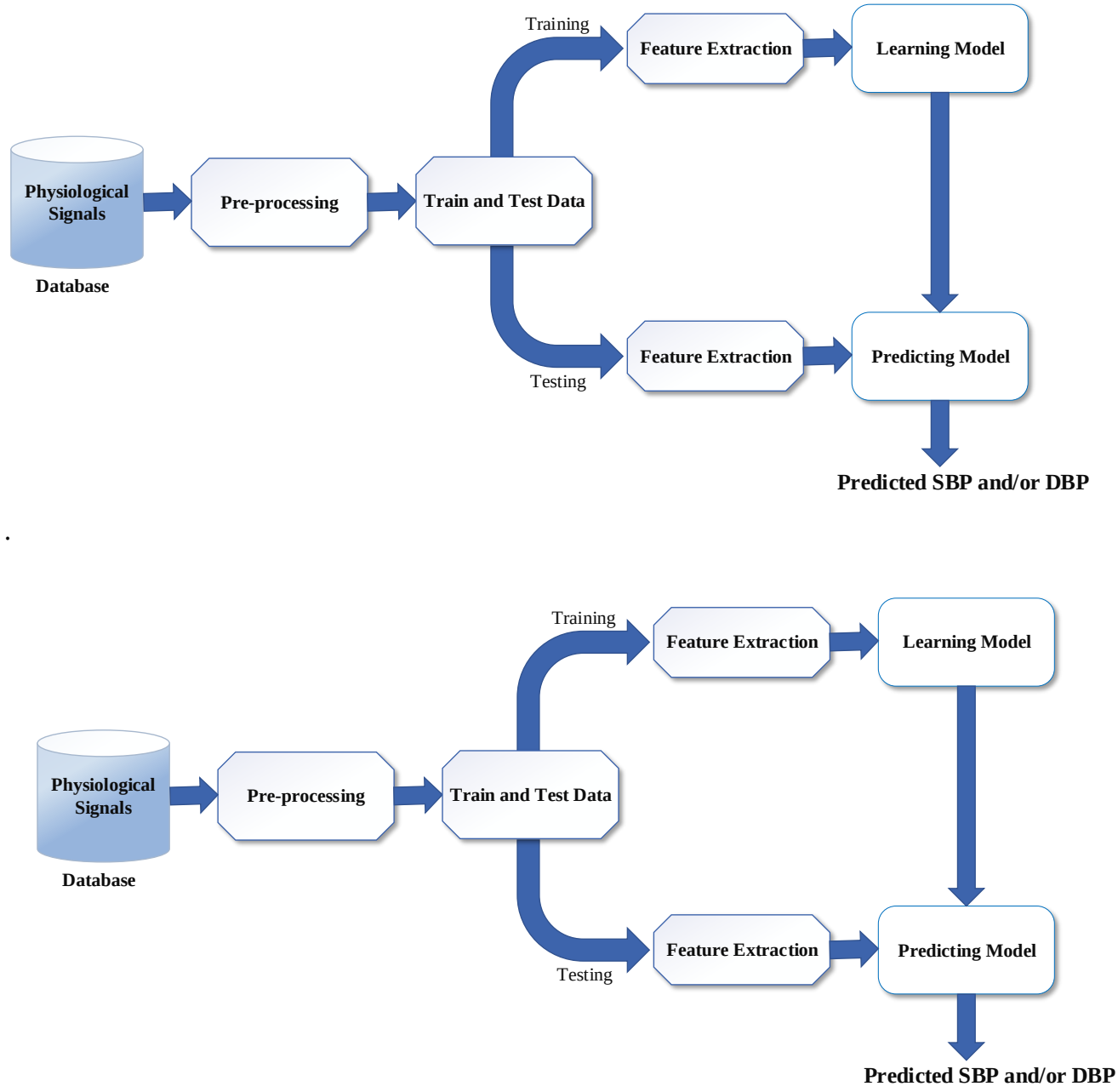

Figure 2-8: *A generic block diagram of most recent cuff-less BP estimations using machine learning techniques*

Most of the studies in this field followed the following design steps:

a) Prepare a database including the ECG and PPG signals as input training data;
b) Pre-process the ECG and PPG signals for de-noising and removing artifacts;
c) Extract features related to BP from the pre-processed signals;

d) BP modelling and possible calibration.

2.4.4.2 Database (ECG and PPG signals)

To train the machine learning or deep learning model for BP estimation variety of physiological signals have been used. Among these signals, ECG and PPG signals are those more employed. The main concern was that both of these signals could be collected non-invasively. PPG signal analyzes and represents blood volume pulsations through back-scattered optical radiation coming from the skin. ECG signal gives the heart electrical activity by utilising electrodes placed on the skin.

As a large amount of data is needed to train the machine learning algorithms, most of the studies employed available online databases for training their proposed system. The MIMIC database has been chosen by many researchers [22, 25, 74, 76, 118, 119] due to the online availability of a wide range of synchronised ECG, PPG, and beat-to-beat BP values. This database was developed by the MIT Lab, and it includes vital signs, medications, demographics, and laboratory tests associated with around 40,000 patients. The MIMIC also provides a waveform database containing multiple physiologic signals recording at 125 Hz. Included in this waveform database are continuous BP waveforms, including ABP that is collected invasively from one of the radial arteries. On the other hand, some studies collected their required database from healthy subjects. The amount of data from MIMIC being used in studies depends both on the complexity of the extracted features and the complexity of the chosen algorithm.

2.4.4.3 Pre-processing

The quality of signals relies on many variables due to different artifacts and distortions, which makes pre-processing an essential step to de-noise and filter the raw signals to be used as an input for the feature extraction step. According to the literature, there are different pre-processing approaches. Wavelet transform (WT) delivers useful information for the analysis of time-domain signals as well as precise frequency and time information. The advantage of using WT as a pre-processing technique includes, but is not limited to, a better phase response compared to Fourier transform [120], flexibility in a different type of signal-to-noise ratio, more efficiency in the matter of computational complexity, and non-steady artifacts. However, the fact that the raw signals will be affected by filtering needs to be considered [121-124].

Empirical mode decomposition (EMD) has been used as a time-space based adaptive analysis method for both non-linear and non-stationary processing series. In general, this method is suitable for original signal analysis; it breaks the signal into different modes without leaving the time domain. However, it exhibits mode mixing, which causes aliasing if transferred to the time-frequency distribution [125-127].

Infinite impulse response (IIR) filters and finite impulse response (FIR) filters are two of the most popular filtering methods that have been used for pre-processing of signals [128-132]. IIR filters work faster than FIR filters because of the smaller amount of coefficients processing needed to execute similar filtering operations, so they are likely to require less memory space. Also, IIR filters are a well-known solution for applications with analog filters or limited phase information such as the Butterworth filter and monitoring signal amplitude. Although the FIR filters are more common than IIR filters, they require further work to set up and extra processing power. Based on the advantages and limitations of each method, a bandpass filter with the combination of a high pass filter (FIR filter) and a low pass filter (IIR filter) was designed [133] to eliminate noise and artifacts.

The Kalman filter is another method that has been used to filter noise and artifacts from raw signals. A joint signal quality index (JSQI) was calculated by fusing the signal quality index (SQI) of ECG and PPG. Through JSQI, this algorithm can adjust measurement noise covariance and provide an automatic artifact detection and rejection mechanism. [76].

As physiological signals always contain parts that have deteriorated due to the different recording systems and artifacts, a pre-processing system needs to make the raw signals ready for feature extraction by removing unreliable data. As described above, one of the most reliable pre-processing techniques is a bandpass filter composed of a low pass filter and a high pass filter in terms of reducing the motion artifacts.

2.4.4.4 Feature Extraction

A feature selection process has been employed by most of the studies before the construction of a BP model so that the irrelevant and redundant features can be removed and the over-fitting problem resolved. The informative features from PPG and ECG signals can be divided into two types. The first type is based on physiological parameters such as heart rate (HR), augmentation index (AI), and

arterial stiffness index. The second type simply includes the shape and timing of signals. There are many approaches to extract features. These include linear regression, genetic algorithm, fast Fourier transform (FFT), and domain-specific methods such as the Pan-Tompkins QRS detector.

FFT was used by Xing and Sun [25] to extract both amplitude and phase features from the ECG and PPG waveforms. This is a robust technique as the identification of the exact location of specific characteristic points on the waveform is not required, and analyzing more than one cardiac cycle at a time is possible. But one of the limitations arising with this method is that the features will be influenced when BP changes rapidly, causing significant errors for the beat-to-beat estimation. Xiao et al. in [134] also used FFT to extract radial pressure waveform features to predict BP using an artificial neural network.

Genetic algorithms are another feature extraction method. It was used by Miao et al. [135] to develop an acceptable fitness level solution for optimal feature selection. The new feature subset was generated, and a fitness function was used to score different subsets, eventually selecting the best one. A random subset was generated, and then the suitability of each feature in the population was assessed by the value of the fitness function calculated in each generation. Then, more optimal features were selected and modified to form a new generation. The developed algorithm was ended when either a maximum number of generations had been realized or a satisfactory fitness level had been achieved.

A combination of a simple Pan-Tompkins algorithm, threshold, and derivation methods was employed by Xu et al. to reduce the cost of system resources and increase the processing speed [136] for extracting ECG and PPG features. Derivative-based algorithm and wavelet modulus maximum algorithms are the most common techniques for extracting PPG signal features [118, 119, 137].

To conclude this section, with the controlling of linear and non-linear transformation techniques and the removal of redundant information, extraction of the most BP-related features is an important step in the accurate estimation of BP. However, the methods that rely on hand-engineered feature extraction have two considerable limitations. The first issue is that calculating several features at once is are difficult due to individual-specific waveforms and the effect of motion artifact. The other one is extracting desired features creates cost challenges in real-time monitoring and it is also time-consuming.

2.4.4.5 BP Modelling Based on Machine Learning Techniques

With recent revolutionary developments in signal processing and the computational power of machine learning, researchers have recognized the remarkable potential of machine learning-based method in the healthcare industry to improve people wellbeing towards cuff-less BP measurement [22-26]. Considering the ability of machine learning to learn the function of a complex system makes it a promising method for BP estimation. If the machine learning-based BP model train well, it can address the latent affecting parameters that cannot be measured in the analytical model. The main idea is to use machine learning to extract surrogate cardiovascular features from the time-domain or the frequency-domain of physiological signals, then train a machine learning-based BP model with those features, and finally estimate the BP through the developed model [29].

Artificial neural networks (ANN) are brain-inspired mathematical models which are used as the primary tool in machine learning. ANN is one of the most promising methods to analyze complex function systems and the non-linear relationship between the input and output data. It mostly consists of input and output layers of computational neurons, as well as middle or hidden layers that transfer the input data to the targeted output data set. ANNs have a significant role in many scientific and industrial applications, such as computer vision, speech recognition, decision making, time series prediction, pattern recognition, and event prediction [118, 138]. Taking into account the fact that ANNs are capable of deriving meaning from highly complex data, this technique has been used by many researchers to estimate non-linear and complex function between BP and related excreted features [25, 139, 140].

ANNs have used the backpropagation neural network to find the minimum value of function error concerning weight using gradient descent. This algorithm is a typical multi-layered feed-forward neural network used to estimate the cuff-less beat-to-beat SBP and DBP [22, 136]. The extracted features from ECG and PPG signals are used as an input layer, and the results showed high accuracy compared to the previous BP estimation design. This training method is probably the most popular algorithm used in industrial applications and has good performance on a wide variety of problems, such as minimizing the mean-square error of the network output. The main drawback of this method is the sensitivity of the algorithm to the initial conditions. Usually, this is taken care of by repeating the training of the algorithm several times to achieve a good performance.

A multilayer feed-forward network (FFNN) based on backpropagation is also a type of ANN used to predict BP [141]. It is considered to be one of the most straightforward methods used for revealing the internal mechanism of a complex problem as it has a robust and flexible learning ability. The optimum features are selected using Levenberg–Marquardt algorithm, and then the SBP and DBP estimated using these features. The FFNN model trained and tested with data recorded from 85 subjects. The performance of the proposed model compared with the conventional maximum amplitude algorithm, adaptive neuro-fuzzy inference system, and NN-based methods. The FFNN model showed the lowest error among other methods [141].

Recent research has revealed that SVM is a powerful tool for classification and regression and has a high noise tolerance [137, 142]. An SVM classifies data by finding the optimal hyperplane that separates the sample into two classes and by optimizing the classification using kernel functions. However, kernel models can be quite sensitive to over-fitting the model selection criterion [143].

Kachuee et al. extracted physical parameters of PPG and used them to train the machine learning algorithm. The authors utilized two different machine learning approaches, ANN and SVM, to estimate the BP. Both models were trained and tested with 4254 records obtained from the MIMIC database. The models evaluated with mean absolute error (MAE) and standard deviation (STD) of estimation errors. The results showed that SVM regression model outperformed the ANN model and achieved less errors [22].

Random forest is a robust and straightforward machine learning algorithm that performs both regression and classification tasks [119]. Simply put, to enhance an accurate and stable prediction, this algorithm makes various decision tree and combines them. A decision tree is the fundamental component of this learning algorithm which is capable of fitting complex datasets. However, this method has a risk of overfitting the data, which implies a low bias, and there is a high low-prediction variance in the model. A bootstrap procedure technique was used to overcome the overfitting typical of regression trees [144].

Chowdhury et al. [145] tested and trained a total of 19 algorithms using the 10-fold cross-validation to find two of the best machine learning algorithms to estimate the BP. The Gaussian process regression (GPR), along with the ReliefF feature selection algorithm selected as the best algorithm among others to design the BP estimation model. The 222 recordings from 126 subjects selected to

evaluate the model and a root mean square error (RMSE) of 6.74 for SBP and 3.59 for DBP estimated. Despite the low error of the proposed method, the results achieved using the engineered and complex feature extraction technique.

Same feature extraction (RReliefF algorithm) as [145] used to select thirteen relevant features from the PPG signal [146]. Amongst 72 patients from the MIMIC database, 41 subjects with high-quality data were selected for the experiment. The results validation was done through 5-fold cross-validation and the LOSO technique. A few types of regression model were considered for the BP modelling; among these methods, the shallow regression tree showed the best performance. The experimental results showed MAE of 4.47 mmHg and 2.02 mmHg for SBP and DBP, respectively.

Zhang et al. [147] used a classification and regression tree (CART) to estimate BP continuously. The data for this study was collected from 18 healthy young participants during three periods of time, namely, 30 minutes at resting position, 45 minutes during exercising, and three minutes during the cooling down period. All the parameters relevant to BP were selected from ECG (AVR, AVL, AVF), PPG, PTT, SPO2 and HR. Compared to linear regression and SVM, this study achieved a higher accuracy which was within the BP standard criteria.

A multivariate partial least-square (PLS) regression method was used by Fujita et al. [148] to estimate SBP. Level Crossing Features (LCF) were used from the contour lines randomly drawn on the second derivative of the PPG signal. To generate training data, 256 subjects from Kanai Hospital with an SBP range of 133.1 ± 18.4 mmHg and aged 62.8 ± 16.8 years participated in the experiment. To evaluate the experimental results, the reference SBP was collected by an automatic BP monitor placed on the left upper arm at rest position for 20 seconds. A low-pass filter and a finite impulse response filter were used to remove the PPG signal's high-frequency noise before feature extraction. Two types of LCF features were extracted: the number of crossings among each contour line and PPG and the overall distance of each contour line lying within the waveform curve. Among the 256 subjects, data related to 180 subjects were used for training and the rest for testing the PLS regression algorithm. Compared to the standard of the British Hypertension Society (BHS), only 38% of the SBP absolute error was within 5 mmHg. Therefore, the proposed method did not meet the expected clinical standard. Moreover, usability for the long- term monitoring was not considered in this experiment.

Chen et al. [149] proposed a genetic algorithm-support vector regression (GA-SVR) model to estimate SBP and DBP. The MIMIC database was employed to evaluate the result of the study. A total of 772 waveform sets, including ECG, PPG, and BP, were selected. A total of fourteen BP related features such as HR, PTT, and characterise of PW were selected. 80 % of the collected data was used as training data and the rest was used for testing data. The experimental results showed a fulfilment estimation error based on the Advancement of Medical Instrumentation and BHS criteria, 3.27 ± 5.52 mmHg for SBP and 1.16 ± 1.97 mmHg for DBP. Compared to traditional PTT-based BP estimation, this study achieved higher accuracy and introduced more relevant PPG signal features.

A restricted Boltzmann machine (RBM) artificial neural network [150] was used to establish a proof of concept for BP monitoring. The MIMIC database was used to validate the result of this study and data related to 250 patients collected for this purpose. All signals went through pre-processing to remove the motion artifacts and noise. Three different regression models with different input data, namely, PTT, 1/PTT, and log (PTT), were established and the mean absolute difference for SBP and DBP are calculated. All the results were within-grade A and B of the BHS standard. However, the six minutes of calibration after each measurement decreases the accuracy of the system. Moreover, the reference BP was collected with an invasive method rather than a non-invasive.

The regression forest technique was employed by Yoshioka et al. [151] to predict continuous BP. At the same time, a non-contact system consisting of a microwave sensor for heartbeat detection and a camera for pulse detection was proposed to monitor vital sign remotely during daily activities of subjects. . The features including age, height, weight, BMI, PTT, and BP were extracted via the ECG and PPG signals in 75 healthy subjects to train and test the BP model. The estimated PTT by this model was highly correlated with the actual value obtained from reference measurement.

The random forest (RF) method was used to measure the ABP by Rui et al. [119]. The MIMIC-II was used as the database, then 285 records based on the availability of ABP, ECG, and PPG signals were selected. Among these records, 18 features were extracted to train rank forest and to evaluate the ABP separately. The results showed more accuracy compared to the PPT-based method; however, the cardiovascular data were excluded from the database. Moreover, the low speed of the RF technique cannot be ignored, which is likely to create some difficulty for real-time monitoring.

Fen Miao et al. [29] extracted 14 features related to BP from the ECG and PPG signals to improve the accuracy of BP measurements. The Genetic algorithm was used to select the most critical features for each subject. The multivariate linear regression (MLR) and the SVR were used to construct the BP model based on the features selected by the genetic algorithm. Pearson's correlation coefficient (CC), the mean difference (MD), and the difference in the SD were calculated for each subject in three static, dynamic and long-term performances. Finapres BP measurement was used as a reference in 73 subjects to evaluate the accuracy of the proposed method. A large correlation was gained between the estimated BP and the reference results for static and dynamic estimation. The long-term estimation showed 20% less correlation compared to previous ones. From one day to three days and then to six months, the estimation error was fairly stable for both SBP and DBP. The overall accuracy of the proposed method increased, but for long-time monitoring, the accuracy of this method is reduced.

Atomi et al. [152] used a PPG signal collected from a wrist watch-type to estimate BP via the data-oriented method. Twenty features were extracted from PPG, as well as an acceleration plethysmogram (APG) and a preliminary questionnaire was used to train BP model. A huge collected data was used to train the machine learning algorithm. A unique cloud system was proposed to deal with BP and life-log data through HTTP, which would solve the data capacity problem. To collect the daily data of the patients, a smartphone application was created. The correlation coefficient between the experiment results with 25 subjects and the estimated result was 0.80. This method showed high accuracy, but it did not meet the level of clinical standard acceptance.

David et al. [153] measured aortic pulse wave velocity by combining ballistocardiography (BCG), a bathroom scale as impedance plethysmography (IPG), and height of the subject in the supine position. The training data set to train the random forest algorithm included IPG and BCG signals collected from 106 subjects. This group included 12 people with CVD history and 28 smokers. The accuracy and feasibility of the results were verified by comparing them with previous techniques, but it still needs to be compared to the gold standard technique. BP monitoring over a long period of time, different populations and different conditions also need to be investigated.

Jun et al. [154] extracted 26 features, including amplitude features, time-domain features, age, and sex of subjects. All these features were fed to a backpropagation neural network algorithm after pre-processing to estimate SBP and DBP. In order to show the efficiency of the approach method, data relating to 10 subjects from the MIMIC II database were used to validate the result. The results showed

a mean error of 5 mmHg and a standard deviation of ±8 mmHg compared to the gold standard. So, the proposed method fits into the clinical standard. However, the small sample size and short measurement period time are not enough to prove the accuracy of the technique.

2.4.4.6 BP Modelling based on Deep Learning Techniques

Deep Learning is a new area of machine learning research and is a highly active research area in the machine learning field. Deep Learning is an artificial intelligence function that imitates the human brain's workings in processing data and creating patterns for use in decision-making. It is also capable of unsupervised learning data that is unstructured or unlabelled.

Lee et al. [155, 156] designed a deep belief network (DBN)-deep neural network (DNN) to estimate SBP and DBP using the oscillometric method. The data set for this experiment was collected from 85 healthy subjects with no history of CVD. Five sets of data, including SBP and DBP, were collected using a cuff-based oscillometric device in a seated position for each subject. As the sample size was very small for such a network, the bootstrap aggregation technique was used to create plenty of training set data to eliminate the overfitting or underfitting. A total of eleven features were extracted, including the features obtained from the oscillometric wave. The results were within the A grade of BHS metric and proved the feasibility of the oscillometric BP measurement technique to increase BP estimation accuracy. Expanding the data set would be an area for future study.

Similar to [155, 156], a DBN-DNN model reported by Argha et al. [157] was used to estimate the BP from the extracted oscillometric waveform envelope (OWE) and beat-by-beat (BBB) features. Seven BBB features were extracted from the time domain of OW using a bootstrap-based method. To validate the experimental results, 155 subjects participated in this experiment. After eliminating the signals with noise and motion artefact, a total of 350 records were selected. The 5-fold cross-validation scheme was used to evaluate the performance of the proposed method, and the MAE of 1.1 mmHg for SBP and 3.0 mmHg for DBP, with a standard deviation error of 2.9 mmHg for SBP and 5.6 mmHg for DBP were estimated compared to a reference value. The results meet the AAMI criteria and prove the importance of BBB features to help improve the accuracy of BP estimation.

Recurrent Neural Network (RNN) models with a contextual layer were used to predict BP values from sequential measurements data [158]. This study's main idea was to add a hidden layer to process

the contextual data and predict the BP from contextual data and sequential data collected by users. To evaluate the proposed model, a database was collected from a wireless home BP monitor. The result was compared with the previous RNN design, and the effectiveness of using a contextual layer to improve the accuracy of predicting BP was obvious.

A new deep RNN consisting of multi-layered long short-term memory (LSTM) networks was proposed by Su et al. [159]. To evaluate the results of this study, the ECG, PPG, and BP signals related to 84 healthy subjects at rest position were recorded for ten minutes. Moreover, the same database was collected for eleven healthy subjects for eight minutes, for a different period, day 1, day 2, day 4, day 6, and after 6 months. To minimize the challenge of temporal dependency in BP measurement, seven features were selected from ECG and PPG signals. The experimental results of the first database showed the root mean square error (RMSE) of 3.90 mmHg for SBP and 2.66 mmHg for DBP. For the second database, the results were achieved the RMSE of 3.84 mmHg for SBP, and 1.80 mmHg for DBP for the first day, 5.25 mmHg for SBP, and 4.78 mmHg for DBP for the second day, 5.80 mmHg for SBP, and 5.0 mmHg for DBP for the fourth day, 5.81 mmHg for SBP, and 5.21 mmHg for DBP after six months. These results were more accurate compared to the previous study.

The DBN-DNN was proposed by Soojeong et al. [160] to train the complex non-linear relationship between artificial feature vectors and the reference BP. The bootstrap technique was used to generate eight artificial features from original oscillometric waveforms. Consequently, a large number of training samples from artificial feature vectors were used to estimate the SBP and DBP. A total of 85 healthy subjects in a seated position participated in validating this experiment. The proposed method with artificial features showed very accurate results.

Su et. al [161] proposed a novel deep RNN consisting of multi-layered LSTM networks to address the accuracy issue over long-term BP monitoring. The authors selected seven features from ECG and PPG signals to train the proposed system. The experimental results were achieved a root mean square error of 3.90 mmHg for SBP and 2.66 mmHg DBP. Although the proposed method met the standard accuracy, it needed to manually extract multi-features from ECG and PPG signals.

2.4.4.7 Results Comparison

Table 2-4 presents a summary of key features, feature extraction algorithms, methods, sample size, and comparison results of the 16 reviewed papers. Samples of results have been carefully extracted from the papers, while some parameters were either unclear or difficult to easily define in the proposed table or not provided/applicable. This comparison includes BP monitoring based on machine learning and deep learning algorithms.

Table 2-4: Summary of key features, feature extraction algorithms, methods, sample size, and comparison results of the selected reviewed papers

Ref.	Key Features	Feature Extraction Algorithm	Methods	Sample Size	Results
[22]	PTT, HR, AI, LASI, IPA	RLR	MLR/ANN/SVM	4254 records /MIMIC	The performance of the method consistent with grade B of BHS standard
[29, 135]	14 features	Genetic algorithm	MLR/SVR	73/Healthy	Mean error of 0.001±3.102 for SBP, Mean error of 0.004±2.199 for DSB
[119]	18 features	Derivate based algorithm	LR/RF	285/ICU/MIMIC	The one-hour beat-to-beat estimation has shown better accuracy in comparison with other systems
[25]	Amplitude and frequency	FFT	ANN	69-MIMIC 23-healthy	The beat-to-beat fitting error was 0.06±7.08 for SBP and 0.01±4.66 for DBP

[158]	SBP, DBP, HR, BMI, gender, age, longitude, and latitude	Not mentioned	RNN-CL	5894/wireless home BP monitoring database	The contextual layer has improved the accuracy of BP estimation
[155]	Not mentioned	FFNN/SVR	DBN-DNN	85/Healthy	Lower standard deviation (SD) error and mean error for SBP and DBP compared to conventional methods
[159]	PTT, HR, RI, ST, Up Time, Systolic volume, Diastolic volume	Not mentioned	Deep RNN/LSTM	84/healthy	Root mean square error of 3.90 for SBP and 2.66 for DBP
[136]	15 features	Derivation and threshold/ Pan-Tompkins algorithm	Backpropagation neural network	7/healthy	Mean SD of SBP is -0.41±2.02 and DBP is 0.46±2.21
[118]	26 features	The wavelet modulus maximum algorithm	Multilayer feed-forward backpropagation ANN	ICU/MIMIC	The mean value of the error of SBP is 4.5 and for DBP is 3.4/ SD of SBP is 6.13 and DBP is 6.13
[137]	Different features for	ANN	SVM	32 surgical cases at the hospital	Mean error is 11.64±8.20 for SBP and 7.61±6.78 for DBP

	different patients				
[146]	PPG cycle morphology	RReliefF algorithm	An ensemble of shallow regression trees	41 / MIMIC	The mean error for SBP is 4.47±5.85 and for DBP is 2.02±2.94
[147]	AVR, AVL, AVF, PPG, SPO2, PTT, and HR	Cross-validation method	Classification and regression trees (CARTs)		The accuracy rate of estimating BP was exceeded by 90%
[124]	PWTT, HR	-	Neural network	Ten/ hospitalised patients	The measured BP error was five compared to hospital data
[148]	LCF	-	Partial least-square regression	256/ Kanai hospital	Only 38% of SBP absolute error was within the BHS criteria
[149]	14 features	Genetic algorithm	SVM and linear regression	MIMIC	Error of 3.27 ± 5.52 mmHg for SBP and 1.16 ± 1.97 mmHg for DBP
[150]	PTT, 1/PTT, log (PTT)	-	Restricted Boltzmann Machine	250/MIMIC	The results are within the BHS criteria.
[157]	7 features	bootstrap-based method	DBN-DNN	151 individual subject	MAE of 1.1±2.9 mmHg for SBP and 3.0±5.6 mmHg for DBP

From Table 2-4, it is clear that most of the studies in the literature were designed using traditional machine learning techniques. The most common machine learning algorithms that have been used to develop proper BP models include linear regression, neural network, support vector machine, and random forest. Comparatively, the PTT based BP measurement techniques in conjunction with machine learning are perhaps the most promising techniques among those tested. Some studies in the literature did exploit the latest deep learning algorithms, namely, LSTM, DNN, RNN and DBN.

However, all these studies required engineered features extraction to extract multi-features from original physiological signals.

As it is considered that BP is the result of various physiological and neurological factors, including feature extraction in a BP estimation model could significantly improve the accuracy of the measurement. With the recent development in signal processing and artificial intelligence, many recent studies have used machine learning and deep learning to develop a continuous and cuff-less BP estimation model. The computational power of such a technique to analyze the non-linear relationship between BP and extracted features and the ability to evaluate big data sets could have a significant impact on increasing BP estimated accuracy. However, as the value of BP can be affected by the state of the cardiovascular system and the existence of some pathologies, the features of physiological signals cannot be fully expressed by geometrical features and there is currently limited knowledge of other effective heuristic features.

2.5 Limitations and Challenges of Existing Works

Accurate measurement of BP is essential to evaluate BP-related risks, diagnose hypertension, monitor the treatment response, and guide the management of diseases. Therefore, the development of cuff-less and continuous BP methods could provide a novel way to overcome various medical problems. The assessment criteria for evaluating the accuracy of BP measurement should therefore be well established before a new measurement system is recommended for clinical use.

Among all existing studies, PTT-based techniques are the most common models being used for cuff-less BP monitoring. However, this study has indicated that there are still issues and challenges that need to be addressed for the pervasive and ubiquitous BP monitoring. First, arterial BP is determined by many other factors in addition to the PTT. Hence, taking only PTT into the estimation cannot fully represent BP. Second, most studies employed PTT to estimate the SBP rather than the DBP. Third, most of the studies have attempted to use cuff-based and regular calibration to remain a high accuracy. However, a simple and cuff-less calibration approach needs to be investigated, taking into account the convenience for patients. Fourth, the PTT/PWV methods could be affected by arterial diseases, and most of the reviewed studies excluded CVD patients from their validation data. It is essential to consider large databases that include both CVD patients and healthy people to investigate the estimation precision and robustness. Finally, as most of the studies compared their results with a

cuff-based technology and used a cuff-based device for calibration, the accuracy of the reference device needs to be discussed in any comparative study.

Importantly, it is crucial that the BP measurement technique meets the standard for evaluating BP measurement accuracy. The difference between the test value and the reference value is considered as determining the accuracy of a device. This accuracy could be calculated in terms of standard deviation, mean absolute difference or absolute difference. Generally, there are four standards with different criteria for evaluation of the accuracy of a BP monitoring device. These standards include the British Hypertension Society (BHS) standard [162], the Association for the Advancement of Medical Instrumentation (AAMI) [163], the IEEE standard for Wearable, Cuff-less Blood Pressure Measuring Devices [164], and the European Society of Hypertension (ESH) evaluation standard [165].

With the current advancements in machine learning and deep learning techniques, many researchers have attempted to develop machine learning-based BP monitoring systems that meet the aforementioned standards. Different algorithms have been developed to firstly select optimal BP features related to the PPG waveform and then other physiological parameters such as age, heart rate, augmentation index (AI), and arterial stiffness. The goal is to monitor BP continuously and non-invasively by combining physiological and mathematical modelling.

Overall, significant achievements have been made towards developing cuff-less and continuous BP monitoring based on these latest algorithms. The accuracy of most machine learning techniques ranges from 80% to 95%, depending on the dataset and model that have been used. However, these techniques were not suitable for the clinical setting due to some important drawbacks, as reported in the current studies.

This study reveals key **limitations** and existing **challenges** faced by the surveyed works:

- Despite most machine learning studies using different calibration techniques to maintain the accuracy of BP measurement, the accuracy of BP measurement reduced with a longer calibration interval. These findings prove that calibration can affect the accuracy of the measurement technique and therefore, should be taken into consideration when designed a new monitoring system. Moreover, most of the calibration techniques were cuff-based.

- Most of the studies in the literature relied on hand-engineered features extraction. However, extracting features from signal waveform is time-consuming and needs additional algorithms. Moreover, in real-time monitoring, calculating several features was time consuming, inconvenient, and cumbersome.

- The evaluation of these studies was conducted in different environments and with different databases, populations, and timeframes which make them incomparable in terms of meeting clinical standards. Most researchers used a small database to validate their results; hence, to achieve the clinical standard, significant amounts of data would need to be generated for analyzing the models. Also, most of the reviewed studies excluded CVD patients from the experiments. This group of people are at high risk and require regular BP monitoring. So, considering people with a CVD history, as well as different age populations, is essential for further validation.

- Although the studies based on deep learning techniques had shown more accuracy, the realizing of the methodology of deep learning black box is opaque. To develop a deep learning method, it is critical that some factors such as algorithm choice, optimization of the number of neurons/layers/training and testing ratio, regularization, normalization, type of gradient descent, and implementation are critical.

- Despite the available public and educational-based tools for machine learning and deep learning, advanced software and technologies with computational power are required to process the vast amount of clinical data.

- The lack of physicians and clinical knowledge in the data science and bioengineering field makes it very difficult to familiarise them with the interpretation of the results. Thus, there is an urgent need for a clinical-friendly trial design to be tested in the real world.

2.6 Overview of the Employed Tools

For the realization of this work, the resources used were:

- The MATLAB© 2019a with a machine equipped with an Nvidia GeForce© GTX 1080 graphics card, which was used to develop and design the proposed models;

- The PhysioNet a web-based resource signals use for the biomedical research community.

2.6.1 MATLAB

MATLAB environment was chosen for this study as it is a matrix-based language and a high-level interactive framework for computational mathematics, visualization, and programming. Utilizing this development environment makes it possible to analyze data, develop algorithms and create models and applications. The apps and built-in functions allow researchers and engineers to quickly explore, transform, filter, and visualize signals. Likewise, the validation of algorithms and applications can be done with immediate visual feedback through plots.

2.6.2 PhysioNet

PhysioNet is a web-based database containing biomedical signals and multi-parameter databases. It is an online open-source archive that is freely accessible and includes 40 GB of digitized physiologic signals which are organized into 21 major databases. The WFDB (Wave Form Data Base) software package is the core of the PhysioToolkit and includes command-line tools. Using WFDB, enables the user to specify the desired database and extract it in the required format. The WFDB package includes a variety of signal processing functions, all written in C and they can be used on Linux or MS-Windows PCs and UNIX workstations. In this study, the chosen database, where the signals of interest were taken from, was MIMIC-III database (Multi-parameter Intelligent Monitoring for Intensive Care).

3 CHAPTER 3 Blood Pressure Measurement Using Continuous Wavelet Transform

3.1 Introduction

In this chapter, the proposed CNN-based method for estimating BP is introduced. We employed a continuous wavelet transform (CWT) and deep convolutional neural network (CNN) to estimate BP. First, the steps for data preparation are explained and then a brief description of CWT is provided. Then, the architecture design of the CNN-based BP estimation model is proposed for continuous and cuff-less BP estimation. Next, the result of the proposed method is evaluated with three different databases. Moreover, the experimental results are compared with selected previous works in the literature. To the best of our knowledge, the proposed model is the first existing study in the literature that shows the effectiveness of using CWT and CNN to estimate the BP by leveraging the CNN technique. Material discussed in this chapter has been previously published [166-168].

3.2 Dataset

The data in this study was obtained from the Medical Information Mart for Intensive Care (MIMIC-III) Waveform Database Matched Subset [169], a subset of the MIMIC-III waveform Database. This database includes multiple physiologic waveforms and numeric time series of vital sign measurements. It contains 22,317 waveform records and 22,247 numeric records collected from 10,282 distinct Intensive Care Unit (ICU) patients that were matched and time-aligned with MIMIC-III clinical database records.

The database provided high-resolution waveform waveforms recording at a sampling frequency of 125 Hz and clinical information on patients that had been hospitalized in the ICU at the Beth Israel Deaconess Medical Centre in 2001. The data was obtained from patients aged 16 years or older, with a mean of 65.8 years, and 44.1% of the subjects were female, and 55.9% of the subjects were male. Each subject could have several recordings with different time lengths, from seconds to a few hours.

In this study, an initial list of patients with available ECG, PPG, SBP, and DBP data was created using the Physionet Bank tool. Patients with empty or a minimal number of samples were then removed from the list. To download the selected patients' data in MATLAB, we developed an

algorithm using the WFDB software package, *wfdb2mat* function [170]. The following steps were taken to synchronize and align the data for each patient.

1. The duration of the recording was specified and based on the requirement of this study; seven minutes of data was collected for each patient.
2. Most of the missing samples occurred within the first minute of recording; therefore, all records were collected after one minute from the start of actual recording time.
3. A 30-second gap was allowed between each one-minute collection interval to avoid the recording of the consecutive pulses.
4. The ECG and PPG waveforms specified as *AVR* and *PLETH* were loaded to the MATLAB environment as a matrix with two labelled columns.
5. The corresponding SBP and DBP, specified as *ABP Sys* and *ABP Dias* were loaded as a matrix with two labelled columns.
6. Both matrices were concatenated together and saved in CSV format for training and testing the network.
7. As each cardiac cycle interval was considered to be 0.6s to 1s, the signals were segmented into the cardiac cycle with a length of 1s as one sample. The summary of these steps is shown in Figure 3-1.

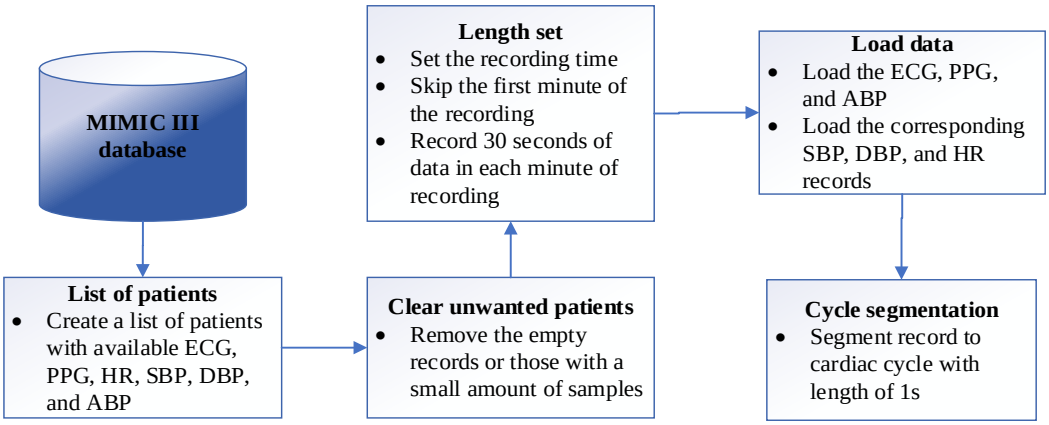

Figure 3-1: The steps to collect data for each patient from MIMIC III database

3.3 Dataset Preparation

For this chapter, we used four parameters for our dataset: ECG, PPG and their corresponding SBP and DSP signals recorded at 125 Hz. In order to fully present the effect of the sampling number on the accuracy of our network, three databases with different data length were created and their results were compared.

Dataset1: The first database was collected from 22 patients and included 200 cardiac samples of ECG, 200 cardiac samples of PPG signals, along 200 synchronized SBP readings.

Dataset 2: The second database was collected from 22 patients and included 250 cardiac samples of ECG, 250 cardiac samples of PPG signals, along 250 synchronized SBP readings.

Dataset 3: The third database was extremely expanded, collected from 120 patients with the same waveform length of seven minutes for each subject. In total, we collected 420 samples of ECG, PPG, SBP, and DBP individually for each patient. In sum, for 120 patients, we collected 50,400 samples equal to 14 hours of training data for each signal. The distributions of SBP and DBP of the final data are shown in Figure 3-2.

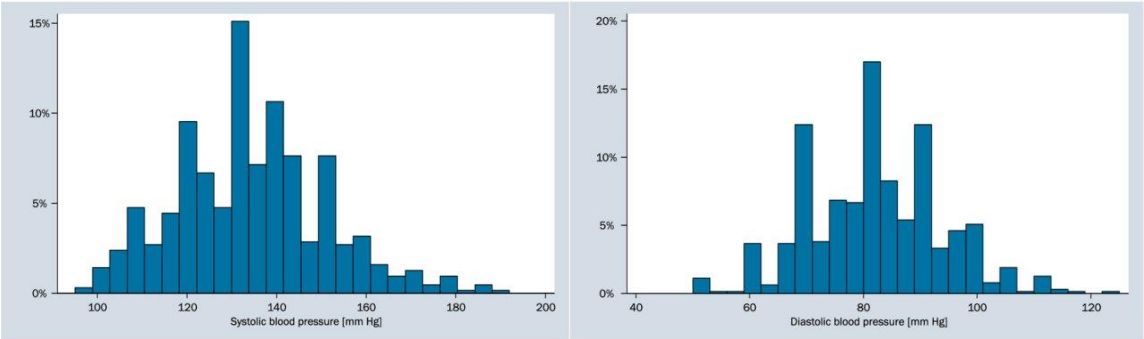

Figure 3-2: The distributions of SBP (left) and DBP (right) in data collected from 120 patients.

3.4 ECG and PPG Scalograms Using CWT

Over the past decades, wavelet theory [171] has become one of the emerging and fast-evolving mathematical and signal processing tools for its many distinct merits. Wavelet transform (WT) can be used for multi-scale analysis of a signal through dilation and translation so that it can extract time-frequency features of a signal effectively.

CWT is one of the most effective techniques for producing a time-frequency analysis of desired signals. This method is suitable for extracting high-frequency components of signals in a short period. The CWT of a signal X(t) ∈ L2(R) could be expressed as Equation (3-1):

$$W(a,b) = \frac{1}{\sqrt{a}} \int_{-\infty}^{\infty} X(t)\, \psi * \left(\frac{t-b}{a}\right) dt \qquad (3\text{-}1)$$

where X(t) is the signal in the time domain, '$*$' operator denotes the complex conjugate and ψ(t) is the mother wavelet scaled by a factor a, where a > 0, and dilated by a factor b.

The absolute value of the CWT coefficients of a signal can be considered as a scalogram, which is a function of time and frequency. Since the ECG is related to heart activity and PPG is a fusion of the microcirculation system that detects the changes in blood volume, their time-frequency domain parameters were essential for this study. Therefore, CWT was used to produce Red-Green-Blue (RGB) images from the selected ECG and PPG signals. Each cardiac cycle was converted to a scalogram over both time and frequency, which can locate different frequency components of the signals.

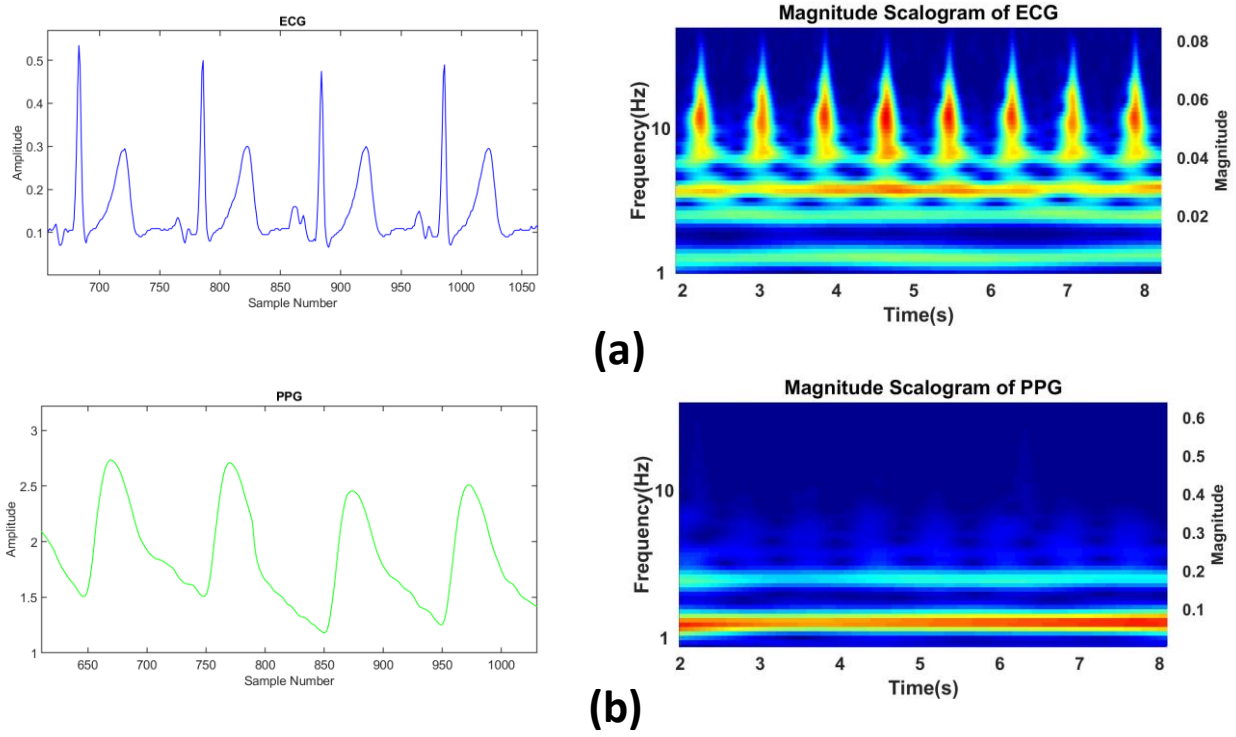

Figure 3-3: *A sample of ECG (a), PPG (b) signals and the corresponding scalograms*

The absolute value of CWT was obtained using the analytic Morse wavelet through the Wavelet toolbox of MATLAB with the symmetry parameter (gamma) equal to 3 and the time-bandwidth product equal to 60.

In total, a dataset containing 400 scalogram images was generated from time-synchronised ECG and PPG for the first dataset, the second dataset consisted of 500 scalogram images of ECG and PPG cardiac samples, and the third dataset consisted of 50,400 scalogram images. A sample of ECG, PPG and their corresponding scalograms created for this study are illustrated in **Error! Reference source not found.**.

3.5 Convolutional Neural Networks

Brain-inspired mathematical models, known as AI, have been used as primary tools in machine learning. They are one of the most promising techniques for recognising patterns of highly complex functions and emulating the nonlinear relationship between inputs and outputs of nonlinear systems. Particularly, the deep learning class of machine learning algorithms have shown promising results in biomedical technologies such as risk assessment for hypertension [33], and echocardiography images analysis [35].

Considering the fact that a convolutional neural network (CNN) is the most popular technique used in deep learning [172], we have found that a CNN-based architecture could be investigated as a continuous and cuff-less BP monitoring technique using the ECG and PPG as input signals. One of the significant benefits of such a method is the ability of CNNs to perform perception tasks, which allows them to learn the BP relevant features from ECG and PPG signals and skip the complicated feature extraction step. Therefore, the first step would be choosing a suitable architecture for the network and then train it with ECG and PPG signals as a training set. The last layer of the network would be a regression layer to estimate BP as the output of the proposed system.

The CNN is a type of deep learning that is widely adopted tools. They are specifically designed for images input. However, recently they have been used for signals, text, and other continuous data. Similar to other deep learning models, the architecture of the CNN is composed of multiple stages. The building block of the CNN contains multiple layers, such as convolution layers, pooling layers, and fully connected layers. CNN can have hundreds of layers that each of them could extract the

different features. The network architecture can vary depending on the nature of the input data and the related application. A small network with only one or two layers might be suitable for a small database, while for a bigger database, a more complicated network with multiple layers might be needed. In general, the input data includes several localized features arranged as a number of feature maps. The multiple of a convolution matrix and a filter matrix is called the feature map. After applying each convolution and pooling layer, the size of the feature maps gets smaller. To combine the features across all frequency bands, after the final CNN layer, one or more fully connected hidden layers are added before feeding them to the output layer.

The main building of CNNs is the convolution layer which computes the number of learnable filters and the dimension of input data (width, height, depth). Filters are usually small, but they can extend based on the full depth of input. If the input data depth is n, a typical filter for a 3D image will be $3 \times 3 \times n$. For a layer with n filters, there will, therefore, be n separate 2D activation maps, which will be stacked along the depth dimension to produce the output volume. The output result of each layer depends on the local position of the input volume, known as the receptive field and it has the same size filter. In other words, each neuron receives their input only from the receptive field in the prior layer, which results in reducing the free parameters and allows CNN to be applied to a large dataset.

After the convolution layer, the pooling layer is typically used for down-sampling and reducing the number of computations, additionally reducing the overfitting. The pooling layer is independently applied to each feature map. It is often placed between two convolutional layers and is responsible for decreasing the number of parameters and calculations in the network. Pooling operations can be applied using Equation (3-2) as:

$$FM[x, y] = f_p \times I_{x,y} \qquad (3\text{-}2)$$

$FM[x, y]$ shows the output feature map, f_p is the pooling function, and $I_{x,y}$ is the input feature map from the previous layer. The pooling operation can be max pooling and average pooling. Max pooling computes a maximum value from the region overlapped by the kernel, whereas average pooling gives an average of all pixel values from the overlapped region.

The extracted feature maps are then sent to activation functions that conduct nonlinear transformations. Nonlinear activation functions are important because otherwise, the network would be a linear predictor, without the ability to learn nonlinear features. The ReLU layer is responsible for replacing all negative values with zeros which are received as inputs. It performs an activation function defined as Equation (3-3):

$$ReLU(x) = \max(0, x) \qquad (3\text{-}3)$$

There are other activation functions that exist in the literature such as sigmoid, tanh, maxout and variants of ReLU. In this study, ReLU is preferred over other functions as it has the power to overcome the vanishing gradient problem.

During the training of the deep neural network, the data distribution of each layer must be constantly changed to prevent early saturation of the nonlinear activation function in the whole network. Accordingly, we utilized batch normalization in the CNN structure to reduce the internal covariate shift, thereby avoiding the vanishing gradient problem and accelerating the training of the CNN network. This had a beneficial impact on the regularisation of the CNN model and the reduction of the dropout utilization. Finally, as the name suggests, in the fully connected layer, all neurons in this layer connected to all the neurons in the previous layers.

3.6 Proposed CNN Regression Model Architecture and Model Training

Following the success of CNN in the fields of speech recognition, emotion recognition, and other speech analysis applications [173-175], a novel CNN-based BP estimation is proposed in this study. The proposed method can detect the knowledge related to BP estimation from ECG and PPG signals by extracting complex BP related features automatically instead of designing them. The engineered features are generally not robust due to noise, scaling, and displacement; however, the extracted features quality has significant effects on the performance of the network. The proposed method can overcome the drawbacks of feature recognition of the PTT-based methods and the low BP prediction accuracy of the non-PTT based methods.

Since deep learning deals efficiently with images, scientists have transformed signals into visual representations based on time-frequency representation. Time-frequency can disclose characteristic signal patterns. It is also a powerful tool for characterising medical signals [176]. The spectrogram

images were used to train a CNN for some medical diagnoses such as automatic atrial fibrillation detection, arrhythmia, sleep disorder, motor impairment neural disorder, and clinical brain death using time-frequency images of bio-signal (ECG, EEG, and EMG) [177, 178]. Besides, research has been conducted to classify various human behaviours using wavelet transformed scalogram image data and deep learning [179, 180]. Inspired by the success of using scalogram image of signals to train the CNN, a deep learning model was constructed and trained with the scalogram of ECG and PPG signals collected from the MIMIC III database. The proposed method is the first to estimate the BP using CWT and CNN. The novelty lies in the usage of scalogram to represent ECG and PPG features and testing its strength in BP estimation.

The design of CNN architecture is challenging and involves several aspects, including the performance metric, loss function, optimization, and hyperparameter setting. The hyperparameter setting includes the number of hidden layers and channels for each layer, the pooling layer, the batch normalization, the activation layers, learning rate, and batch size [181]. Although there are various pre-trained CNN networks such as AlexNet, GoogLeNet, and ResNet, this study utilized a novel CNN network designed to suit the complexity of the selected training dataset. Creating a network required determining a network configuration to provide the most control over the network and optimizing the results.

In this study, two CNN with different architectures were created, with the number of convolutional layers ranging from 4 to 5 layers. The CNN architectures were designed inspired by successful architectures in computer vision [182]. This architecture's primary concern is to extract a wide range of features and is not restricted to specific feature types. The first CNN has included four convolutional layers obtained through the process of trial and error. Each convolutional layer was followed by batch normalization, an activation layer, and an average-pooling layer. The input data was fed into the convolutional layers with filter size W×H and kernel size N, where W and H are the filter width and height, respectively, and N is the filter depth. The proposed CNN structure is presented in Table 3-1

During the training of the deep neural network, the data distribution of each layer must be constantly changed for preventing the early saturation of the nonlinear activation function in the whole network. The batch normalization was implemented for regularization after each convolutional layer and to speed up the process of network learning using internal normalization values [183]. The batch normalization was placed between the convolutional and ReLU layer to stabilize the learning process

and to reduce the number of epochs. Furthermore, the batch normalization reduces the scale gradients of the input values and network parameters; thus, a relatively high learning rate is applied to the CNN without divergence risk [184]. This has a beneficial impact on the regularization of the CNN model and the reduction of the dropout utilization [185]. In the normalization step, the mean and variance of the input are determined. Specifically, for a k-dimensional input batch $x = \{x_1, \ldots, x_k\}$, the batch normalization is calculated using the following equation **Error! Reference source not found.** :

$$\mathrm{Norm}(x_i) = \frac{x_i - E(x_i)}{\sqrt{\mathrm{Var}(x_i)}} \qquad (3\text{-}4)$$

where $\mathrm{Norm}(x_i)$ is the batch normalization of the training dataset, $E(x_i)$ is the batch mean, and $\mathrm{Var}(x_i)$ is the batch variance.

After the convolutional feature extraction, the average pooling layer is adopted for reducing the spatial size of the feature representation. This reduces the number of parameters and the computational load. The pooling layer is independently applied to each feature map. In this study, the average-pooling layer was employed in the pooling layer owing to its advantage for extracting high-level features [186]. The average pooling layer greatly reduces the number of training parameters of the CNN model and reduces the risk of CNN model over-fitting.

The extracted features were then sent to the ReLU layer that performs the nonlinear transformation. Otherwise, the network would have behaved as a linear predictor without the ability to extract the nonlinear features. The dropout layer was then applied to avoid overfitting, which causes the deep learning network to fail in predicting additional or future data. After all the convolutional layers were implemented, the outputs were fed to the fully connected layer and regression layer.

To convert the traditional CNN classification network to a regression model, the fully connected layer of size two according to the number of output (SBP and DBP) and a regression layer was replaced the softmax layer and classification output layer. The fully connected layer multiplied the input by a weight matrix and added a bias vector. The regression layer computes the mean-squared-error loss for regression problems. The mean square error (MSE) is given by Equation (3-5) :

$$\boldsymbol{MSE} = \sum_{\boldsymbol{n=1}}^{\boldsymbol{R}} \frac{(\boldsymbol{t_i} - \boldsymbol{y_i})^2}{\boldsymbol{R}} \qquad (3\text{-}5)$$

where t_i is the estimated BP, y_i is the actual value, and R is the total number of values in the testing dataset. The pseudo algorithm for the proposed CNN regression network is shown in Figure 3-4.

Pseudo Code for the proposed CNN network

A. Parameter initialization:

Segment of labelled training patterns, $Z=\{(x_i, y_i, \ldots), \ldots\ldots, (x_n, y_n, \ldots)\}$

Set Initial learning rate as = 0.001

Minibatchsize as = 60

Epochs as = 30

B. Dataset preparation:

Divide data in the ratio of 7:3 among training and testing sets

C. Training Phase:

I. Initialize regression networks layers

(a) Convolutional layers

for i from 1 to N do , *N is total rows in samples*

for j from 1 to M do, *M is column in total samples*

$$\boldsymbol{FM = [\,i\,,j\,] = I[\,i,j\,] \times K[x\,,y]}$$

end for

end for

where, i , j are positions in input samples and x,y are kernel element positions.

(b) Initialize batch normalization and rectified linear layer to normalize channels and setting negative values to zero.

(c) Apply average pooling on the feature map as,

$$\mathbf{FM} = \frac{\mathbf{1}}{\mathbf{M \times N}} \sum_{\mathbf{i=1}}^{\mathbf{M}} \sum_{\mathbf{j=1}}^{\mathbf{N}} \mathbf{FM[i\,,j]}$$

With varying value stride of [1 1] and [2 2], and padding of [0 0 0 0]

(d) Set regularisation ratio in dropout layer as 20% to suspend some of neurons to go into the next layers, aiming to avoid overfitting.

(e) For fully connected layer

for i from 1 to m do

for j from 1 to n do

$$\boldsymbol{Weight - Matrix = FM\,[\,i\,,j\,]\,x\,W[\,i\,,j\,] + bias}$$

end for

end for

where, m is row and n is column of feature map from previous layers.

(f) Regression layer compute a loss value based on the half-mean-squared-error given as,

$$MSE = \sum_{n=1}^{R} \frac{(t_i - y_i)^2}{R}$$

where R is the number of responses, t_i is the target output, and y_i is the network's prediction for response i.

D. Repeat training phase to update weight until loss is minimum.

Figure 3-4: The pseudo-code of the proposed CNN regression network

3.6.1 First CNN-based BP Model

To predict the continuous BP and solve the regression problem, the layers of the network were created, and a regression layer were included at the end of the network. The first layer defined the size

and type of the input data, and then generated an image input layer of the same size as the training images. The middle layers of the network defined the core architecture of the network, where most of the computation and learning take place. The final layers defined the size and type of output data. For regression problems, a fully connected layer was added at the end of the network.

Table 3-1: Details of the architecture for proposed CNN

	Layers	Size and Definition
1	Image Input	41x125x2 RGB images
2	Conv_1	8 3x3x3 convolutions with stride [1 1] and padding 'same'
3	Batchnorm_1	Batch normalization with 8 channels
4	Relu_1	ReLU
5	Avegpool_1	2x2 average pooling with stride [2 2] and padding [0 0 0 0]
6	Conv_2	16 3x3x8 convolutions with stride [1 1] and padding 'same'
7	Batchnorm_2	Batch normalization with 16 channels
8	Relu_2	ReLU
9	Avegpool_2	2x2 average pooling with stride [2 2] and padding [0 0 0 0]
10	Conv_3	32 3x3x16 convolutions with stride [1 1] and padding 'same'
11	Batchnorm_3	Batch normalization with 32 channels
12	Relu_3	ReLU
13	Avegpool_3	2x2 average pooling with stride [2 2] and padding [0 0 0 0]
13	Conv_4	32 3x3x32 convolutions with stride [1 1] and padding 'same'
14	Batchnorm_4	Batch normalization with 32 channels
15	Relu_4	ReLU
16	Dropout	20% dropout
17	FC1	2
18	Regression Output	mean-squared-error with response 'Response'

This model had four convolutional layers (C1 to C4), one fully connected layer, and one regression layer. The ECG and PPG scalograms passed through the proposed network as input data. The input data was sorted as a 41×125×2 array, where 41 is the height and 125 is the width of the images. The first convolutional layer (C1) had eight kernels of size (3×3×3) applied at a stride setting of 2. This

was followed by a batch normalization layer with eight channels to normalize the estimations of the network when training starts. A ReLU layer was used to improve the efficiency of the training process, and an average pooling layer with a stride of two implied respectively. The second convolutional layer (C2) had 16 kernels of size (3×3×8) which was applied to the input with a stride of two pixels. Correspondingly, this was followed by batch normalization, ReLU, and average pooling layers. The third convolutional layer (C3) had 32 kernels of size (3×3×16) and the same layer was followed as the previous one. The last convolutional layer (C4) had 32 kernels of size (3×3×32) and was followed by a fully connected layer of two neurons. To reduce overfitting, a dropout layer that performed regularization with a dropout ratio of 20% was used before a fully connected layer. A regression layer was then used to estimate the SBP from the final fully connected layer. The details of the architecture for CNN are presented in Figure 3-5 and Table 3-1.

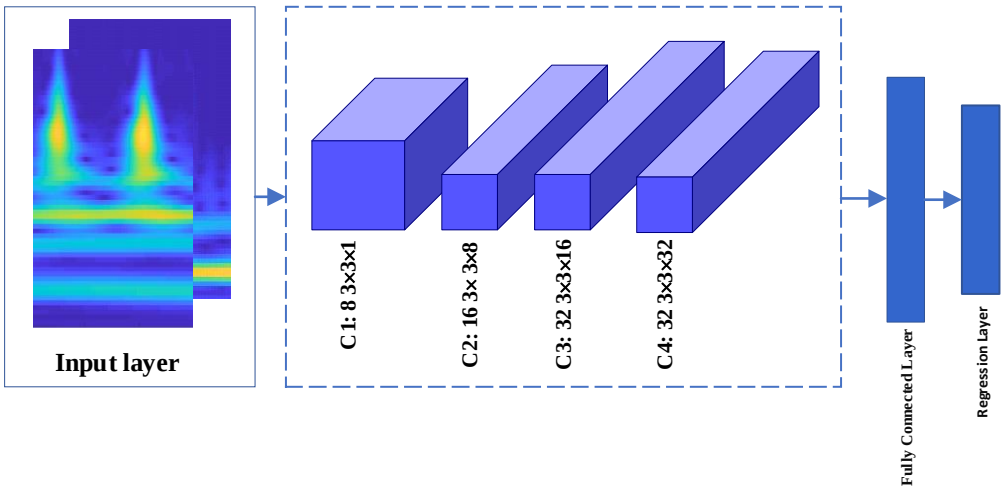

Figure 3-5: Proposed CNN architectures for BP estimation using scalogram

3.6.2 Optimized CNN-based BP Model

To improve the accuracy and decrease network complexity, a simple, yet effective BP measurement method based on optimized CNN architecture is proposed. To optimize the accuracy of the BP measurement and decrease the error rate, a larger database was generated for the second method. As a larger dataset was used for this method, adding more convolutional layers with less stride factor would extract more features for the input data. Increasing unnecessary layers would only lead to overfitting the network and adding more layers beyond a certain threshold would lead to irregularities in the data. A model with few layers cannot learn the regression problem, whereas a model with too

many layers can learn it too well and overfit the training dataset, So using the trial and error method, an extra layer was added to our previous design.

Table 3-2: Details of optimized CNN network architecture with five convolutional layers

	Layers	Size and Definition
1	Image Input	41x125x2
2	Conv_1	8 3x3x3 convolutions with stride [1 1] and padding 'same'
3	Batchnorm_1	Batch normalization with 8 channels
4	Relu_1	ReLU
5	Avegpool_1	2x2 average pooling with stride [2 2] and padding [0 0 0 0]
6	Conv_2	16 3x3x8 convolutions with stride [1 1] and padding 'same'
7	Batchnorm_2	Batch normalization with 16 channels
8	Relu_2	ReLU
9	Avegpool_2	2x2 average pooling with stride [2 2] and padding [0 0 0 0]
10	Conv_3	32 3x3x16 convolutions with stride [1 1] and padding 'same'
11	Batchnorm_3	Batch normalization with 32 channels
12	Relu_3	ReLU
13	Avegpool_3	2x2 average pooling with stride [2 2] and padding [0 0 0 0]
14	Conv_4	32 3x3x32 convolutions with stride [1 1] and padding 'same'
15	Batchnorm_4	Batch normalization with 32 channels
16	Relu_4	ReLU
17	Avegpool_4	2x2 average pooling with stride [2 2] and padding [0 0 0 0]
18	Conv_5	64 3x3x32convolutions with stride [1 1] and padding 'same'
19	Batchnorm_5	Batch normalization with 64 channels
20	Relu_5	ReLU
21	Dropout	20% dropout
22	FC1	2
23	Regression Output	mean-squared-error with response 'Response'

The test and trial technique was performed over a number of layers, kernel size, batch size, and learning rate for hyperparameter optimization in training. The second proposed CNN architecture had

two inputs, ECG and PPG signals, five convolutional layers, the first four layers were the same as in our first design and the last convolutional layer (C5) had 64 kernels of size (3×3×32) and was followed by a fully connected layer of one neuron. The output of these feature extraction convolutional layers went into a fully connected layer with one neuron. Finally, the fully connected layer was connected to a regression layer to address the regression problem of the design. To reduce the overfitting, a dropout layer that performed regularization with a dropout ratio of 20% was used before the fully connected layer. A regression layer was then used to estimate the SBP from the final fully connected layer. The details of the architecture for optimized CNN are presented in Figure 3-6 and Table 3-2.

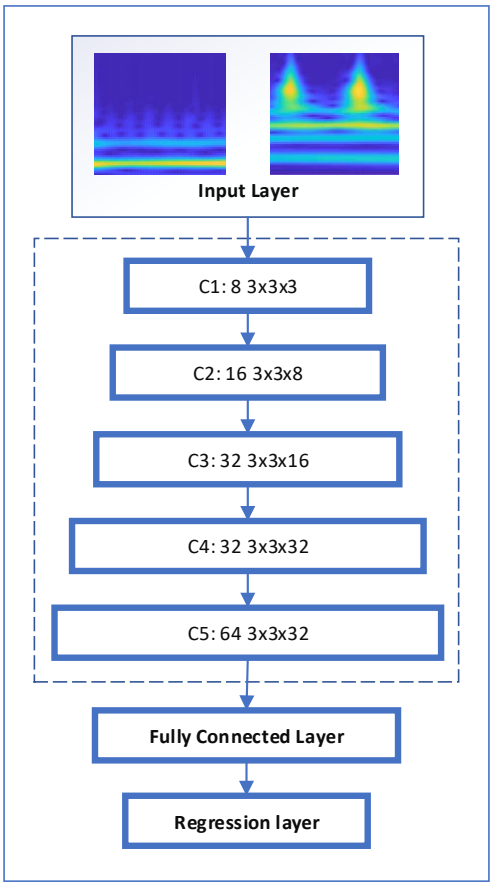

Figure 3-6: Optimized proposed CNN architectures for BP estimation using scalogram

3.7 Model Training and Experimental Results

To evaluate the performance of the proposed model, the dataset was divided into two training and testing sets. The first 70% of the selected dataset was considered for training, and the rest for testing. The CNN model was obtained by training with the Stochastic gradient descent [187] optimizer. In

order to find the best accuracy, five parameters were chosen for learning rate as 0.00005, 0.0001, 0.0005, 0.001, 0.005. The learning rate of 0.001 resulted in higher accuracy among other parameters and a piecewise drop of 0.1 for every epoch was used. The standard gradient descent algorithm updated the network parameters (weights and biases) to minimize the loss function by taking small steps at each iteration in the direction of the negative gradient of the loss (Equation 3-6),

$$\theta_{l+1} = \theta_l - \alpha \nabla E(\theta_l) \qquad (3\text{-}6)$$

In the above equation, l is the iteration number, $\alpha > 0$ is the learning rate, θ is the parameter vector, and $E(\theta)$ is the loss function. In the standard gradient descent algorithm, the gradient of the loss function, $\nabla E(\theta)$, is evaluated using the entire training set, and the standard gradient descent algorithm uses the entire data set at once. By contrast, at each iteration, the Stochastic gradient descent algorithm evaluates the gradient and updates the parameters using a subset of the training data.

The training process was conducted with 30 epochs, as higher value results in longer training time without any changes in performance. A mini-batch size of 60 was used empirically as for values lower than 60; the performance dropped down. Two experiments were then performed with three different datasets, as explained to illustrate our testing results. Table 3-3 presents the results of the first proposed CNN against the first two databases.

This study defines the accuracy evaluation index for the regression model of BP estimation, as shown in Equation (3-7), where x represents the number of correct estimations and y represents the total number of model estimations.

$$\text{Accuracy} = 100 * \frac{\text{Number of correct estimation}}{\text{Total number of testing data}} \qquad (3\text{-}7)$$

Moreover, the RMSE obtained from Equation (3-8) was used as an indicator for evaluating the performance of the estimation model.

$$\text{RMSE} = \sqrt{\frac{\sum(x_i - y_i)^2}{n}} \qquad (3\text{-}8)$$

where x_i is the estimated BP, y_i is the actual value, and n is the total number of values in the testing dataset.

Table 3-3: Comparison of two datasets for the first CNN model

Number of Images	RMSE for SBP (mmHg)	Accuracy (%)	Number of Subjects
500 RGB images	6.51	84.32	22
400 RGB images	7.79	82.76	22

Aiming to achieve the best generalization, less error, and meeting the BP standards requirements, the size of the database increased significantly. Consequently, the proposed CNN architecture was modified to improve the accuracy of BP monitoring. The second proposed network validated against all three datasets, and the results are shown in Table 3-4.

Table 3-4: Comparison of Three datasets for optimized CNN model

Number of Images	RMSE for SBP (mmHg)	Accuracy (%)	Number of Subjects
400 RGB images	7.79	82.76	22
500 RGB images	5.43	87.42	22
50400 RGB images	3.21	90.05	120

The results showed that the first, second, and third databases achieved a high accuracy of 82.27%, 87.42%, and 90.05%, respectively. Experimental results indicated that the RMSE of 7.79 mmHg for the first method, 5.43 mmHg for the second and 3.21 mmHg for the third database were achieved. The results confirm a larger database and modified CNN structure performed with the highest accuracy and the least error rate. These results were achieved without performing any complicated feature extraction or pre-processing techniques.

3.8 Comparison and Discussion

The experimental results demonstrated a low error rate with high accuracy, confirming that the proposed CNN models are suitable and feasible where the features are not immediately apparent or difficult to extract.

Also, the experimental results of the proposed automated features extraction models were compared with traditional works in the literature that used engineered feature extraction techniques. Looking at individual related papers, Mishra et al. [188] used ECG and PPG signals with the PTT approach and reported the RMSE of 11 for SBP. Yoon et al. [189] achieved lower error but used a small amount of data. Nidigattu et al. [190] employed extensive signal processing and feature engineering. The authors extracted a total of 39 features from the time domain and six features from frequency and then normalized the features before training their models. They employed three types of machine learning methods to estimate the BP and calculated the RMSE for SBP. They used data related to 140 individual healthy subjects of just over three minutes as their database. It is reported that the RMSE of 5.86 mmHg, 9.50 mmHg, and 10.30 mmHg were calculated for the random forest, support vector machine, and k-nearest neighbours respectively. Su et al. [191] used a modern LSTM with the PTT approach and achieved the lowest error rates among the other studies.

Table 3-5: Comparison with well-established related work concerning dataset size, RMSE, and the use of engineered features

Model	Number of subjects	RMSE for SBP (mmHg)	Engineered Features
PTT (Pulse Transit Time) [188]	32 healthy subjects	11	Yes
Pulse wave analysis (PWA) and pulse arrival time (PAT) [189]	MIMIC, 23 subjects	10.6	Yes
Three types of machine learning [190]	140 healthy subjects	5.86, 9.50,10.30	Yes
PTT approach [191]	84	3.73	Yes
Optimized CNN with the third dataset	120	3.21	No

The performance obtained from the proposed CWT+CNN method compared with other studies in this field are given in Table 3-5. The accuracy of the proposed automated features extraction method was compared with the studies using engineered features extraction. The main concern of this comparison is to show the improvement of the proposed method without using the features extraction phase in terms of RMSE. The first column indicates the method that used to estimate the SBP and the following column illustrates the number of subjects, and error rate, where the last column shows the use of engineered feature extraction. The proposed CNN model was tested and trained with 50400 scalogram images. These RGB images were obtained by applying CWT to ECG and PPG signals of 120 subjects from the MIMIC III database. From Table 3-5, it is clear that the proposed CNN-based-SBP estimation model showed the least errors in comparison to the other methods. The comparison demonstrates that the CNN model outperforms other traditional algorithms.

The results of the proposed CNN-based model confirm that this method does not need any manual features extraction and can produce a learning model. It can perform the feature phase itself and get rid of the dependence on designing features. It also can overcome the limitations of traditional methods relying on expert experience in signal processing. Moreover, eliminating the features extraction phase decreases the complexity of the measurement. Overall, the proposed model achieves competitive accuracy, reliability, and ease of implementation.

4 CHAPTER 4 Blood Pressure Measurement Using Time Series of ECG and PPG Signals and Deep Learning Networks

4.1 Introduction

Extracting BP-related features can often be a complicated task since the ECG and PPG signals could easily be influenced by motion artifacts, drugs, illness, and other external influencers. Thus, employing a model to extract related features automatically instead of designing features is necessary. This chapter aims to develop an accurate continuous BP estimation model based on the correlation between PTT and BP. To ensure that all critical points of the ECG and PPG signals were included in each sample of the training dataset, a series of pre-processing steps were performed before feeding the collected signals to a deep learning network. The two most promising deep learning BP estimation models are proposed to estimate the SBP and DBP using time series of ECG and PPG signals. Incipiently, the CNN-based model is designed and validated with the time series dataset. Then an optimized LSTM-based model is proposed and validated with the same dataset. Finally, a comparison between each proposed method is provided. Material discussed in this chapter has been previously published [192].

4.2 Database

The MIMIC III database described in *Chapter 3*, with 120 subjects were used to evaluate the performance of the proposed model in the current chapter. Moreover, the performance of proposed BP models in both chapters compared with the same database. A total of 50,400 cardiac cycles were extracted from 120 patients, equal to 14 hours of training data for each required signal. This data included 420 samples of the ECG, PPG, SBP, and DBP individually for each patient.

4.3 Pulse Transit Time Approach to BP Estimation

As described in *Chapter 2*, the relationship between BP and PTT has been well studied [193, 194], and PTT is recognized as a valid and well-accepted method for measuring BP [195, 196]. PTT has been used to develop wearable devices for continuous BP measurement as it can be estimated from

ECG and PPG signals conveniently [197]. Moreover, due to the simplicity of this method, it can be used for a wide range of patients regardless of age or their underlying conditions.

The relationship between BP and PWV was first theoretically validated by Moens and Korteweg [198]. PTT is related to PWV, and both have demonstrated an indirect relationship with BP [8]. The PTT-based method uses a more straightforward design for BP measuring devices and solves the drawback of lack of comfort for the patient in long-term monitoring. The Moens–Korteweg equation defines PWV as a function of the vessel and fluid characteristics (Equation 4-1):

$$PWV = \frac{L}{PTT} = \sqrt{\frac{Eh}{\rho D}} \qquad (4\text{-}1)$$

where L is the vessel length, PTT is the time that a pressure pulse takes to propagate through the length of the vessel, E is the elasticity of the artery, h is the wall thickness of arterial, ρ is the blood density, and D is the artery diameter [79].

Hughes [199] proposed a theoretical model that describes the close relationship between BP and the elasticity of the artery E as shown below in Equation (4-2):

$$E = E_0\, e^{\gamma P} \qquad (4\text{-}2)$$

where $E_0$is Young's modulus for zero pressure of the vessel wall, γ is the vessel parameter, and P is the BP value. Using Equations (4-1) and (4-2), a close correlation between PTT and BP is clear.

4.4 Pre-processing and R-peak Detection

As the main objective of this study was to eliminate feature extraction techniques, it was essential to ensure that all key points related to the PTT features were available in each segmented cardiac cycle. For this purpose, the R-peak of ECG signals was detected after the pre-processing step. Using the detected index, the length of each cardiac cycle centred on R-peaks was calculated. The same approach was taken to align all the samples, and the same length as the cardiac cycle was used to resample the PPG and BP signals.

To perform an accurate measurement, the ECG signal (considered to be the most important component in BP estimation) needs to be presented as cleanly and clearly as possible. Therefore, the

first step was to pre-process the ECG signals, then analyze the ECG signal to locate R-peaks on the ECG waves. These peaks were then used as the centre point for resampling the cardiac intervals. The following procedure was utilized to pre-process the ECG signal and resample the ECG and the PPG, with the aim to include all the PTT related points in each cardiac cycle.

4.4.1 Baseline Wander Removal

Generally, baseline wandering is the noise artifacts that affect ECG signals. The source of these artifacts is often respiration and usually lies between 0.15 and 0.2 Hz. To reduce the irregularities in beat morphology, the removal of baseline wander is necessary [200]. In this study, the baseline wander of the ECG waveform was eliminated by shifting the signal baseline, aiming to represent the correct amplitude. To remove the trend, a low order polynomial was fitted to the signal and the polynomial was used to detrend it. An example of an ECG signal before and after detrending is shown in Figure 4-1.

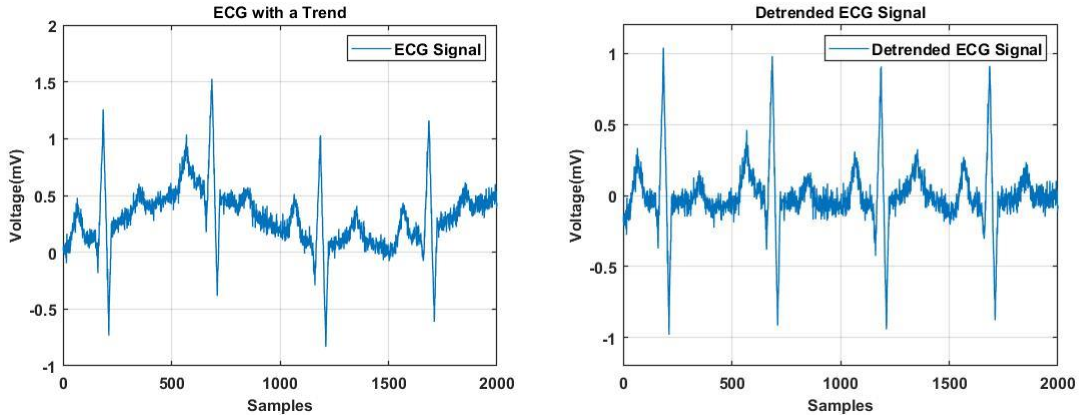

Figure 4-1: A sample of the original and the de-trended ECG signal

4.4.2 Denoising

ECG signals are often noisy due to random body movements, poor contact of electrodes, and electrical activities of other muscles in the body [201]. Generally, the ECG signal can be buried in noise which can result in the detection of unwanted peaks. Accordingly, the ECG signal must be de-noised and presented as a clear waveform before peak detection. However, standard filters cannot remove the noise sufficiently, as ECG is a non-stationary signal [202].

There are several methods used for de-noising signals, including wavelet transform [203-205], Savitzky-Golay filtering [206, 207], and adaptive filtering [208]. In this study, the Savitzky-Golay filtering was used to remove the ECG signal noise as it has previously shown better performance compared with other commonly used de-noising methods [201]. This method is based on a local least-squares polynomial approximation which was firstly proposed by Savitzky and Golay [209]. To implement the Savitzky-Golay smoothing filter, the sgolayfilt function in MATLAB was utilized. This function computes the smoothing polynomial coefficients, delays the alignment, and performs the transit effects at the start and end of the data record. An example of a noisy and denoised ECG signal is shown in Figure 4-2.

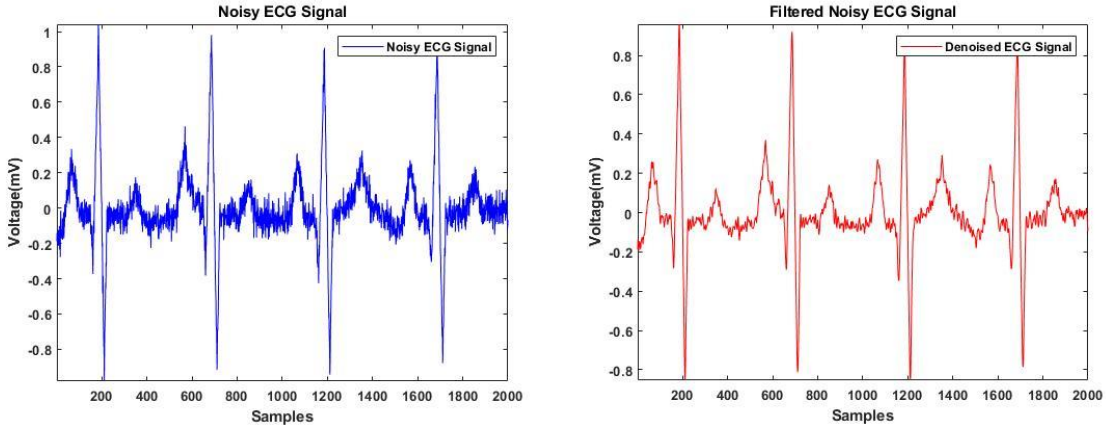

Figure 4-2: sample of noisy and de-noised ECG signal using the Savitzky-Golay smoothing filter

4.4.3 Peak Detection

In this study, the thresholding method was selected for peak detection. To optimize signal amplitude changes and reduce peak detection error, the ECG and PPG signals were normalized based on their corresponding value range. The R-peak of ECG signals was detected by thresholding peaks above 0.5 mV. Moreover, to avoid detecting unwanted peaks, the minimum peak distance was set by 125 samples, which was equal to one cardiac cycle in this study. The indexes related to the R-peak were used to resample the cardiac cycle (centred on the R-peak) and aimed to include all the PTT-related points. In order to align the ECG, PPG and BP signals in the same length, the calculated length of the ECG cardiac cycle was used to time-synchronize the corresponding PPG and BP. Figure 4-3 illustrates a sample of peak detection for a subject.

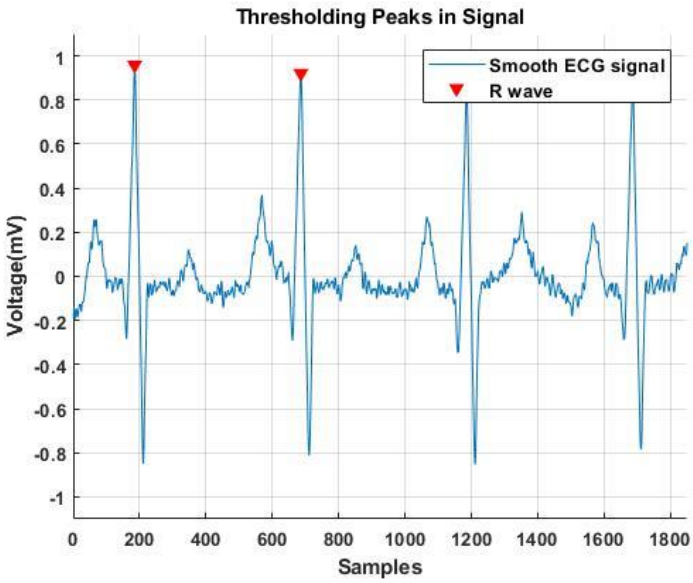

Figure 4-3: A sample of R-wave detection

The proposed pseudo-code of the whole process is presented in Figure 4-4.

Pseudo Code for Peak Detection

1: Detrend the ECG signal by removing the baseline wander
2: Denoised the ECG signal using Savitzky-Golay filtering
3: R-peak detection;

threshold peaks above 0.5 mV
set 'MinPeakHeight' to 0.5
set 'MinPeakDistance' to 125
use logical indexing to find the locations of the R waves
find the related index
store index to an array

4: Resample the ECG Signal based on the index of R-peak
5: Find the corresponding PPG and BP signal

Figure 4-4: Pseudo Code for Peak Detection

4.5 CNN Model for BP Estimation

The same optimized CNN architecture from *Chapter 3* was used for this experiment. The proposed CNN architecture had five convolutional layers which were the core of the network, followed by a fully connected layer with two neurons and a regression layer to address the regression problem. The last two layers were developed for calculating the SBP and DBP. Overfitting is a common problem for a network with high variance. To reduce the overfitting of the training data and improve the performance of the network, a regularization layer with a dropout ratio of 20% was considered before the fully connected layer.

The model has been tested and trained with time series of ECG and PPG signals that were obtained after pre-processing steps in section 4-4. As explained in section 4-4, to include all the critical points of signals related to PTT, the entire database was resampled and time-synchronized based on the R-peak of the ECG signal. The database was included a total of 420 samples of ECG, PPG, SBP, and DBP that collected individually from 120 subjects from the MIMIC III database. A total of 50,400 cardiac cycles for each signal was utilized as CNN input. Each cardiac cycle was a vector of 1×125 dimension. The details of the proposed architecture for an optimized CNN are presented in Figure 4-5 and Table 4-1.

Table 4-1: CNN architecture of the proposed model with time series of the ECG and PPG signal as input data

	Layer	Size and Definition
1	Conv_1	8 3x3x1 convolutions with stride [1 1] and padding 'same'
2	Batchnorm_1	Batch normalization with 8 channels
3	Relu_1	ReLU
4	Avegpool_1	2x2 average pooling with stride [2 2] and padding [0 0 0 0]
5	Conv_2	16 3x3x8 convolutions with stride [1 1] and padding 'same'
6	Batchnorm_2	Batch normalization with 16 channels
7	Relu_2	ReLU
8	Avegpool_2	2x2 average pooling with stride [2 2] and padding [0 0 0 0]
9	Conv_3	32 3x3x16 convolutions with stride [1 1] and padding 'same'

10	Batchnorm_3	Batch normalization with 32 channels
11	Relu_3	ReLU
12	Avegpool_3	2x2 average pooling with stride [2 2] and padding [0 0 0 0]
13	Conv_4	32 3x3x32 convolutions with stride [1 1] and padding 'same'
14	Batchnorm_4	Batch normalization with 32 channels
15	Relu_4	ReLU
16	Avegpool_4	2x2 average pooling with stride [2 2] and padding [0 0 0 0]
17	Conv_5	64 3x3x32 convolutions with stride [1 1] and padding 'same'
18	Batchnorm_5	Batch normalization with 64 channels
19	Relu_5	ReLU
20	Dropout	20% dropout
21	FC1	2
22	Regression Output	mean-squared-error with response' Response'

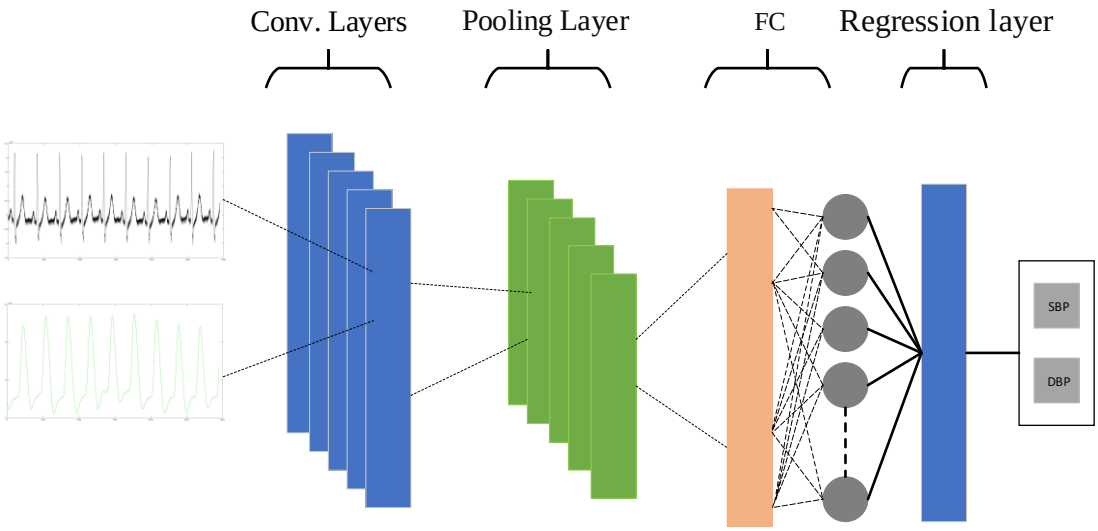

(a)

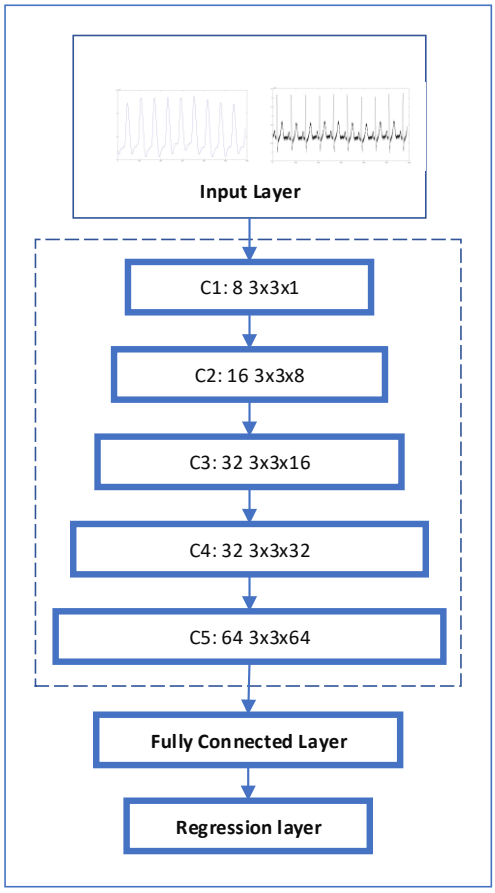

(b)

Figure 4-5: (a) CNN structure (b) CNN layers

4.5.1 Experimental Results and Comparison

The performance of the proposed CNN for cuff-less BP measurement using PTT and ECG was evaluated and compared with the actual SBP and DBP from the MIMIC III database. The dataset was divided into training and testing set by subject to avoid an abnormally high prediction accuracy. The data relating to the first 70% of subjects were selected to train and the remaining data were used for testing the network. Stochastic gradient descent with an initial learning rate of 0.001 was used, and a piecewise drop of 0.1 for every epoch was considered. The training process was conducted with 30 epochs as a higher value results in a longer training time without any performance changes. A mini-batch size of 60 was used as the experiment showed that at a value lower than 60, it not only didn't enhance better results but also reduced the performance. The RMSE was used as an evaluation metric and the training progress shows how RMSE decreased in both training and validation with an increase

in the number of iterations. Figure 4-6 showed the training progress in terms of RMSE and loss per iteration. The RSME and loss function results show that this model was working accurately.

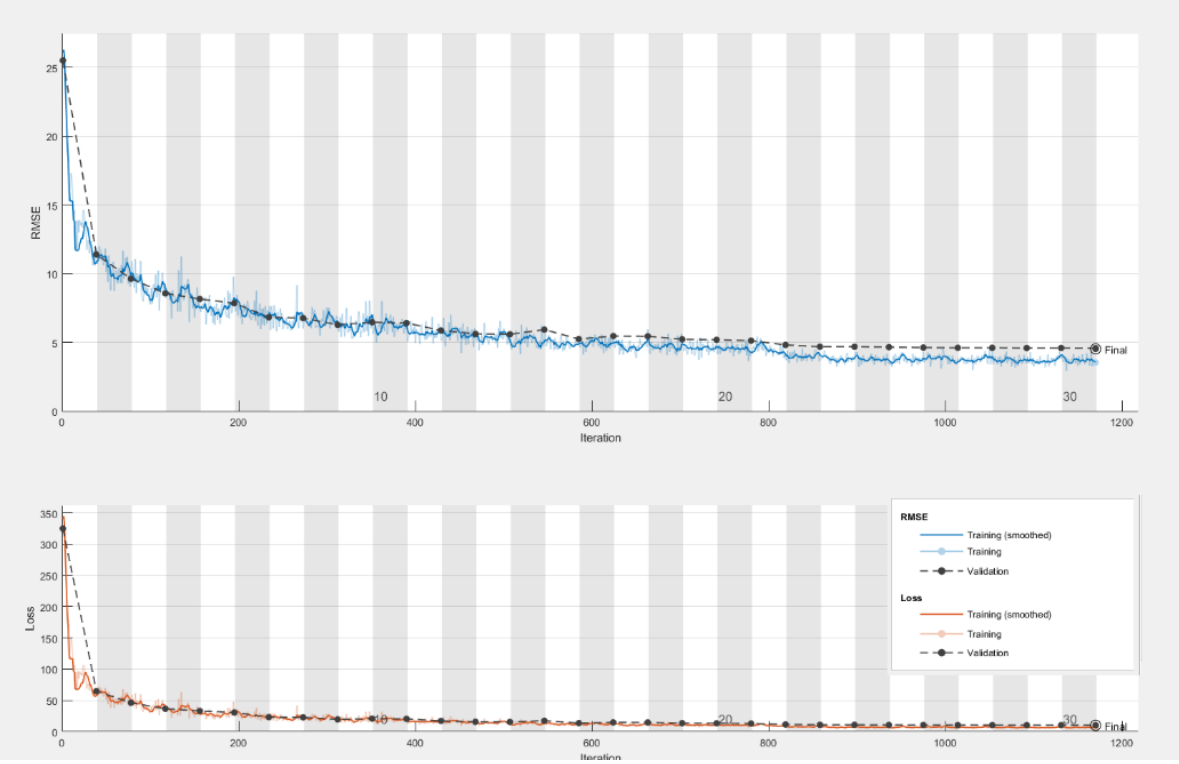

Figure 4-6: Training loss and accuracy at every iteration

Moreover, the performance of the proposed method for SBP and DBP estimation against the reference SBP and DBP are shown in Figure 4-7. A reasonable correlation has been illustrated between the majority of the points and the reference BP.

The performance of the proposed network using the ECG and PPG signals was evaluated based on the accuracy of the network on the testing dataset. For this purpose, the number of correct estimations within the acceptable error margin $\leq$ 5mmHg set by AAMI standard was calculated. The accuracy was calculated using Equation (3-7) from *Chapter 3*. The accuracy of 92.43% and 87.31% is achieved for SBP and DBP estimation by the proposed method, respectively.

Moreover, to ascertain the accuracy of the model, the difference between the model estimated BP values and the actual BP values were computed. This difference was referred to as model error, as it

reflects how well the model fits the experimental data for each experimental setting. The model error values for all subjects were computed using RMSE as described in Equation (3-8) in C*hapter 3*.

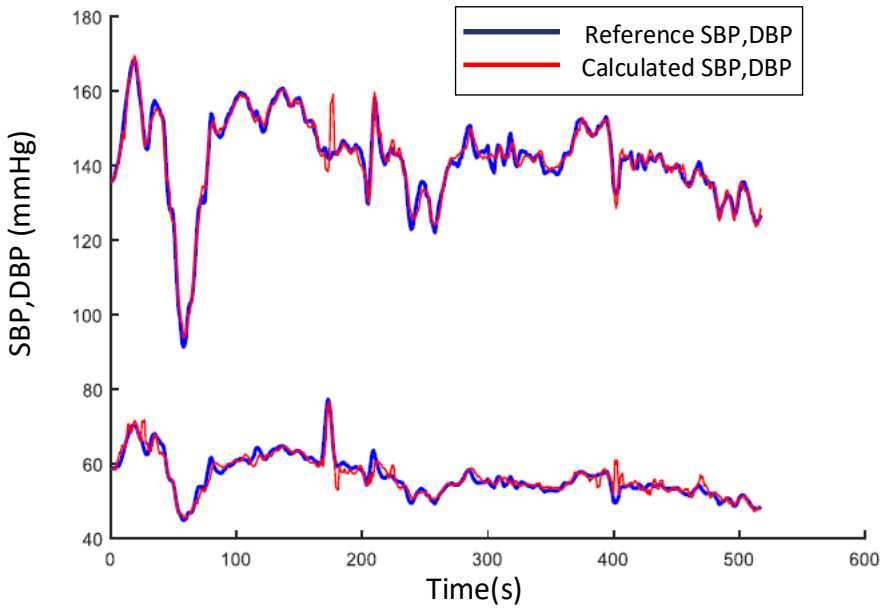

Figure 4-7: Systolic (up) and Diastolic (down) BP calculated from time series of signals

For SBP, the RMSE of 3.21 mmHg reduced to 3.02 mmHg compared to the proposed model in *Chapter 3*. Moreover, the RMSE of 6.52 mmHg was calculated for DBP. The results confirmed that PTT features are important for the improvement of BP estimation and for decreasing errors in determining BP.

4.6 Long Short-term Memory Model for BP Estimation

To demonstrate the proposed CNN regression-based method's superiority, a long short-term memory (LSTM) network is also used to estimate the SBP and DBP with the same database. The LSTM is one of the most promising networks in the field of time series data estimations.

LSTM is a type of recurrent neural network (RNN) design, which has demonstrated remarkable healthcare applications performance. LSTM was utilized by Chauhan and Vig [210] to detect arrhythmia in ECG signals with no requirement for prior information about abnormalities or handcrafted features. An LSTM-based network was used by Tan et al. [211] to classify normal and

coronary artery disease from the ECG signal. Lo et al. [212] proposed an LSTM-based network to estimate BP from ECG and PPG signals. Similarly, Zhao et al. [213] and Tanveer et al. [214] utilized LSTM-based networks to estimate BP.

LSTM was first introduced by Hochreiter and Schmidhuber in 1997 [215]. The primary goal of LSTM development was to overcome the vanishing gradient issues that occur with RNNs during long-term processing. The overall structure of the LSTM model can be subdivided into three stages (also known as gates), namely an input, output, and forget gate. The input gate controls the degree of long-term-memory input to the most recent memory. The output gate controls the impact of short-term memory on long-term memory. The forget gate is used to bypass some selective information. Due to the gate structure, the LSTM can memorize and exhibit better processing time-series performance.

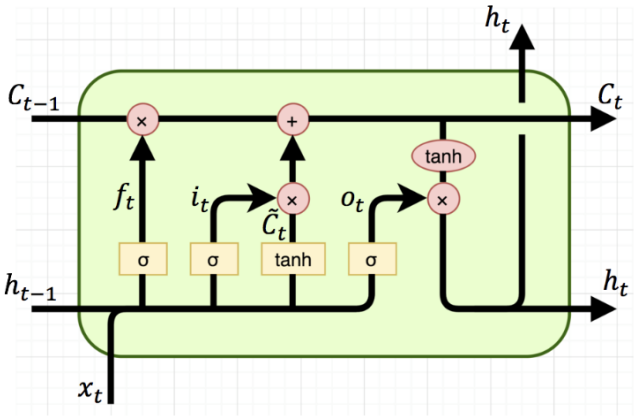

Figure 4-8: Structure of an LSTM cell [216]

The overall structure of the LSTM is shown in Figure 4-8. Where x_t is the input vector, C_{t-1} is a memory from the previous block, h_{t-1} is output from the previous block, C_t is a memory from the current block, h_t is the output of the current block and f_t, i_t, o_t are the calculation methods of the forgetting gate, the input gate, and the output gate, respectively.

4.6.1 Proposed LSTM Network Design

The accuracy of BP estimation could be increased by considering the time-domain variations of relevant features. LSTM has shown promising results in the modelling of complex time series [214].

Following the success of Su et al. [191] in increasing the BP estimation accuracy using LSTM, an LSTM-based BP estimation model for comparative purposes was employed in this study.

This Network is included of an input layer, an LSTM layers, a fully connected layer, and a regression output layer. LSTM hidden layers are chosen to be 128 units and two fully connected layers of size two. The same database, as explained in *Section 4.2*, was used to evaluate the LSTM network design. The training data was fed into the LSTM layer in the form of a 125× 1 vector for each sample. The output vector y_t was calculated as:

$$h_t = \vartheta(x_t, c_{t-1}, h_{t-1}) \quad (4\text{-}3)$$

$$y_t = \sigma W_y h_t + b_y \quad (4\text{-}4)$$

where x_t and $y_t$refer to the input and output in the state *t*, respectively, c_t represents the cell vector while h_t refers to the hidden vector, σ is the logistic sigmoid function, *W* terms denote weight matrices, the *b* denote bias vectors, and ϑ is the operator of the hidden layer. The equations of the LSTM memory cell ϑ can be generalized as follows:

$$i_t = \sigma\,(W_i.[x_t, h_{t-1}] + b_i) \quad 4\text{-}5)$$

$$f_t = \sigma\,(W_f.[x_t, h_{t-1}] + b_f) \quad (4\text{-}6)$$

$$o_t = \sigma\,(W_o.[x_t, h_{t-1}] + b_o) \quad (4\text{-}7)$$

$$\widetilde{c_t} = tanh\,(W_c.[x_t, h_{t-1}] + b_c) \quad (4\text{-}8)$$

$$c_t = (\widetilde{c_t} \times i_t + c_{t-1} \times f_t) \quad (4\text{-}9)$$

$$h_t = tanh\,(c_t) \times o_t \quad (4\text{-}10)$$

where i_t represents the input gate equation, f_t refers to the forget gate equation, and o_t represents the output gate equation. The input gate indicates the amount of information needing to be kept, the forget gate indicates the previous information needs to be removed, and the output gate determines the amount of information needing to become output in the next step. The data was then fed into a fully

connected layer and a regression layer after passing through the LSTM layers to predict SBP and DBP.

4.6.2 Experimental Results and Comparison

The performance of the proposed LSTM with the same database as described in *Section 4-2* was evaluated. The dataset from 120 different subjects was divided into training (70%, 84 subjects) and test (30%, 36 subjects) to train and test the LSTM. The network was trained for 60 epochs with a minibatch size of 30 using the Stochastic gradient solver with a learning rate of 0.001. The effectiveness of the proposed network was addressed by computing the RSME between the estimated SBP and DBP and the ground truth. The model error values for all subjects were computed using RMSE as described in Equation (3-8) in *Chapter 3*. The RSME of 18.90 mmHg and 26.69 mmHg was calculated for SBP and DBP, respectively. These findings did not fit within the AAMI error of margin.

4.7 Comparison and Discussion

A comparison between the performance of the proposed CNN and LSTM, which were trained and tested with the same database in terms of RMSE, is given in Table 4-2.

Table 4-2: Evaluation of the best performing algorithm for SBP and DBP estimations

Model	RMSE of SBP (mmHg)	RMSE of DBP (mmHg)
CNN model	3.02	5.22
LSTM model	18.90	22.69

The results of the LSTM-based BP model were compared with the results of the CNN-based model based on the RSME values. The lower value of RSME indicates that the proposed CNN-based outperformed the LSTM-based model. This may be because the CNN-based model could extract better BP-related features than the LSTM-based model.

Table 4-3 summarizes a comparison between the CNN-based model employed in this study and other well-established related works by the same investigators. In general, comparing findings across different studies in this field is difficult due to the use of different evaluation metrics. Therefore, only the studies utilizing RSME metrics were chosen for comparison. The first column shows the BP

estimation model used and the following columns report the number of patients, SBP error rate, and DBP error rate. The last column indicates the use of engineered feature extraction.

Table 4-3: Comparison of the proposed method with well-established related work in terms of methodology, dataset, estimation error and use of engineered features

Method Used	Number of subjects	RMSE for SBP (mmHg)	RSME for DBP (mmHg)	Engineered Feature extraction
PTT, linear regression [188]	32 healthy subjects	5.16	5.36	Yes
Random forest, SVM, KNN [190]	140 healthy subjects	5.86, 9.50,10.30	5.30, 8.30, 8.25	Yes
Autoregressive moving average (ARMA) models [217]	15 subjects	6.49	4.33	Yes
PTT, LSTM [191]	84	3.73	2.43	Yes
Our work	120	3.02	5.22	No

Mishra et al. [188] used ECG and PPG signals with a PTT approach and reported an RMSE of 5.16 and 5.36 for SBP and DBP, respectively. Nidigattu et al. [190] employed extensive signal processing and feature engineering. The authors extracted a total of 39 features from the time domain and six features from frequency and then normalized the features before training their models. They employed three types of machine learning methods to estimate the BP and calculated the RMSE for SBP. They used data from 140 individual healthy subjects just over 3 minutes as their database. They reported RMSE calculations of 5.86 mmHg, 9.50 mmHg, and 10.30 mmHg for the random forest, support vector machine, and k-nearest neighbours respectively. In [217] Zadi et al. showed the calculation of systolic and diastolic BP from PPG measurements using a viable method for continuous and non-invasive measurement of BP, however, using a very small dataset (15 subjects only). Su et al. [191] used a modern LSTM with the PTT approach and achieved the lowest error compared with the other studies. However, the authors did not split their train and test data based on subjects. The data relating to a subject used in the training set might be used in the testing set, which results in abnormally high BP measurement accuracy. The CNN model used in the current study achieved results comparable to Su et al. [191]. Even though eliminating the complex engineered features extraction approach and

choosing training and testing dataset based on the subjects, suggesting that our proposed method is well suited to BP measurement Table 4-3.

4.8 Conclusion

In this chapter, we proposed two cuff-less and continuous BP measurement methods using deep learning networks and PTT-based methods on selected patients from the MIMIC III database. The CNN model performed better when compared with the LSTM model. The results showed that CNN could be trained simultaneously with several patients' data. More importantly, the results showed that the estimated SBP and DBP were highly correlated with the actual SBP and DBP. Therefore, the proposed approach shows promise as a potential method for increasing the accuracy of BP measurement from ECG and PPG signals. It achieved a low error rate and an acceptable regression coefficient. Moreover, as the proposed network learns to extract the related features from ECG and PPG signals intelligently, signal pre-processing and complex engineering feature extraction will eventually not be required, which will decrease the complexity of the model, and improve the processing time.

5 CHAPTER 5 Blood Pressure Measurement Using Features Extraction Techniques

5.1 Introduction

Although different deep learning-based methods with promising results have been proposed in previous chapters, this chapter intends to suggest how to improve BP estimation accuracy to a higher level. In this manner, two different models are proposed, aiming to find the best approach for BP measurement. Since previous studies have shown that machine learning-based BP regression models work well with manual features extraction, firstly, an SVR-based BP measurement was conducted to estimate BP. In order to train the proposed SVR model, a set of features that commonly used across previous studies was selected.

Secondly, a novel hybrid system that combines our optimized CNN model with the SVR model is proposed where CNN is used as a trainable feature extractor and SVR used as the regression operator. We demonstrated that a hybrid CNN-SVR model could effectively exploit feature interactions from feed-forward directions to learn more in-depth features of ECG and PPG signals and their corresponding SBP and DBP. The proposed hybrid CNN-SVR model for BP measurement is considered the first hybrid CNN-SVR model in the known literature.

5.2 Database

This chapter aims to set a comparison between the experimental results of our previous proposed methods and the proposal in this current chapter. To do so, the MIMIC III database described in *Chapter 3* was used to evaluate the performance of the proposed model in the current chapter. The Database includes the information of 120 patients, which consists of 420 samples of the ECG, PPG, SBP, and DBP data for each patient. A total of 50,400 cardiac cycles were extracted from these 120 patients, equal to 14 hours of training data for each signal.

5.3 Features Selection

Among all existing signals, ECG and PPG signals are the most fundamental signals that are employed to calculate BP. To enhance the accepted accuracy of the BP estimation model, it is

necessary to select the useful features and accurately extract the related features from ECG and PPG signals. Based on the best performance of recent studies, a total of 11 BP-related features, including HR, PTT, and characteristics of PPG waveforms, were carefully chosen from those studies. The definition of all selected features is given in Table 5-1.

Table 5-1: Definitions of selected features

Features	Definition
f_1: HR	The time distance between two R_R intervals
f_2: PTT peak	The time distance between ECG R peak and the peak of simultaneously PPG
f_3: PTT foot	The time distance between ECG R peak and the bottom of simultaneously PPG
f_4: PIR	The ratio of PPG peak to PPG bottom
f_5: T1	The time delay between the systolic and diastolic peak
f_6: DT	Diastolic time
f_7: ST	Systolic time
f_8: T_s	Time from cycle start to systolic PPG peak
f_9: T_d	Time from systolic PPG peak to cycle end
f_{10}: AI	Augmentation Index
f_{11}: LAF	Large artery stiffness

5.3.1 Heart Rate (HR)

Heart rate (HR) is holding the peripheral resistance and cardiac output at a constant level, as well as affecting the stroke volume. The acceleration of HR, due to the shortened diastolic, causes the reduction of blood flows in the peripheral blood vessels while increasing the blood flows to the aorta. These changes result in increasing both SBP and DBP and vice versa [218]. In this study, the HR is calculated as the interval of the two neighbouring ECG R-waves.

5.3.2 PTT's Features

The close relationship of the PTT with the BP values was described in *Chapter 2* through the Moens-Korteweg equation. Two different PTT features were considered by calculating the time between the R-peak of the ECG signal and the specific point of PPG evaluated in each cardiac cycle.

As illustrated in Figure 5-1, the PTT peak was defined as the distance between the R-peak of the ECG signal and the PPG peak, while the PTT foot was defined as the distance between the R-peak of the ECG signal and the PPG foot point.

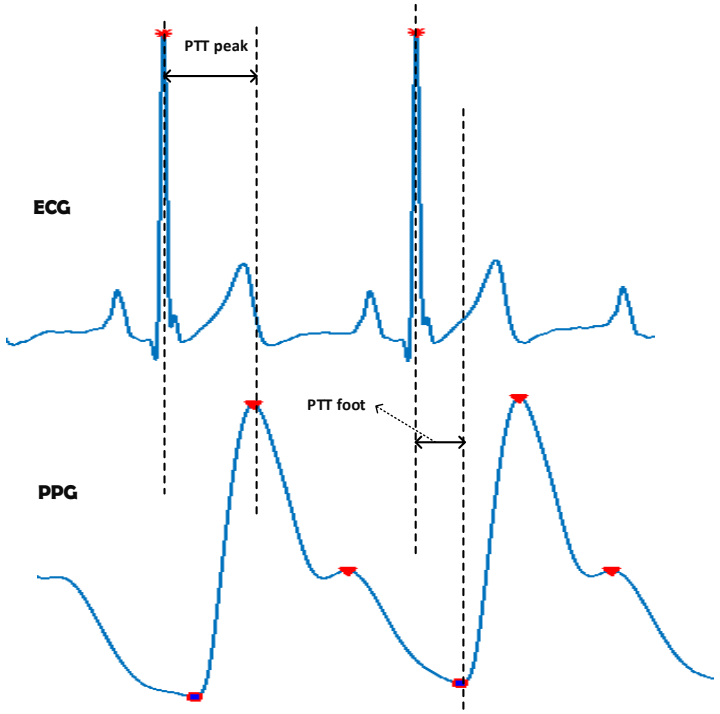

Figure 5-1: The PTT peak is the distance between the R-peak of the ECG signal and the PPG peak, and the PTT foot is the distance between the R-peak of the ECG signal and the PPG foot

All systolic peaks are inevitably located between two subsequent R-peaks as the PTT peak interval starts from the R-peak of the ECG signal and it ends up on the peak of the PPG signal of the same cardiac cycle. To search the location of its maximum point, the algorithm analyzes each portion of the PPG signal between two consecutive R peaks. The maxima and minima detection routines were implemented for each cardiac cycle to locate the PPG systolic peaks and feet. All the maximum and minimum points in the PPG signal were detected, as shown in Figure 5-2.

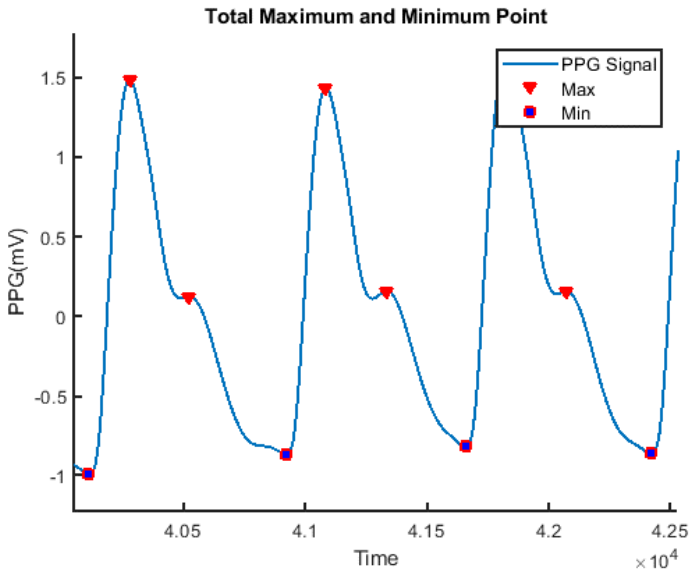

Figure 5-2: Maximum and minimum points of the PPG signal

All the maxima and minima point of the PPG signal can be identified in very noisy areas of the signal or correspondence of non-physiological wave benefits to the simplicity of the detection algorithm.

5.3.3 PPG Characteristic Points

In this study, to find an optimal characteristic point of the PPG signal for estimating SBP and DBP, several features including systolic time (ST), diastolic time (DT), large artery stiffness index (LAF), PPG peak intensity ratio (PIR), augmentation index (AI), and the time delay between the systolic and diastolic peak (T1) were extracted. The extracted features are defined below:

- Systolic Time (ST), as shown in Figure 5-3, ST is described as a relative time from PPG foot to PPG peak, which also presents the whole cardiac output changes [219].

- Diastolic Time (DT), as shown in Figure 5-3, DT is defined as the relative time for PPG peak to PPG foot which changes with peripheral resistance [219].

- Large Artery Stiffness index (LAF) is the time interval between the systolic peak and diastolic peak, which measures arterial stiffness [220].

- PIR is the ratio of PPG peak intensity to PPG bottom intensity, reflecting arterial vasomotion [87]. These changes can be observed in terms of PIR regarding arterial diameter changes with peripheral resistance and blood volume. The arterial diameter change Δd is theoretically reflected by PIR during one cardiac cycle from systole to diastole. The PIR is derived from Equation (5-1).

$$PIR = e^{\alpha \Delta d} \qquad (5\text{-}1)$$

where α is a constant related to the optical absorption coefficients in the light path.

- Augmentation Index (AI), as illustrated in Figure 5-3, is defined as the ratio of the diastolic peak and systolic peak, which measure the arteries wave reflection using Equation (5-2) [220].

$$AI = \frac{x}{y} \qquad (5\text{-}2)$$

- The time delay between the systolic and diastolic peak (T1), as shown in Figure 5-3, is the systolic and diastolic peaks which are two maxima of the signal. In each PPG wave, the systolic peak is the absolute maximum, whereas the diastolic peak is the relative one. As all filtered systolic and diastolic peaks are detected, the T1 can be simply calculated.

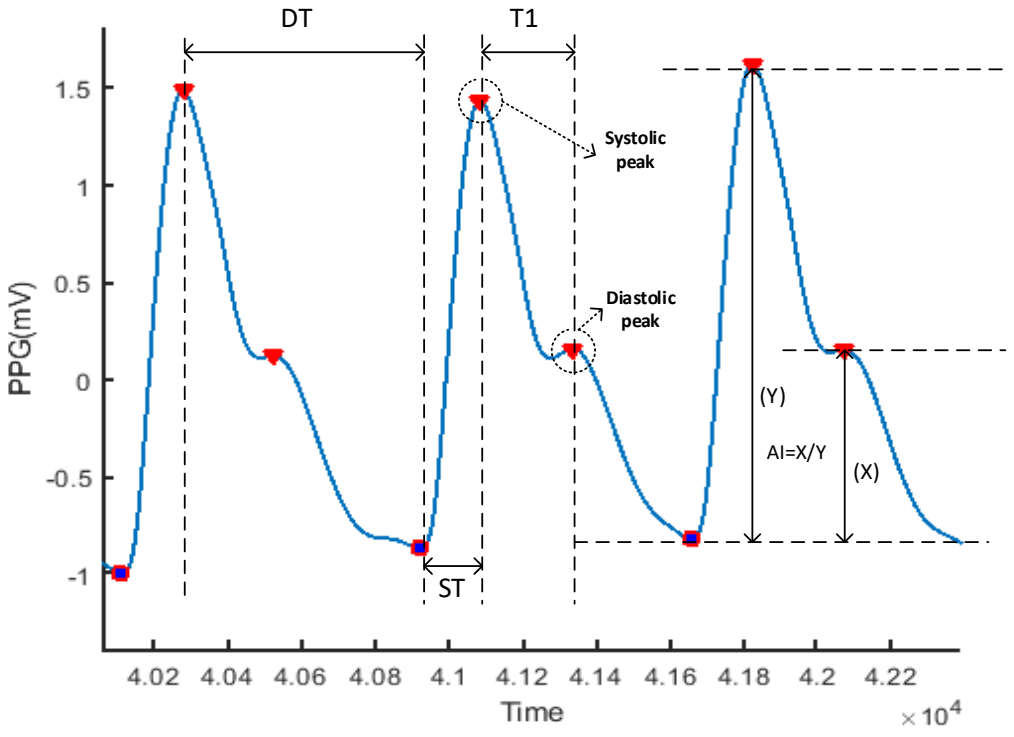

Figure 5-3: The schematic diagram of PPG Characteristic features

5.4 SVR Model

Different models can be used to solve classification, regression, and abnormality detection problems. A support vector machine (SVM) is one method that can overcome these problems. An SVM encompasses a range of different models divided into linear not-separable vector machines, linear separable SVMs, and non-linear SVMs. Using the Kernel function, which is detailed in *Section 5.4.1*, the non-linear SVM converts linearly non-separable problems into linearly separable problems, from low dimensional space to high-dimensional space. The SVM algorithm works for both classifications as well as for regression applications. The regression or the function approximation version of SVM is referred to as support vector machine regression (SVR) [221].

The SVR model's main idea is to map the input space into a high-dimensional feature space by non-linear mapping and then linearly solving nonlinear problems [221]. The power of this model to deal with the non-linear relationship of input and output data makes it suitable to address the non-linear relation between the features extracted from ECG and PPG signals and the actual BP. Therefore, an

SVR model using complex characteristics of the human physiological index, which was explained in *Section 5.3.3* is proposed to predict SBP and DBP.

5.4.1 Kernel Function Selection

In some cases, the data is not linearly separable in the original, so the kernel function is used to map the projection of input space to a higher dimension where a linear separation is feasible. The goal is that after the transformation to the higher dimensional space, the classes are now linearly separable in this higher dimensional feature space. Therefore, support vector machine models can use the kernel function $K(x, x')$ to establish a non-linear support machine. Different kernel functions produce different algorithms for mapping the data into different dimensional spaces. The polynomial kernel functions, Gaussian Radial Basis Function (RBF), and sigmoid kernel function are the most common kernel functions at present [5].

In this study, the RBF kernel was adopted in the SVR algorithm by mapping the original feature space $x = (PTT, HR, \dots)$ onto the new feature space $x' = (x_1, x_2, x_3, \dots x_n)$. Therefore, the new set of the BP indicator data was expressed by a linear regression formula in the feature space to determine a nonlinear mapping model between ECG and PPG signals and BP. The SVR model did not establish based on a polynomial kernel function and a sigmoid kernel function. The polynomial SVR model needs a prolonged parameter optimization process to convergence, and the sigmoid SVM model has fast parameter optimization, but the predictions are poor. Moreover, fewer parameters are required for the RBF kernel than the polynomial kernel; the number of parameters can contribute to the complexity of the overall system.

5.4.2 Description of Proposed SVR

SVR has a unique ability to solve the nonlinear regression problem. The nonlinear mapping $\varphi(x)$ mapped the input sample x into a high-dimensional feature space and then estimated the regression function through a linear model built in this feature space. The main idea was to use non-linear mapping to map the input space onto a high-dimensional feature space. The non-linear model is shown in Equation (5-3) :

$$f(x, \omega) = \omega \cdot \varphi(x) + b \qquad (5\text{-}3)$$

where $x = (PTT, HR, \dots), \omega$ is the weight vector, and b is the threshold. The ω and b can be obtained through the following optimization Equation (5-4).

$$\min \frac{1}{2} \| \omega \|^2 + c \sum_{i=1}^{1} (\xi_i + \xi_i^*), \qquad (5\text{-}4)$$

is subject to:

$$y_i - (\omega^T x_i + b) < \varepsilon + \xi_i$$

$$(\omega^T x_i + b) - y_i < \varepsilon + \xi_i^*$$

$$\xi_i + \xi_i^* \geq 0$$

where C is a penalty factor, ε is the loss function, and ξ_i and ξ_i^* are different relaxation factors. The solution of Equation (5-3) is as follows:

$$f(x) = \sum_i^l (-\alpha_i + \alpha_i^*) K(x_i, x) + b, \qquad (5\text{-}5)$$

where α_i and α_i^* are Lagrange multipliers, l is the number of SVs, and $K(x_i, x)$ is a kernel function.

After comparing different kernel functions, the RBF kernel was chosen to be used in this study. Unlike the linear kernel, the RBF kernel transforms the database into a non-linear high dimensional space, making it possible to overcome the non-linear relationship between features and BP. Also, compare with the polynomial kernel, it has less model complexity due to fewer tuning parameters. The RBF is shown as Equation (5-6) :

$$K(x_i, x) = \exp(-\gamma \| x - x_i \|^2) \qquad (5\text{-}6)$$

where γ is the kernel parameter. The kernel parameter, gamma (γ), can adjust the influence of a training sample. The larger value will decrease under the influence of the training sample.

Considering Equations (5-4) and (5-6), selecting the proper value for C(penalty factor), gamma(γ), and ε (loss function) can effectively increase the accuracy of the SVR model. The C Parameter can balance the prediction error in the training set [222]. Additionally, a smaller C makes the decision surface smoother, whereas a larger C allows the model more freedom to use more samples as support

vectors so that all the training samples can be accurately classified or predicted. A larger Gamma, γ, has less influence on the training sample.

5.4.3 SVR BP Model

The features described in *Section 5-1*, including HR, PTT features, and PPG features, were extracted and combined using the dataset from *Chapter 3*. These features were used to train and test the SVR model. To evaluate the SVR method, the database was split into training and testing; 70% of the subjects were selected for training and 30% of the rest for the testing dataset.

To establish an SVR model to predict the SBP and DBP using the optimal parameters C and γ, the parameters were set to (100, 10) for C , (100, 10) for γ , and [0.01,1] for ε. These values were chosen based on the promising results achieved by Zhang et al. [223], which were achieved by the optimization function created on 10-fold cross-validation. The proposed SVR model was implemented in the MATLAB environment.

The detailed of SBP and DBP prediction process using the SVR model is shown in Figure 5-4. After extraction and combination of features, the data was divided into training and test set. Then the SVR model was established based on the optimal parameter of RBF kernel (C, γ, ε), and then the training dataset was used to train the SVR model. The testing dataset was fed to a trained network in the next step to estimate the SBP and DBP.

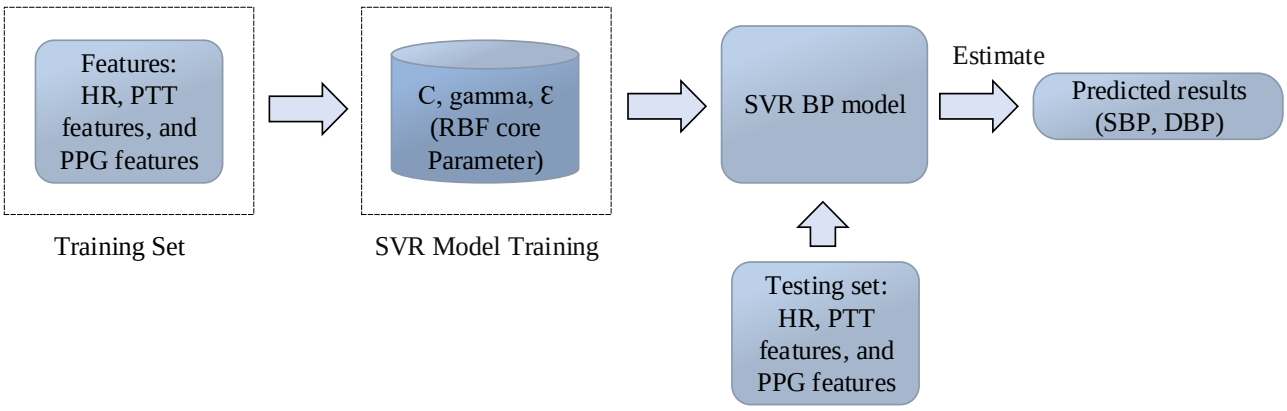

Figure 5-4: Schematic diagram of SBP and DBP estimation using SVR model

The prediction results of SVR model using hand-engineered features were evaluated in terms of accuracy and RMSE. For this purpose, the number of correct estimations within the acceptable error margin ≤ 5mmHg set by AAMI standard was calculated. Equation (3-7) from *Chapter 3* was used to calculate the performance accuracy of the SVR model. The experimental results show that the SVR model reaches an SBP estimation accuracy of 93.52 % and DSB estimation accuracy of 90.12 %.

The RMSE is the difference between the model estimated BP values and the actual BP values were computed. This difference was referred to as model error; it reflects how well the model fits the experimental data for each experimental setting. The model error values for all subjects were computed using RMSE as described in Equation (3-8) in *Chapter 3*. The RMSE of 2.37 mmHg and 4.18 mmHg for SBP and DBP were calculated, respectively.

From the performance evaluation results, it can be confirmed that the SVR model with manual features extraction outperformed the CNN model using the PTT technique (*Chapter 4*) as indicated in Table 5-2.

Table 5-2: The performance of the SVR model with features extraction compared to the CNN model based on the PTT technique

Model	RMSE of SBP (mmHg)	RMSE of DBP (mmHg)	Accuracy of SBP	Accuracy of DBP
SVR	2.37	4.18	93.52	90.12
CNN using PTT technique	3.02	5.22	92.43	87.31

The results indicated that the estimated BP values obtained by the SVR ensemble estimator were closer to the reference SBP and DBP. Therefore, the proposed SVR algorithm offers accurate BP estimates compared with the CNN model from *Chapter 4*. This implies that extracting BP-related features was a critical factor for enhancing the BP model's generalisation ability. Although the SVR model using hand-engineered features achieved better performance than other models without feature extraction, the previous study's main gap remained to be addressed.

5.5 Hybrid CNN-SVR BP Model

The proposed methods described in *Chapter 3*, *Chapter 4*, and the present chapter show significant performance improvement in measuring BP. Nevertheless, there is still room to improve the performance of the proposed models and reduce their complexity. The following method proposed aim to address the main research gap of eliminating complex engineered feature extraction techniques while increasing the performance of the model.

However, the results of our SVR model with manual features extraction show that extracting more BP-related features could improve the accuracy of the BP measurement. Therefore, we propose a hybrid CNN-SVR as a novel BP measurement model. To the best of the author's knowledge, there is no literature on exploiting the benefit of the hybrid architecture of CNN and SVR for BP measurement.

This model employs the optimized CNN model (*Chapter 3*) to extract robust features from the time series of the ECG and PPG signals and present them to the SVR network (*Section 5.4.2*). The three stages of the proposed method are:

Firstly, the time series of the ECG and PPG signals from the dataset in *Chapter 3* are fed into the proposed CNN model for training the CNN network.

Secondly, the CNN network was employed to extract representative features from the time series of ECG and PPG signals.

Finally, the extracted features by the CNN network were applied as input to the SVR for BP estimation. The proposed hybrid CNN-SVR method did not use any engineered feature extraction techniques for the ECG and PPG signals. The proposed model is suitable for wearable monitoring devices and real-time monitoring.

5.5.1 The Architecture of the CNN-SVR Combined Model

The structure of the proposed hybrid CNN-SVR model is shown in Figure 5-5.

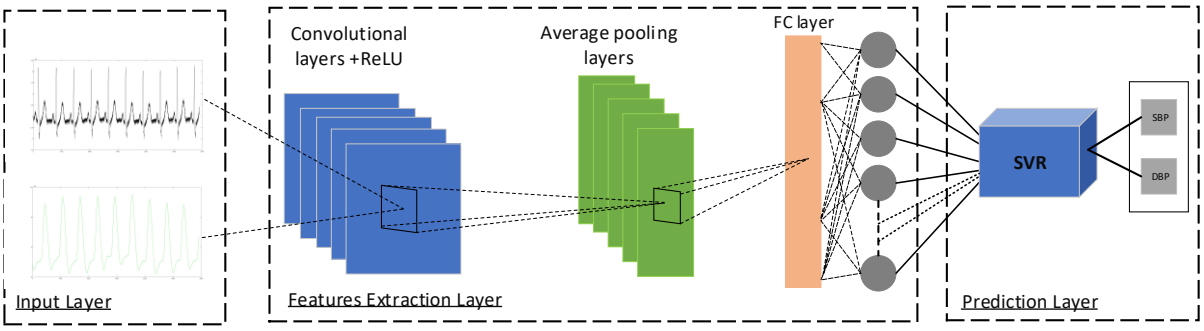

Figure 5-5: Structure of CNN-SVR model

The CNN-based network (as described in *Chapter 3*) includes convolutional layers, pooling layers, fully connected layers, batch normalization, ReLU, and dropout. The last output layer of the proposed CNN is replaced with an SVR model from *Section 5.4.3* to design the hybrid CNN-SVR model.

In the output units of the last layer of the CNN network, there are estimated probabilities for the input samples. An activation function calculates each output probability. The activation function input is the linear combination of the outputs from the previously hidden layer with trainable weights, plus a bias.

For features extraction with CNN, five convolutional layers are used. Each convolutional layer is followed by batch normalization, ReLU, and average pooling layers. Batch normalization can robustly handle overfitting and underfitting problems. To reduce the overfitting, a dropout regularization technique with a dropout ratio of 20% is employed before the fully connected layer.

The last layer in the CNN model is replaced with an SVR with an RBF kernel. Then, the SVR takes the outputs from the hidden layer as a new feature vector for training. Once the SVR is well trained, it carries out the regression step and estimates SBP and DBP with automatically extracted features from CNN. In this case, SVR shows a better ability to handle high dimension regression problems in comparison to the simple linear combination. Furthermore, the combination of CNN and SVR networks can benefit from the advantages of each individual layer and enhance the accuracy of the estimation.

5.5.2 Model Training and Experimental Results

To implement the hybrid CNN-SVR model, firstly, the ECG and PPG signals were fed to the CNN as an input map. After the CNN was well trained with several input maps, the corresponding feature vector can be automatically extracted for each input map. An activation function calculates each output probability. The activation function input is the linear combination of the previously hidden outputs with trainable weights, plus a bias term. Looking at the hidden layer's output values is meaningless but only makes sense to the CNN network itself; however, these values can be treated as features for any other classifiers. Then, the SVR replaced the last layer and took the CNN outputs as a new feature vector for training. Once the SVR has been well trained, the well-trained SVR performed the regression task to predict the SBP and DBP. The implementation of the proposed hybrid CNN-SVR is shown in Figure 5-6.

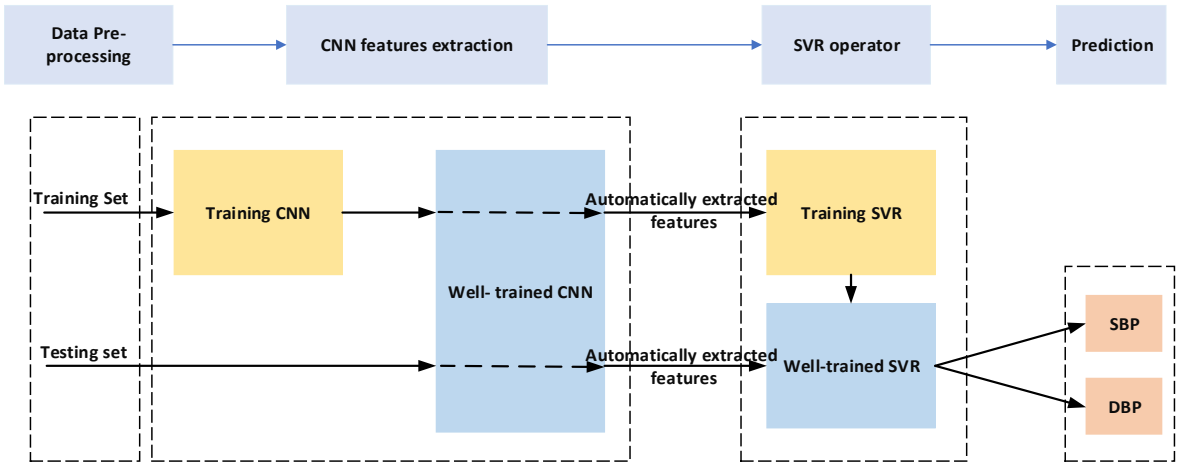

Figure 5-6: Implementation process of the Hybrid CNN-SVR model

To evaluate the feasibility of the hybrid CNN-SVR model for BP measurement, the data related to 70% of the selected subjects from MIMIC III database (*Section 5.2*) were assigned to the training samples and the rest were assigned to the test samples to prevent overlapping the subjects of the training set with that of in the test set. The CNN network of the CNN-SVR combined model trained with the Stochastic gradient descent [187] optimizer with an initial learning rate of 0.001 and a piecewise drop of 0.1 for every epoch was considered. The training process was conducted with 30 epochs, as a higher value results in longer training time without any changes in performance. Results

of a series of experiments showed that a mini-batch size of 60 should be used in the experiment as a value lower than 60, neither enhanced the results nor improved the performance accuracy.

For the SVR of the hybrid CNN-SVR model, the SVR model was adopted from *Section 5.4.3* and radial basis kernel function (RBF). To establish an SVR model to predict the SBP and DBP using the optimal parameters C and γ, the parameters were set to (100, 10) for C and (100, 10) for γ.

5.5.2.1 Accuracy Performance

To evaluate the BP estimation accuracy of the proposed method, three measurement methods were selected. They included accuracy as shown in (**Error! Reference source not found.**), RMSE as shown in Equation (5-8), the total mean absolute error (MAE) as shown in Equation (5-9), and total standard deviation error (STD) as shown in Equation (5-10), was calculated as evaluation metrics. The following equations defined these three measurements.

$$\text{Accuracy } = 100 * \frac{\text{Number of correct estimation}}{\text{Total number of testing data}} \qquad 5\text{-}7)$$

$$RMSE = \sqrt{\frac{\sum_{i=1}^{n}(x_i - y_i)}{n}} \qquad (5\text{-}8)$$

$$MAE = \frac{\sum_{i=1}^{n}|x_i - y_i|}{n} \qquad (5\text{-}9)$$

$$STE = \sqrt{\frac{\sum_{i=1}^{n}(x_i - y_i - ME)^2}{n-1}} \qquad (5\text{-}10)$$

Subject to:

$$ME = \frac{\sum_{i=1}^{n}(x_i - y_i)}{n}$$

where ME is the mean error x_i is the estimated BP, y_i is the actual value, and n is the total number of values in the testing data.

Figure 5-7 shows the average results of the actual and the predicted SBP and DBP for all patients. It is shown that the hybrid CNN-SVR model for SBP and DBP estimation generates values close to the actual values, with the highest estimation accuracy among all proposed methods.

The proposed model achieved an estimation error of 1.23±2.45 mmHg for SBP and 3.08 ± 5.67 for DBP, which would also pass the AAMI standard criteria. Moreover, the RMSE of 1.89 mmHg and 3.91 mmHg for SBP and DBP respectively, were calculated using hybrid CNN-SVR. It was found that, the hybrid CNN-SVR model's training time is 344 minutes, and the testing time is 0.1673 seconds.

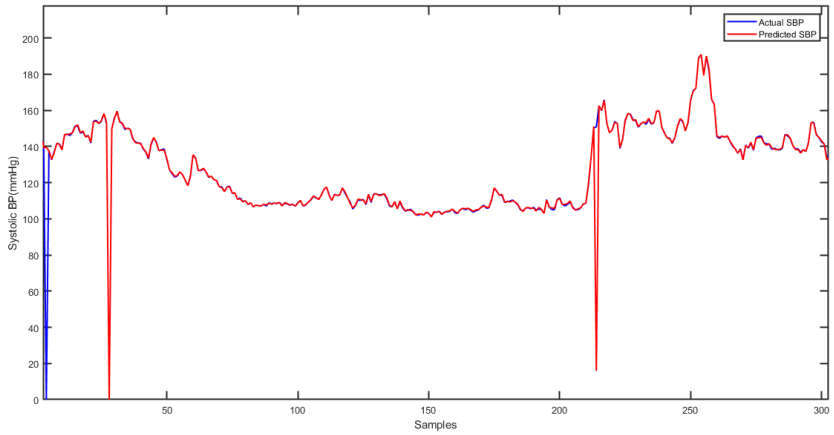

(a)

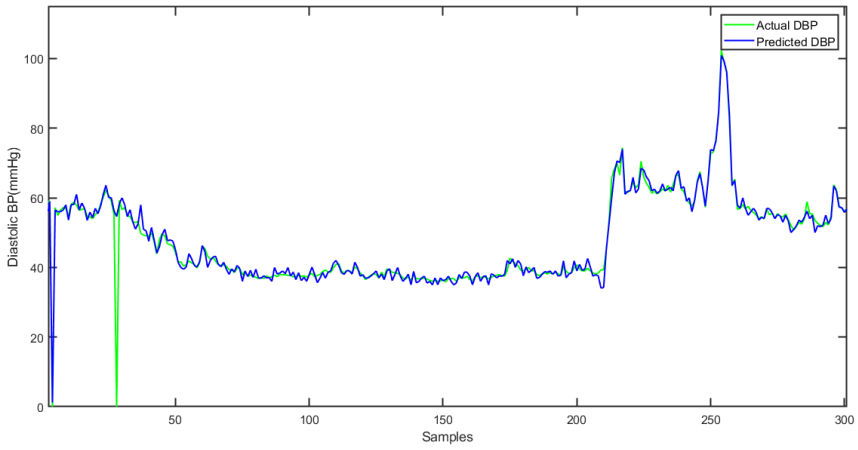

(b)

Figure 5-7: Comparison between predicted and actual (a) SBP; (b) DBP

Table 5-3 indicates that our novel hybrid CNN-SVR model achieved lower RMSE on the testing data than the SVR model. It shows that the regression performance and generalization ability of CNN are better improved by combined with the SVR model.

Table 5-3: Performance comparison of the SVR model and hybrid CNN-SVR model

Model	RMSE of SBP (mmHg)	RMSE of DBP (mmHg)
Hybrid CNN-SVR	1.89	3.91
SVR	2.37	4.18

Table 5-4 shows the results of the hybrid CNN-SVR model against the AAMI standard. The AAMI standard requires a study population of at least 85 subjects; this study included 120 subjects for evaluating the results. Also, the AAMI requires a mean error of less than 5mmHg for non-invasive BP measurement and standard devotion error of more than 8 mmHg. It can be seen from Table 5-4 that the hybrid CNN-SVR model fully satisfies the AAMI criteria for non-invasive and continuous SBP and DBP measurement.

Table 5-4: Performance evaluation based on the AAMI standard

		Mean Error	Standard Deviation	Subjects
AAMI standard	SB, DBP	≤5(mmHg)	≤8 (mmHg)	≥ 85
Hybrid CNN-SVR Model	SBP	1.23	2.45	120
	DBP	3.08	5.67	

As shown in Table 5-5, there are two calculation results. This is because the proposed CNN-SVR algorithm consists of two stages: one is the model's training stage, and the other is the testing stage of the model. The above one is a combination of CNN and CWT, using ECG and PPG signals' scalograms to train the CNN model parameters. The below one is to extract the feature using the trained CNN model as a feature extractor and then input the extracted representative features into the SVR for BP estimation. As shown in Table 5-5, the accuracy of CNN+CWT is 90.05 %; the accuracy of hybrid CNN-SVR has increased to 96.83 %. The training time of the CWT+CNN model is 874 minutes, and the training time of the hybrid CNN-SVR is 344 minutes, as the CWT part is removed. Therefore, although the proposed hybrid CNN-SVR method adds an SVR part based on CNN, the

training time was decreased. In terms of the test time, the proposed CWT+CNN method needs 78 seconds. The hybrid CNN-SVR test time is 0.01673 seconds, which is also obviously better than the proposed CWT+CNN model in Chapter 3. The test time reduction is of great significance for the proposed method using to estimate the BP from time series of ECG and PPG signals.

Table 5-5: *A comparison results of proposed CWT+CNN and proposed hybrid CNN-SVR*

Model	RMSE of SBP (mmHg)	RMSE of DBP (mmHg)	Accuracy of SBP	Accuracy of DBP	Training Time (m)	Testing Time (s)
CWT+CNN	3.21	-	90.05	-	874	78
Hybrid CNN-SVR	1.89	3.91	96.83	92.47	344	0.1673

5.5.2.2 Comparison Results with Related Work

A comparison between the performance of the proposed CNN-SVR BP model and the related work is shown in Table 5-6. To achieve a fair comparison, the studies that reported their results with the same evaluation metric and database were considered in this study. The proposed study using the combination of CNN and SVR to predict BP achieved better performance in comparison with the selected studies. The MAE for SBP was significantly lower, and the MAE for both SBP and DBP were within the AAMI standard criteria.

Regarding using a feature extraction technique, Kachuee et al. [224], Slapničar et al. [225], Chen et al. [149], Khalid et al. [226], Ertuğrul et al. [227], and Wang et al. [228] proposed a feature extraction-based technique to estimate BP. Although some of these studies reported acceptable results [149, 226] [227] [228], they still used various time consuming and complex feature extraction techniques. Among these studies, only two papers [229] [230] used the CNN technique without features extraction. However, the error results and the number of subjects is not within the required BP standard. Another CNN-based model [230] was chosen for this comparison used a sufficient number of subjects for the experiment. Nevertheless, this method used the calibration technique, and the error margin is not acceptable by BP standard.

Table 5-6: *Comparison of hybrid CNN-SVR BP model performance with other works in terms of methodology, database, use of engineered features, and estimation error*

Model	Number of Subjects	Engineered Feature extraction	SBP Error (mmHg)	DBP Error (mmHg)
Classical ML[224]	MIMIC II, 1000 subjects	Yes	MAE:11.17	MAE:5.35
ResNet [225]	MIMIC III, 510 subjects	Yes	MAE:9.43	MAE:6.88
GA-SVR [149]	MIMIC III, 772 set waveforms	Yes	MAE: 3.27	MAE: 1.16
Regression tree [226]	Queensland, 32 subjects	Yes	MAE: 4.82	MAE: 3.25
ELM [227]	MIMIC II, 4254 records	Yes	MAE: 4.25	MAE: 3.95
ANN [228]	MIMIC II, 90 subjects	Yes	MAE: 4.02	MAE: 2.27
CNN [229]	Unspecified, 62 Subjects	No	MAE: 9.61	MAE: 6.73
CNN [230]	MIMIC II, 379	No	MAE: 9.30	MAE: 5.12
Hybrid CNN-SVR	MIMIC III, 120 subjects	No	MAE: 1.23	MAE: 3.08

Looking at individual related works in Table 5-6, Kachuee et al. [224] proposed a method that employs pre-processed physiological features and machine learning model using the PTT approach and calibration. The database divided into training and test set based on the number of subjects, where they showed a promising result according to the British Hypertension Society (BHS). Slapničar et al. [225] used the deep-learning spectro-temporal ResNet and a large dataset to estimate the BP. The PPG

features used to train and test the proposed model and divided based on the number of subjects achieved reasonable accuracy; however, just the PPG signal used to estimate the BP.

Chen et al. [149] used the SVR model and fourteen features from ECG and PPG signals to estimate the BP. The accuracy of BP estimation increased significantly. The database was randomly divided into training and test set, which might cause the overlapping of the subjects in the training and testing datasets. Khalid et al. [226] employed three PPG features to train and test different machine learning algorithms aiming to find the best model to estimate BP. A small database used to evaluate the models; the training data included the old subjects while the test dataset included young subjects. Although the proposed model achieved promising results, the study is limited to 32 subjects and hand-engineered PPG features. Ertuğrul et al. [227] proposed extreme learning machines (ELM) model using the time-frequency domain and statistical features. The results were within the standard criteria, but they used very small amount of data (only five subjects) and the training and testing database divided randomly. In [228], Wang et al. conducted the BP estimation using ANN and multitaper method (MTM) to extract the BP-related features. However, the database randomly split into training and testing dataset.

The hybrid CNN-SVR BP model proposed in the study was estimated with higher accuracy and least error while avoiding overlapping the subjects of the training set with that of the test set by dividing them based on the number of subjects. The proposed hybrid CNN-SVR BP model is the first CNN and SVR combination that targets BP estimation to the best of our knowledge. This novel hybrid model fills the research gaps by utilizing CNN that can extract robust features automatically instated of design and calculate them and provide them to the SVR model. Then, SVR reconstructs the non-linear relationship between the in-depth features extracted by CNN and BP.

In sum, the proposed hybrid CNN-SVR method can be easily applied to a hand-held device for the following reasons:

1) It is possible to estimate BP values using a short or long database. The results of this study using different database lengths as explained in section 3-3 were confirmed that the proposed method can process both small and big database. The acceptable results were achieved using a database that included 22 subjects with 200 samples and 120 subjects with 50400 samples for each signal, equal to 14 hours of data related to ECG, PPG, SBP, and DBP.

2) It is possible to combine various inputs such as ECG and PPG signals to utilize the measurable biomedical signal according to the requirement of the measurement devices. For instance, various studies investigated the possibility of measuring BP using pulse oximetry signals [231, 232].

3) The comparison between the proposed CWT+CNN model using scalogram images of ECG and PPG signals and hybrid CNN-SVR using time series of ECG and PPG signals confirms that using raw signal decrease the training and testing time. Moreover, by removing the CWT part the complexity of the model was decreased. Notably, a hand-held device application has the advantage that there is no need for additional equipment or special conditions (synchronization, etc.) for converting signals to images or feature extraction. Moreover, the ECG and PPG signals can be easily measured from mobile device such as smartphone and watch to estimate the BP.

6 CHAPTER 6 Conclusion

6.1 Introduction

The main objective of this thesis was to propose a novel deep learning-based BP measurement model to achieve cuff-less and continuous estimation of BP measurement. This study aimed to develop an accurate BP measurement system that meets the clinical standards and is suitable for real-life monitoring. This research investigated the development of a cuff-less continuous and calibration-free BP estimation tool with unsupervised feature extraction. Moreover, it contributed to the field of knowledge in biomedical by considering the existing challenges, limitations and research gaps that were identified in this study [233].

Different deep learning-based BP models were proposed and evaluated in this study to find the best implementation method. The proposed hybrid CNN-SVR model demonstrated a solution for continuous estimation of BP measurement on consumer wearable devices. This method is suitable for measuring continuous BP and has the benefits of unsupervised feature learning and not requiring constant calibration; these are currently two considerable limitations for commercial estimation of BP measurement devices.

This chapter presents the original and significant contributions achieved through this study, with some suggestions for further research in this area.

6.2 Concluding Remarks

The goals of this study have been achieved by proposing and implementing a method for estimating SBP and DBP with a combination of deep learning and machine learning algorithms. This successfully demonstrates how this model can be used to accurately estimate the SBP and DBP of patients continuously and non-invasively without using the cuff-based technique. Besides, it contributes to the literature by overcoming two considerable limitations of previous studies in this field; hand-engineered features and a regular calibration system.

Two different CNN-based algorithms were proposed and developed, aiming to find an optimized CNN network for BP estimation [167, 168, 234]. To predict the BP and solve the regression problem, the layers of the network were created, and a regression layer was included at the end of the network.

Both models were trained and evaluated with the same database using scalograms of ECG and PPG signals. The scalograms of the ECG and PPG signals were created using CWT. The performance of our optimized CNN network with five convolutional layers achieved a low error rate that falls within the acceptable standards range. It can be concluded that the obtained results are sufficient for many practical medical applications. To the best of our knowledge, the proposed model is the first existing study in the literature that shows the effectiveness of using CWT and CNN to estimate BP.

Furthermore, the network design was extended to decrease network complexity and achieve a simple yet effective performance based on the correlation between PTT and BP. To ensure that all critical points of the ECG and PPG signals are included in each sample of the training dataset, a series of pre-processing steps were performed before the collected signals were fed to the deep learning network. Two different networks were implemented to predict the SBP and DBP. The proposed CNN algorithms were trained with the ECG and PPG signals, and then an optimized LSTM algorithm was trained with the same database. The CNN achieved better performance results than the LSTM. The results demonstrated that CNN could be trained simultaneously with several patients' data. More importantly, the results show that the estimated SBP and DBP are highly correlated with the actual SBP and DBP. Therefore, the proposed approach can be considered as a potential method for increasing the accuracy of BP measurement from the ECG and PPG signals. The proposed model is suitable and feasible for real-life scenarios where the relevant features are not obvious or are difficult to perform. The proposed CNN-based algorithms [235], which trained with ECG and PPG signals, showed less error and greater accuracy than other reported PTT-based technique in the literature.

Subsequently, an SVR-based BP measurement model was conducted aiming to prove that the proposed CNN-based BP measurement model using unsupervised feature extraction could achieve a comparable result to machine learning-based BP regression models with hand-engineered features. The proposed SVR algorithms were trained with a set of features commonly used across previously discussed studies. The results were indicated that the proposed CNN-based BP model achieved results comparable to the SVR model, despite eliminating complex engineered features.

Finally, to improve BP estimation accuracy to a higher level, a novel hybrid system that combines the optimized CNN model with an SVR model was proposed where CNN is used as a trainable feature extractor and SVR performed as the regression operator. We demonstrated that a hybrid CNN-SVR model could effectively exploit feature interactions from feed-forward directions to learn more in-

depth features of ECG and PPG signals and their corresponding SBP and DBP. The proposed hybrid CNN-SVR model for BP measurement consider being the first hybrid CNN-SVR model that exists in the known literature on BP measurement. In terms of MAE ± STD, the model achieves an overall accuracy of 1.23 ± 2.45 mmHg for SBP and 3.08 ± 5.67 for DBP.

6.3 Contributions

The primary research contributions of this thesis are:

- To the best of our knowledge, the use of CWT for obtaining the scalograms of the ECG and PPG signals and applying them to a CNN-based model to estimate BP is a novel approach. The model was validated against three datasets, and the results based on 120 subjects indicated that the proposed model possesses less error compared to the other reported methods. Moreover, it resolves the problem of feature extraction, which requires further signal processing steps.

- Two deep learning models, the optimized CNN model and the LSTM model based on the correlation between PTT and BP, were proposed to find better deep learning architecture for continuous and cuff-less BP estimation. Both models were trained with time series of ECG and PPG signals. The same number of subjects with the same lengths of data were utilized for training the proposed models that were then evaluated using the RMSE metric. The lower value of RSME indicates that the proposed CNN-based model outperforms the LSTM-based model. Therefore, it could be summarized that CNN models can extract better BP-related features compared to LSTM models.

- Different deep learning and machine learning models were proposed, trained, and compared to determine the best performance. Among all the investigated methods, the hybrid CNN-SVR model performed better in estimating the SBP and DBP. The proposed hybrid BP model provides a less complex solution than existing studies, which have estimated SBP and DBP by utilizing CNN and SVR models. In addition, this model is a low-complex model providing many in one solution in an unobtrusive way using two signals and offering a cost-effective, safer and convenient mode of health monitoring in and out of the clinical setting.

- Proposing a novel hybrid CNN-SVR method for continuous and cuff-less BP measurement can be considered as the main contribution of this research. The time series of ECG and PPG signals were input into the optimized CNN model to complete the training of the CNN model. Then the optimized CNN was used as features extractors to extract representative features from ECG and PPG signals. Finally, the extracted feature vectors were input into SVR that used for BP estimation. The proposed method can effectively reduce the CNN's model parameters and estimation time and effectively improve BP estimation accuracy.

- The overall performance of the proposed hybrid model was evaluated with data related to 120 subjects from the MIMIC III database. According to AAMI standard protocol, the ME and SDE between the predicted BP and actual BP were calculated. The measurement error has an ME value no more than 5 mmHg and an SD of less than 8 mmHg, which meet the criteria of the AAMI standard protocol. The proposed model achieved an estimation error of 1.23 ± 2.45 mmHg for SBP and 3.08 ± 5.67 for DBP, all of which comply with AAMI protocol standard criteria. The results confirm that the proposed CNN-SVR method need not any manual feature extraction and signal processing operations on the time series of data during the whole BP estimation process. It can eliminate the dependence on manual feature extraction and overcome the limitations of traditional methods relying on regular calibration. The hybrid CNN-SVR model is the first continuous and cuff-less BP estimation model based on CNN-SVR in the literature.

- The proposed methodology has the capability to estimate DBP and SBP simultaneously from the same network without any need for individual training for each subject. Moreover, the proposed hybrid model could be easily extended and adapted to different types of databases of various sizes, targeting compatibility within the clinical environment.

6.4 Outcome and Benefits

The potential outcome and benefit of this study should include:

- The proposed hybrid model can estimate SBP and DBP simultaneously, with a minimum number of sensors using only ECG and PPG signals. Hence, it offers a safer and potentially

more convenient approach for health monitoring and enables practical usability for real-time analysis, such as with mobile and embedded platforms (wearable devices).

- The development of a hybrid CNN-SVR BP estimation framework eliminates the necessity for training the model for each new user or calibration to maintain measurement accuracy. This makes the proposed methodology more robust for utilization in the healthcare environment.

- The proposed method can be efficiently utilized in a hand-held device application owing to the flexibility of CNN architecture to deal with various inputs such as ECG and PPG signals. Due to its calibration-free and unsupervised feature learning ability from the collected signal, the proposed method has high prospects for application in wearable BP monitoring devices. Moreover, there is no need for a special condition or additional algorithms for feature extraction, making it very cost-effective. Managing and predicting hypertension with a combination of the deep learning method and wearable technology could be a significant step forward in CVD treatment.

- The proposed methods can be employed in wearable and smart devices and integrated with cloud computing technology. The wearable devices could collect signals and information, and then the cloud platforms could process the data using embedded CNN models. So, this model could play a major role in the continuous estimation of BP measurement and early diagnosis of hypertension, consequently leading to a decrease in the rate of morbidity and mortality associated with CVD.

6.5 Future Works

This study may lead to the following future research directions:

- The database used in this study has a sampling rate of 125 Hz, it is expected that with a database with a higher sampling rate, the performance of the model will be improved. However, it should be investigated whether a new BP estimation model structure needs to be developed for a high sampling rate database.

- From a wearable application perspective, the average BP value and age of the subject in the MIMIC III database was higher than the total average of the general public, as this data was obtained from patients in ICU. To improve the performance of this study, further experiments could be conducted using data collected through consultations in clinical environments with medical experts.

- Although the proposed model was evaluated with data collected from clinical settings, the integration of the proposed model into wearable and clinical devices needs to be investigated.

- To further improve the results, the size and diversity of the database could be increased and demographic and clinical data, including age, gender, and height of the subjects that influence BP, could be considered as input information. Moreover, this study could be extended by involving physiological parameters such as respiratory rate and SpO2, aiming to use mobile phone platforms.

- The accuracy of the proposed method could be verified by adopting a standard calibration for long–term monitoring, such as one week, one month, or a few months, as the accuracy of the proposed model's measurements might decrease over longer periods of monitoring.

References

[1] M. J. Banet, Z. Zhou, M. S. Dhillon, R. J. Kopotic, A. S. Terry, and I. H. VISSER, "Vital sign monitor for measuring blood pressure using optical, electrical and pressure waveforms," ed: Google Patents, 2013.

[2] S. S. Lim *et al.*, "A comparative risk assessment of burden of disease and injury attributable to 67 risk factors and risk factor clusters in 21 regions, 1990–2010: a systematic analysis for the global burden of disease study 2010," *The Lancet,* vol. 380, no. 9859, pp. 2224-2260, 2012.

[3] T. G. Pickering, D. Shimbo, and D. Haas, "Ambulatory blood-pressure monitoring," *New England Journal of Medicine,* vol. 354, no. 22, pp. 2368-2374, 2006.

[4] E. Dolan *et al.*, "Superiority of ambulatory over clinic blood pressure measurement in predicting mortality," *Hypertension,* vol. 46, no. 1, pp. 156-161, 2005.

[5] S. R. Group, "A randomized trial of intensive versus standard blood-pressure control," *N Engl J Med,* vol. 2015, no. 373, pp. 2103-2116, 2015.

[6] S. R. Steinhubl, E. D. Muse, P. M. Barrett, and E. J. Topol, "Off the cuff: rebooting blood pressure treatment," *The Lancet,* vol. 388, no. 10046, p. 749, 2016.

[7] Y.-L. Zheng *et al.*, "Unobtrusive sensing and wearable devices for health informatics," *IEEE Transactions on Biomedical Engineering,* vol. 61, no. 5, pp. 1538-1554, 2014.

[8] A. E. Moran *et al.*, "Cost-effectiveness of hypertension therapy according to 2014 guidelines," *New England Journal of Medicine,* vol. 372, no. 5, pp. 447-455, 2015.

[9] G. Cohuet and H. Struijker-Boudier, "Mechanisms of target organ damage caused by hypertension: therapeutic potential," *Pharmacology & Therapeutics,* vol. 111, no. 1, pp. 81-98, 2006.

[10] S. Ahmad, M. Bolic, H. Dajani, V. Groza, I. Batkin, and S. Rajan, "Measurement of heart rate variability using an oscillometric blood pressure monitor," *IEEE Transactions on Instrumentation and Measurement,* vol. 59, no. 10, pp. 2575-2590, 2010.

[11] A. Silvani *et al.*, "Sleep-dependent changes in the coupling between heart period and blood pressure in human subjects," *American Journal of Physiology-Regulatory, Integrative and Comparative Physiology,* vol. 294, no. 5, pp. R1686-R1692, 2008.

[12] S. Ahmad *et al.*, "A Prototype of An Integrated Blood Pressure and Electrocardiogram Device for Multi-Parameter Physiologic Monitoring," in *IEEE Instrumentation and Measurement Technology Conference (I2MTC)*, 2010: IEEE, pp. 1244-1249.

[13] *World Health Organization (WHO)." Global Health Observatory (GHO) data," [Online]. Available : http://www.who.int/mediacentre/factsheets/fs317/en/. [Accessed Aguest 10, 2017].*

[14] M. H. Forouzanfar *et al.*, "Global, regional, and national comparative risk assessment of 79 behavioural, environmental and occupational, and metabolic risks or clusters of risks in 188 countries, 1990–2013: a systematic analysis for the global burden of disease study 2013," *The Lancet,* vol. 386, no. 10010, pp. 2287-2323, 2015.

[15] S. Sidney *et al.*, "Recent trends in cardiovascular mortality in the united states and public health goals," *JAMA Cardiology,* vol. 1, no. 5, pp. 594-599, 2016.

[16] *American Heart Association, "Heart Disease and Stroke Statistics 2017 At-a-Glance," 2017. Available at: http://healthmetrics.heart.org/wp-content/uploads/2017/06/Heart-Disease-and-Stroke-Statistics-2017-ucm_491265.pdf. [Accessed July. 14, 2018].*

[17] *New Zealand Ministry of Health, " Mortality and Demographic data 2015," 2015. [Online]. Available : https://www.health.govt.nz/publication/mortality-2015-data-tables . [Accessed Feb. 23, 2018].*

[18] *New Zealand Ministry of Health, "NZ Health Survey: Annual update of key results," 2014-2015. [Online]. Available: http://www.moh.govt.nz/notebook/nbbooks.nsf/0/997AF4E3AAE9A767CC257F4C007DDD84/$file/annual-update-key-results-2014-15-nzhs-dec15-1.pdf. [Accessed Jan. 23, 2018].*

[19] R. M. McLean, S. Williams, J. I. Mann, J. C. Miller, and W. R. Parnell, "Blood pressure and hypertension in new zealand: results from the 2008/09 adult nutrition survey," *The New Zealand Medical Journal (Online),* vol. 126, no. 1372, 2013. [Online serial]. Available: http://www.nzma.org.nz/journal/read-the-journal/all-issues/2010-2019/2013/vol-126-no-1372/article-mclean. [Accessed Dec.21,2017].

[20] J. J. Rutherford, "Wearable technology," *IEEE Engineering in Medicine and Biology Magazine,* vol. 29, no. 3, pp. 19-24, 2010.

[21] X.-R. Ding *et al.*, "Continuous blood pressure measurement from invasive to unobtrusive: celebration of 200th birth anniversary of carl ludwig," *IEEE Journal of Biomedical and Health Informatics,* vol. 20, no. 6, pp. 1455-1465, 2016.

[22] M. Kachuee, M. M. Kiani, H. Mohammadzade, and M. Shabany, "Cuff-Less High-Accuracy Calibration-Free Blood Pressure Estimation Using Pulse Transit Time," in *IEEE International Symposium on Circuits and Systems (ISCAS)*, 2015: IEEE, pp. 1006-1009.

[23] Y. Li, Z. Wang, L. Zhang, X. Yang, and J. Song, "Characters available in photoplethysmogram for blood pressure estimation: beyond the pulse transit time," *Australasian Physical & Engineering Sciences in Medicine,* vol. 37, no. 2, pp. 367-376, 2014.

[24] E. Monte-Moreno, "Non-invasive estimate of blood glucose and blood pressure from a photoplethysmograph by means of machine learning techniques," *Artificial Intelligence in Medicine,* vol. 53, no. 2, pp. 127-138, 2011.

[25] X. Xing and M. Sun, "Optical blood pressure estimation with photoplethysmography and FFT-based neural networks," *Biomedical Optics Express,* vol. 7, no. 8, pp. 3007-3020, 2016.

[26] J. C. Ruiz-Rodríguez *et al.*, "Innovative continuous non-invasive cuffless blood pressure monitoring based on photoplethysmography technology," *Intensive Care Medicine,* vol. 39, no. 9, pp. 1618-1625, 2013.

[27] S. S. Mousavi, M. Hemmati, M. Charmi, M. Moghadam, M. Firouzmand, and Y. Ghorbani, "Cuff-less blood pressure estimation using only the ECG signal in frequency domain," in *8th International Conference on Computer and Knowledge Engineering (ICCKE)*, 2018: IEEE, pp. 147-152.

[28] S. S. Mousavi, M. Hemmati, M. Charmi, M. Moghadam, M. Firouzmand, and Y. Ghorbani, "Cuff-Less blood pressure estimation using only the ecg signal in frequency domain," in *2018 8th International Conference on Computer and Knowledge Engineering (ICCKE)*, 2018: IEEE, pp. 147-152.

[29] F. Miao *et al.*, "A Novel Continuous Blood Pressure Estimation Approach Based on Data Mining Techniques," *IEEE Journal of Biomedical and Health Informatics,* vol. 21, no. 6, pp. 1730-1740, 2017.

[30] Z.-Q. Zhao, P. Zheng, S.-t. Xu, and X. Wu, "Object detection with deep learning: A review," *IEEE Transactions on Neural Networks and Learning Systems,* vol. 30, no. 11, pp. 3212-3232, 2019.

[31] A. B. Nassif, I. Shahin, I. Attili, M. Azzeh, and K. Shaalan, "Speech recognition using deep neural networks: A systematic review," *IEEE Access,* vol. 7, pp. 19143-19165, 2019.

[32] G. Antipov, M. Baccouche, S.-A. Berrani, and J.-L. Dugelay, "Effective training of convolutional neural networks for face-based gender and age prediction," *Pattern Recognition,* vol. 72, pp. 15-26, 2017.

[33] J. C. Rodrigues *et al.*, "ECG strain pattern in hypertension is associated with myocardial cellular expansion and diffuse interstitial fibrosis: a multi-parametric cardiac magnetic resonance study," *European Heart Journal–Cardiovascular Imaging,* vol. 18, no. 4, pp. 441-450, 2016.

[34] M. Saeki *et al.*, "Left ventricular layer function in hypertension assessed by myocardial strain rate using novel one-beat real-time three-dimensional speckle tracking echocardiography with high volume rates," *Hypertension Research,* vol. 38, no. 8, p. 551, 2015.

[35] A. Madani, R. Arnaout, M. Mofrad, and R. Arnaout, "Fast and accurate view classification of echocardiograms using deep learning," *Digital Medicine,* vol. 1, no. 1, p. 6, 2018.

[36] W. M. van Everdingen *et al.*, "Comparison of strain parameters in dyssynchronous heart failure between speckle tracking echocardiography vendor systems," *Cardiovascular Ultrasound,* vol. 15, no. 1, p. 25, 2017.

[37] "Ministry of Health, "Cardiovascular Disease Risk Assessment and Management for Primary Care, "" *Wellington: Ministry of Health,* 2018.

[38] "World Health Organization (WHO). Cardiovascular diseases (CVDs), [Online]. Available : https://www.who.int/news-room/fact-sheets/detail/hypertension

[39] S. Rastegar, H. GholamHosseini, and A. Lowe, "Non-invasive continuous blood pressure monitoring systems: current and proposed technology issues and challenges," *Physical and Engineering Sciences in Medicine,* vol. 43, no. 1, pp. 11-28, 2020.

[40] A. Wessels and D. Sedmera, "Developmental anatomy of the heart: a tale of mice and man," *Physiological Genomics,* vol. 15, no. 3, pp. 165-176, 2003.

[41] L. Carnevale, A. Celesti, M. Fazio, and M. Villari, "A Big Data Analytics Approach for the Development of Advanced Cardiology Applications," *Information,* vol. 11, no. 2, p. 60, 2020.

[42] A. V. Chobanian *et al.*, "Seventh report of the joint national committee on prevention, detection, evaluation, and treatment of high blood pressure," *Hypertension,* vol. 42, no. 6, pp. 1206-1252, 2003.

[43] J. S. Williams, S. M. Brown, and P. R. Conlin, "Blood-pressure measurement," *N Engl J Med,* vol. 360, no. 5, p. e6, 2009.

[44] "Understanding Blood Pressure Readings," *American Heart Association. [Online],* vol. https://www.heart.org/en/health-topics/high-blood-pressure/understanding-blood-pressure-readings

[45] A. Ostadfar, *Biofluid mechanics: Principles and applications*. Academic Press, 2016.

[46] P. L. Marino and K. M. Sutin, *The ICU book*. Williams & Wilkins Baltimore: , 1998.

[47] M. Antonelli *et al.*, "Hemodynamic monitoring in shock and implications for management," *Intensive Care Medicine,* vol. 33, no. 4, pp. 575-590, 2007.

[48] N. Ghasemzadeh and A. M. Zafari, "A brief journey into the history of the arterial pulse," *Cardiology research and practice,* vol. 2011, 2011.

[49] W. Harvey and G. Whitteridge, *An anatomical disputation concerning the movement of the heart and blood in living creatures*. Blackwell Scientific Publications, 1976.

[50] W. B. Fye, "Disorders of the heartbeat: a historical overview from antiquity to the mid-20th century," *The American Journal of Cardiology,* vol. 72, no. 14, pp. 1055-1070, 1993.

[51] M. Ward and J. A. Langton, "Blood pressure measurement," *Continuing Education in Anaesthesia, Critical Care & Pain,* vol. 7, no. 4, pp. 122-126, 2007.

[52] B. Beate H. McGhee, MN, APN and Elizabeth J. Bridges, Maj, USAF, NC, "Monitoring Arterial Blood Pressure: What You May Not Know," *Crit. Care Nurse,* vol. 22, pp. 60-79, 2002.

[53] T. L. Marek Brzezinski, Martin J. London, "Radial artery cannulation: a comprehensive review of recent anatomic and physiologic investigations," *International Anesthesia Research Society,* vol. 109(6), no. 6, 2009.

[54] H. L. Li-wei, M. Saeed, D. Talmor, R. Mark, and A. Malhotra, "Methods of blood pressure measurement in the ICU," *Critical care medicine,* vol. 41, no. 1, p. 34, 2013.

[55] E. Chung, G. Chen, B. Alexander, and M. Cannesson, "Non-invasive continuous blood pressure monitoring: a review of current applications," *Frontiers of medicine,* vol. 7, no. 1, pp. 91-101, 2013.

[56] H. E. Hoff and L. A. Geddes, "Graphic registration before Ludwig; the antecedents of the kymograph," *Isis,* vol. 50, no. 1, pp. 5-21, 1959.

[57] L. Peter, N. Noury, and M. Cerny, "A review of methods for non-invasive and continuous blood pressure monitoring: Pulse transit time method is promising?," *Irbm,* vol. 35, no. 5, pp. 271-282, 2014.

[58] B. S. Alpert, D. Quinn, and D. Gallick, "Oscillometric blood pressure: a review for clinicians," *Journal of the American Society of Hypertension,* vol. 8, no. 12, pp. 930-938, 2014.

[59] A. S. Meidert *et al.*, "Evaluation of the radial artery applanation tonometry technology for continuous noninvasive blood pressure monitoring compared with central aortic blood pressure measurements in patients with multiple organ dysfunction syndrome," *Journal of Critical Care,* vol. 28, no. 6, pp. 908-912, 2013.

[60] J. Peňáz, "The blood pressure control system: a critical and methodological introduction," in *Psychosomatics in Essential Hypertension*, vol. 144: Karger Publishers, 1970, pp. 125-150.

[61] G. Parati, R. Casadei, A. Groppelli, M. Di Rienzo, and G. Mancia, "Comparison of finger and intra-arterial blood pressure monitoring at rest and during laboratory testing," *Hypertension,* vol. 13, no. 6_pt_1, pp. 647-655, 1989.

[62] J. Fortin *et al.*, "Continuous non-invasive blood pressure monitoring using concentrically interlocking control loops," *Computers in Biology and Medicine,* vol. 36, no. 9, pp. 941-957, 2006.

[63] D. Perloff *et al.*, "Human blood pressure determination by sphygmomanometry," *Circulation,* vol. 88, no. 5, pp. 2460-2470, 1993.

[64] Z. Taha, L. Shirley, and M. A. M. Razman, "A review on non-invasive hypertension monitoring system by using photoplethysmography method," *Movement, Health & Exercise,* vol. 6, no. 1, 2017.

[65] M. Forouzanfar, S. Ahmad, I. Batkin, H. R. Dajani, V. Z. Groza, and M. Bolic, "Coefficient-free blood pressure estimation based on pulse transit time–cuff pressure dependence," *IEEE Transactions on Biomedical Engineering,* vol. 60, no. 7, pp. 1814-1824, 2013.

[66] S. H. a. M. Staber, " Oscillometric blood pressure measurement used for calibration of the arterial tonometry method contributes significantly to error," *European Journal of Anaesthesiology,* vol. 23, no. 9, pp. 781–787, 2006.

[67] V. Kontis *et al.*, "Contribution of six risk factors to achieving the 25× 25 non-communicable disease mortality reduction target: a modelling study," *The Lancet,* vol. 384, no. 9941, pp. 427-437, 2014.

[68] N. R. Campbell, D. T. Lackland, and M. L. Niebylski, "High blood pressure: why prevention and control are urgent and important—a 2014 fact sheet from the World Hypertension League and the International Society of Hypertension," *The Journal of Clinical Hypertension,* vol. 16, no. 8, pp. 551-553, 2014.

[69] J. M. Meinders and A. P. Hoeks, "Simultaneous assessment of diameter and pressure waveforms in the carotid artery," *Ultrasound in Medicine & Biology,* vol. 30, no. 2, pp. 147-154, 2004.

[70] S. Weber, P. Scharfschwerdt, T. Schauer, T. Seel, U. Kertzscher, and K. Affeld, "Continuous wrist blood pressure measurement with ultrasound," *Biomedical Engineering/Biomedizinische Technik,* 2013.

[71] J. Seo, S. J. Pietrangelo, H.-S. Lee, and C. G. Sodini, "Noninvasive arterial blood pressure waveform monitoring using two-element ultrasound system," *IEEE Transactions on Ultrasonics, Ferroelectrics, and Frequency Control,* vol. 62, no. 4, pp. 776-784, 2015.

[72] J. Joseph, P. Nabeel, M. I. Shah, and M. Sivaprakasam, "Arterial compliance probe for calibration free pulse pressure measurement," in *IEEE International Symposium on Medical Measurements and Applications (MeMeA)*, 2016: IEEE, pp. 1-6.

[73] A. M. Zakrzewski and B. W. Anthony, "Arterial blood pressure estimation using ultrasound: Clinical results on healthy volunteers and a medicated hypertensive volunteer," in *39th Annual International Conference of the IEEE Engineering in Medicine and Biology Society (EMBC)*, 2017: IEEE, pp. 2154-2157.

[74] B. Escobar and R. Torres, "Feasibility of Non-Invasive Blood Pressure Estimation Based on Pulse Arrival Time: A MIMIC Database Study," in *Computing in Cardiology Conference (CinC)*, 2014: IEEE, pp. 1113-1116.

[75] Z. Tang *et al.*, "A chair-based unobtrusive cuffless blood pressure monitoring system based on pulse arrival time," *IEEE Journal of Biomedical and Health Informatics,* 2016.

[76] Q. Zhang *et al.*, "Cuff-less blood pressure measurement using pulse arrival time and a Kalman filter," *Journal of Micromechanics and Microengineering,* vol. 27, no. 2, p. 024002, 2017.

[77] Y. Zheng, C. C. Poon, B. P. Yan, and J. Y. Lau, "Pulse Arrival Time Based Cuff-Less and 24-H Wearable Blood Pressure Monitoring and its Diagnostic Value in Hypertension," *Journal of Medical Systems,* vol. 40, no. 9, p. 195, 2016.

[78] S. Rajala, T. Ahmaniemi, H. Lindholm, and T. Taipalus, "Pulse arrival time (PAT) measurement based on arm ECG and finger PPG signals-comparison of PPG feature detection methods for PAT calculation," in *39th Annual International Conference of the IEEE Engineering in Medicine and Biology Society (EMBC)*, 2017: IEEE, pp. 250-253.

[79] A. Hennig and A. Patzak, "Continuous blood pressure measurement using pulse transit time," *Somnologie-Schlafforschung und Schlafmedizin,* vol. 17, no. 2, pp. 104-110, 2013.

[80] J.-Q. Li *et al.*, "Design of a continuous blood pressure measurement system based on pulse wave and ECG signals," *IEEE journal of translational engineering in health and medicine,* vol. 6, pp. 1-14, 2018.

[81] Z. Shen, F. Miao, Q. Meng, and Y. Li, "Cuffless and continuous blood pressure estimation based on multiple regression analysis," in *2015 5th International Conference on Information Science and Technology (ICIST)*, 2015: IEEE, pp. 117-120.

[82] R. Payne, C. Symeonides, D. Webb, and S. Maxwell, "Pulse transit time measured from the ECG: an unreliable marker of beat-to-beat blood pressure," *Journal of Applied Physiology,* vol. 100, no. 1, pp. 136-141, 2006.

[83] X. Ding, W. Dai, N. Luo, J. Liu, N. Zhao, and Y. Zhang, "A Flexible Tonoarteriography-Based Body Sensor Network for Cuffless Measurement of Arterial Blood Pressure," in *IEEE 12th International Conference on Wearable and Implantable Body Sensor Networks (BSN),*, 2015: IEEE, pp. 1-4.

[84] X. Ding, W. Dai, N. Luo, J. Liu, N. Zhao, and Y. Zhang, "A Flexible Tonoarteriography-Based Body Sensor Network for Cuffless Measurement of Arterial Blood Pressure," in *IEEE 12th International Conference on Wearable and Implantable Body Sensor Networks (BSN)*, 2015: IEEE, pp. 1-4.

[85] W. Chen, T. Kobayashi, S. Ichikawa, Y. Takeuchi, and T. Togawa, "Continuous estimation of systolic blood pressure using the pulse arrival time and intermittent calibration," *Medical and Biological Engineering and Computing,* vol. 38, no. 5, pp. 569-574, 2000.

[86] Z. Tang *et al.*, "A chair–based unobtrusive cuffless blood pressure monitoring system based on pulse arrival time," *IEEE Journal of biomedical and health informatics,* vol. 21, no. 5, pp. 1194-1205, 2016.

[87] X.-R. Ding, Y.-T. Zhang, J. Liu, W.-X. Dai, and H. K. Tsang, "Continuous cuffless blood pressure estimation using pulse transit time and photoplethysmogram intensity ratio," *IEEE Transactions on Biomedical Engineering,* vol. 63, no. 5, pp. 964-972, May 2016.

[88] X.-R. Ding and Y.-T. Zhang, "Photoplethysmogram intensity ratio: A potential indicator for improving the accuracy of PTT-based cuffless blood pressure estimation," in *2015 IEEE 37th Annual International Conference of the Engineering in Medicine and Biology Society (EMBC)*, 2015: IEEE, pp. 398-401.

[89] X.-R. Ding and Y.-T. Zhang, "Photoplethysmogram intensity ratio: A potential indicator for improving the accuracy of PTT-based cuffless blood pressure estimation," in *IEEE 37th Annual International Conference of the Engineering in Medicine and Biology Society (EMBC)*, 2015: IEEE, pp. 398-401.

[90] X.-R. Ding, Y.-T. Zhang, and H. K. Tsang, "A New Modeling Methodology For Continuous Cuffless Blood Pressure Measurement," in *IEEE-EMBS International Conference on Biomedical and Health Informatics (BHI)*: IEEE, pp. 264-267.

[91] W.-H. Lin, H. Wang, O. W. Samuel, and G. Li, "Using a New PPG Indicator to Increase The Accuracy of PTT-Based Continuous Cuffless Blood Pressure Estimation," in *39th Annual International Conference of the IEEE Engineering in Medicine and Biology Society (EMBC)*, 2017: IEEE, pp. 738-741.

[92] J. Liu, Y.-T. Zhang, X.-R. Ding, W.-X. Dai, and N. Zhao, "A preliminary study on multi-wavelength PPG based pulse transit time detection for cuffless blood pressure measurement," in *IEEE 38th Annual International Conference of the Engineering in Medicine and Biology Society (EMBC)*, 2016: IEEE, pp. 615-618.

[93] J. Liu, Y. Li, X.-R. Ding, W.-X. Dai, and Y.-T. Zhang, "Effects of cuff inflation and deflation on pulse transit time measured from ECG and multi-wavelength PPG," in *IEEE 37th Annual International Conference of the Engineering in Medicine and Biology Society (EMBC)*, 2015: IEEE, pp. 5973-5976.

[94] I. C. Jeong and J. Finkelstein, "Introducing contactless blood pressure assessment using a high speed video camera," *Journal of medical systems,* vol. 40, no. 4, pp. 1-10, 2016.

[95] Y. Sun and N. Thakor, "Photoplethysmography revisited: from contact to noncontact, from point to imaging," *IEEE Transactions on Biomedical Engineering,* vol. 63, no. 3, pp. 463-477, 2016.

[96] S. Ghosh, A. Banerjee, N. Ray, P. W. Wood, P. Boulanger, and R. Padwal, "Continuous blood pressure prediction from pulse transit time using ECG and PPG signals," in *2016 IEEE Healthcare Innovation Point-Of-Care Technologies Conference (HI-POCT)*, 2016: IEEE, pp. 188-191.

[97] A. Visvanathan, A. Sinha, and A. Pal, "Estimation of Blood Pressure Levels From Reflective Photoplethysmograph Using Smart Phones," in *IEEE 13th International Conference on Bioinformatics and Bioengineering (BIBE)*, 2013: IEEE, pp. 1-5.

[98] M. Atef, L. Xiyan, G. Wang, and Y. Lian, "PTT based continuous time non-invasive blood pressure system," in *IEEE 59th International Midwest Symposium on Circuits and Systems (MWSCAS)* 2016: IEEE, pp. 1-4.

[99] A. D. Junior, S. Murali, F. Rincon, and D. Atienza, "Methods for reliable estimation of pulse transit time and blood pressure variations using smartphone sensors," *Microprocessors and Microsystems,* vol. 46, pp. 84-95, 2016.

[100] W.-X. Dai, Y.-T. Zhang, J. Liu, X.-R. Ding, and N. Zhao, "Dual-Modality Arterial Pulse Monitoring System for Continuous Blood Pressure Measurement," in *IEEE 38th Annual International Conference of the Engineering in Medicine and Biology Society (EMBC)*, 2016: IEEE, pp. 5773-5776.

[101] C. Yang and N. Tavassolian, "Pulse Transit Time Measurement Using Seismocardiogram, Photoplethysmogram, and Acoustic Recordings: Evaluation and Comparison," *IEEE Journal of Biomedical and Health Informatics,* 2017.

[102] M. H. van Velzen, A. J. Loeve, S. P. Niehof, and E. G. Mik, "Increasing accuracy of pulse transit time measurements by automated elimination of distorted photoplethysmography waves," *Medical & Biological Engineering & Computing,* pp. 1-12, 2017.

[103] B. Ibrahim, V. Nathan, and R. Jafari, "Exploration and Validation of Alternate Sensing Methods for Wearable Continuous Pulse Transit Time Measurement Using Optical and Bioimpedance Modalities," in *39th Annual International Conference of the IEEE Engineering in Medicine and Biology Society (EMBC)*, 2017: IEEE, pp. 2051-2055.

[104] A. M. Carek, J. Conant, A. Joshi, H. Kang, and O. T. Inan, "SeismoWatch: Wearable Cuffless Blood Pressure Monitoring Using Pulse Transit Time," *Proceedings of the ACM on Interactive, Mobile, Wearable and Ubiquitous Technologies,* vol. 1, no. 3, p. 40, 2017.

[105] Y. Chen, S. Cheng, T. Wang, and T. Ma, "Novel blood pressure estimation method using single photoplethysmography feature," in *39th Annual International Conference of the IEEE Engineering in Medicine and Biology Society (EMBC)*, 2017: IEEE, pp. 1712-1715.

[106] D. Buxi, J.-M. Redouté, and M. R. Yuce, "Blood pressure estimation using pulse transit time from bioimpedance and continuous wave radar," *IEEE Transactions on Biomedical Engineering,* vol. 64, no. 4, pp. 917-927, 2017.

[107] J. Sola *et al.*, "Noninvasive and nonocclusive blood pressure estimation via a chest sensor," *IEEE Transactions on Biomedical Engineering,* vol. 60, no. 12, pp. 3505-3513, 2013.

[108] V. Prabhu, P. Kuppusamy, A. Karthikeyan, and M. Sucharitha, "A novel approach for non-invasive measurement of mean arterial pressure using pulse transit time," *Multimedia Tools and Applications,* pp. 1-15, 2018.

[109] W.-H. Lin, H. Wang, O. W. Samuel, and G. Li, "Using a New PPG Indicator to Increase The Accuracy of PTT-Based Continuous Cuffless Blood Pressure Estimation," in *2017 39th Annual International Conference of the IEEE Engineering in Medicine and Biology Society (EMBC),* , 2017: IEEE, pp. 738-741.

[110] X.-R. Ding, Y.-T. Zhang, and H. K. Tsang, "A New Modeling Methodology For Continuous Cuffless Blood Pressure Measurement," in *2016 IEEE-EMBS International Conference on Biomedical and Health Informatics (BHI)*: IEEE, pp. 264-267.

[111] J. Liu, Y.-T. Zhang, X.-R. Ding, W.-X. Dai, and N. Zhao, "A preliminary study on multi-wavelength PPG based pulse transit time detection for cuffless blood pressure measurement," in *2016 IEEE 38th Annual International Conference of the Engineering in Medicine and Biology Society (EMBC)*, 2016: IEEE, pp. 615-618.

[112] J. Liu, Y. Li, X.-R. Ding, W.-X. Dai, and Y.-T. Zhang, "Effects of cuff inflation and deflation on pulse transit time measured from ECG and multi-wavelength PPG," in *2015 IEEE 37th Annual International Conference of the Engineering in Medicine and Biology Society (EMBC)*, 2015: IEEE, pp. 5973-5976.

[113] M. Atef, L. Xiyan, G. Wang, and Y. Lian, "PTT based continuous time non-invasive blood pressure system," in *2016 IEEE 59th International Midwest Symposium on Circuits and Systems (MWSCAS)* 2016: IEEE, pp. 1-4.

[114] A. Visvanathan, A. Sinha, and A. Pal, "Estimation of Blood Pressure Levels From Reflective Photoplethysmograph Using Smart Phones," in *2013 IEEE 13th International Conference on Bioinformatics and Bioengineering (BIBE),* , 2013: IEEE, pp. 1-5.

[115] W.-X. Dai, Y.-T. Zhang, J. Liu, X.-R. Ding, and N. Zhao, "Dual-Modality Arterial Pulse Monitoring System for Continuous Blood Pressure Measurement," in *2016 IEEE 38th Annual International Conference of the Engineering in Medicine and Biology Society (EMBC),* , 2016: IEEE, pp. 5773-5776.

[116] B. Ibrahim, V. Nathan, and R. Jafari, "Exploration and Validation of Alternate Sensing Methods for Wearable Continuous Pulse Transit Time Measurement Using Optical and Bioimpedance Modalities," in *2017 39th Annual International Conference of the IEEE Engineering in Medicine and Biology Society (EMBC),*, 2017: IEEE, pp. 2051-2055.

[117] Y. Chen, S. Cheng, T. Wang, and T. Ma, "Novel blood pressure estimation method using single photoplethysmography feature," in *2017 39th Annual International Conference of the IEEE Engineering in Medicine and Biology Society (EMBC),* , 2017: IEEE, pp. 1712-1715.

[118] J. Xu, J. Jiang, H. Zhou, and Z. Yan, "A Novel Blood Pressure Estimation Method Combing Pulse Wave Transit Time Model and Neural Network Model," in *39th Annual International Conference of the IEEE Engineering in Medicine and Biology Society (EMBC)*, 2017: IEEE, pp. 2130-2133.

[119] R. He, Z.-P. Huang, L.-Y. Ji, J.-K. Wu, H. Li, and Z.-Q. Zhang, "Beat-to-Beat Ambulatory Blood Pressure Estimation Based on Random Forest," in *IEEE 13th International Conference on Wearable and Implantable Body Sensor Networks (BSN)*, 2016: IEEE, pp. 194-198.

[120] M. Sifuzzaman, M. Islam, and M. Ali, "Application of wavelet transform and its advantages compared to Fourier transform," *Journal of Physical Science,* vol. 13, no. 0972-8791, pp. 121-134, 2009.

[121] R. Aggarwal, J. K. Singh, V. K. Gupta, S. Rathore, M. Tiwari, and A. Khare, "Noise reduction of speech signal using wavelet transform with modified universal threshold," *International Journal of Computer Applications,* vol. 20, no. 5, pp. 14-19, 2011.

[122] H.-y. ZHAO and C.-h. JI, "Noise reduction technology based on wavelet transform and realization in Matlab [J]," *Ordnance Industry Automation,* vol. 2, p. 028, 2006.

[123] M. Kachuee, M. M. Kiani, H. Mohammadzade, and M. Shabany, "Cuffless blood pressure estimation algorithms for continuous health-care monitoring," *IEEE Transactions on Biomedical Engineering,* vol. 64, no. 4, pp. 859-869, 2017.

[124] Q. Lu and E. Dai, "A New Blood Pressure Estimation Method Based on Neural Network Algorithm Model," in *IOP Conference Series: Materials Science and Engineering*, 2018, vol. 382, no. 5: IOP Publishing, p. 052027.

[125] Z. Wu and N. E. Huang, "Ensemble empirical mode decomposition: a noise-assisted data analysis method," *Advances in Adaptive Data Analysis,* vol. 1, no. 01, pp. 1-41, 2009.

[126] M. E. Torres, M. A. Colominas, G. Schlotthauer, and P. Flandrin, "A Complete Ensemble Empirical Mode Decomposition with Adaptive Noise," in *IEEE International Conference on Acoustics in Speech and Signal Processing (ICASSP)*, 2011: IEEE, pp. 4144-4147.

[127] Y. Wang *et al.*, "A Method of Denoising And Decomposing Cuff Pressure Based on Improved Empirical Mode Decomposition," in *Biomedical Engineering and Environmental Engineering: Proceedings of the 2014 2nd International Conference on Biomedical Engineering and Environmental Engineering (ICBEEE 2014), December 24–25, 2014, Wuhan, China*, 2014: CRC Press, p. 77.

[128] R. Vetter, L. Rossini, A. Ridolfi, J. S. I. CAROS, and M. Correvon, "Monitoring device and method for estimating blood constituent concentration for tissues with low perfusion," ed: U.S. Patent No. 9,687,162. 27 Jun., 2017.

[129] A. Patel, J. Li, B. Finegan, and M. McMurtry, "Aortic pressure estimation using blind identification approach on single input multiple output non-linear wiener systems," *IEEE Transactions on Biomedical Engineering,* vol. 65, no. 6, pp. 1193-1200, 2018, doi: 10.1109/TBME.2017.2688425.

[130] Y. Wang, F. Ding, and L. Xu, "Some new results of designing an IIR filter with colored noise for signal processing," *Digital Signal Processing,* vol. 72, pp. 44-58, 2018.

[131] P. J. Chowienczyk, S. E. Brett, and A. Y. M. Guilcher, "Apparatus and method for measuring blood pressure," ed: U.S. Patent No. 9,289,138. 22 Mar., 2016.

[132] K. Murakami, M. Yoshioka, and J. Ozawa, "Non-Contact Pulse Transit Time Measurement Using Imaging Camera, and Its Relation to Blood Pressure," in *14th IAPR International Conference on Machine Vision Applications (MVA)*, 2015: IEEE, pp. 414-417.

[133] Z. Xu *et al.*, "Improved PT Algorithm Applied to A Wearable Integrated Physiological Parameters System," in *IEEE and Internet of Things (iThings/CPSCom) of Green Computing and Communications (GreenCom), IEEE International Conference on and IEEE Cyber on Physical and Social Computing*, 2013: IEEE, pp. 1756-1762.

[134] H. Xiao, M. Butlin, I. Tan, A. Qasem, and A. Avolio, "Estimation of pulse transit time from radial pressure waveform alone by artificial neural network," *IEEE Journal of Biomedical and Health Informatics,* vol. 22, no. 4, pp. 1140 - 1147, July 2017.

[135] F. Miao *et al.*, "A novel continuous blood pressure estimation approach based on data mining techniques," *IEEE Journal of Biomedical and Health Informatics,* vol. 21, no. 6, pp. 1730-1740, Nov. 2017.

[136] Z. Xu, J. Liu, X. Chen, Y. Wang, and Z. Zhao, "Continuous blood pressure estimation based on multiple parameters from eletrocardiogram and photoplethysmogram by back-propagation neural network," *Computers in Industry,* vol. 89, pp. 50-59, 2017.

[137] Y. Zhang and Z. Feng, "A SVM Method for Continuous Blood Pressure Estimation from a PPG Signal," in *Proceedings of the 9th International Conference on Machine Learning and Computing*, 2017: ACM, pp. 128-132.

[138] T. H. Wu, G. K.-H. Pang, and E. W.-Y. Kwong, "Predicting Systolic Blood Pressure Using Machine Learning," in *7th International Conference on Information and Automation for Sustainability (ICIAfS),* , 2014: IEEE, pp. 1-6.

[139] T. H. Wu, G. K.-H. Pang, and E. W.-Y. Kwong, "Predicting Systolic Blood Pressure Using Machine Learning," in *7th International Conference on Information and Automation for Sustainability (ICIAfS)*, 2014: IEEE, pp. 1-6.

[140] P. Li *et al.*, "Novel wavelet neural network algorithm for continuous and noninvasive dynamic estimation of blood pressure from photoplethysmography," *Science China Information Sciences,* vol. 59, no. 4, p. 042405, 2016.

[141] M. Forouzanfar, H. R. Dajani, V. Z. Groza, M. Bolic, and S. Rajan, "Feature-based neural network approach for oscillometric blood pressure estimation," *IEEE Transactions on Instrumentation and Measurement,* vol. 60, no. 8, pp. 2786-2796, 2011.

[142] I. Saini, A. Khosla, and D. Singh, "Classification of RR-Interval and blood pressure signals using support vector machine for different postures," *International Journal of Computer Theory and Engineering,* vol. 4, no. 3, p. 391, 2012.

[143] G. C. Cawley and N. L. Talbot, "On over-fitting in model selection and subsequent selection bias in performance evaluation," *Journal of Machine Learning Research,* vol. 11, no. Jul, pp. 2079-2107, 2010.

[144] H. F. Golino *et al.*, "Predicting Increased Blood Pressure Using Machine Learning," *Journal of obesity,* vol. 2014, 2014.

[145] M. H. Chowdhury *et al.*, "Estimating Blood Pressure from the Photoplethysmogram Signal and Demographic Features Using Machine Learning Techniques," *Sensors,* vol. 20, no. 11, p. 3127, 2020.

[146] G. Slapničar, M. Luštrek, and M. Marinko, "Continuous Blood Pressure Estimation from PPG Signal," *Informatica 42,* vol. 42, no. 1, pp. 33-42, Mar. 2018.

[147] B. Zhang, Z. Wei, J. Ren, Y. Cheng, and Z. Zheng, "An Empirical study on Predicting Blood Pressure using Classification and Regression Trees," *IEEE Access,* vol. 6, pp. 21758-21768, 2018.

[148] D. Fujita, A. Suzuki, and K. Ryu, "PPG-based systolic blood pressure estimation method using PLS and level-crossing feature," *Applied Sciences,* vol. 9, no. 2, p. 304, 2019.

[149] S. Chen, Z. Ji, H. Wu, and Y. Xu, "A Non-Invasive Continuous Blood Pressure Estimation Approach Based on Machine Learning," *Sensors,* vol. 19, no. 11, p. 2585, 2019.

[150] V. R. Ripoll and A. Vellido, "Blood pressure assessment with differential pulse transit time and deep learning: a proof of concept," *Kidney Diseases,* vol. 5, no. 1, pp. 23-27, 2019.

[151] M. Yoshioka and S. Bounyong, "Regression-forests-based estimation of blood pressure using the pulse transit time obtained by facial photoplethysmogram," in *2017 International Joint Conference on Neural Networks (IJCNN)*, 2017: IEEE, pp. 3248-3253.

[152] K. Atomi, H. Kawanaka, M. S. Bhuiyan, and K. Oguri, "Cuffless Blood Pressure Estimation Based on Data-Oriented Continuous Health Monitoring System," *Computational and Mathematical Methods in Medicine,* vol. 2017, 2017.

[153] D. Campo *et al.*, "Measurement of aortic pulse wave velocity with a connected bathroom scale," *American Journal of Hypertension,* 2017.

[154] J. Xu, J. Jiang, H. Zhou, and Z. Yan, "A novel Blood Pressure estimation method combing Pulse Wave Transit Time model and neural network model," in *2017 39th Annual International Conference of the IEEE Engineering in Medicine and Biology Society (EMBC)*, 2017: IEEE, pp. 2130-2133.

[155] S. Lee and J.-H. Chang, "Oscillometric blood pressure estimation based on deep learning," *IEEE Transactions on Industrial Informatics,* vol. 13, no. 2, pp. 461-472, 2017.

[156] S. Lee and J.-H. Chang, "Deep learning ensemble with asymptotic techniques for oscillometric blood pressure estimation," *Computer Methods and Programs in Biomedicine,* vol. 151, pp. 1-13, 2017.

[157] A. Argha, J. Wu, S. W. Su, and B. G. Celler, "Blood Pressure Estimation From Beat-by-Beat Time-Domain Features of Oscillometric Waveforms Using Deep-Neural-Network Classification Models," *IEEE Access,* vol. 7, pp. 113427-113439, 2019.

[158] X. Li, S. Wu, and L. Wang, "Blood Pressure Prediction via Recurrent Models with Contextual Layer," in *Proceedings of the 26th International Conference on World Wide Web*, 2017: International World Wide Web Conferences Steering Committee, pp. 685-693.

[159] Peng Su, Xiao-Rong Ding, Yuan-Ting Zhang, Jing Liu, Fen Miao, and N. Zhao, "Long-term Blood Pressure Prediction with Deep Recurrent Neural Networks," *IEEE Conference on Biomedical and Health Informatics (BHI).* 2018.

[160] S. Lee and J.-H. Chang, "Oscillometric blood pressure estimation based on deep learning," *IEEE Transactions on Industrial Informatics,* vol. 13, no. 2, pp. 461-472, 2016.

[161] P. Su, X.-R. Ding, Y.-T. Zhang, J. Liu, F. Miao, and N. Zhao, "Long-term blood pressure prediction with deep recurrent neural networks," in *2018 IEEE EMBS International Conference on Biomedical & Health Informatics (BHI)*, 2018: IEEE, pp. 323-328.

[162] E. O'Brien *et al.*, "The British Hypertension Society protocol for the evaluation of blood pressure measuring devices," *J Hypertens,* vol. 11, no. Suppl 2, pp. S43-S62, 1993.

[163] A. ANSI, "& ANSI/AAMI SP10: 2002/A1: 2003," *American National Standard. Manual, Electronic, or Automated Sphygmomanometers,* 2002.

[164] I. S. Association, "IEEE standard for wearable cuffless blood pressure measuring devices," *IEEE Std,* pp. 1708-2014, 2014.

[165] E. O'Brien *et al.*, "European Society of Hypertension International Protocol revision 2010 for the validation of blood pressure measuring devices in adults," *Blood Pressure Monitoring,* vol. 15, no. 1, pp. 23-38, 2010.

[166] S. Rastegar, H. Gholamhosseini, A. Lowe, F. Mehdipour, and M. Lindén, "Estimating Systolic Blood Pressure Using Convolutional Neural Networks," *Studies in Health Technology and Informatics,* vol. 261, pp. 143-149, 2019.

[167] S. Moghaddam Mansouri, H. Gholamhosseini, A. Lowe, and M. Lindén, "Systolic Blood Pressure Estimation from Electrocardiogram and Photoplethysmogram Signals Using Convoluional Neural Networks," *EJBI,* vol. 16, no. 2, pp. 2-34, 2020.

[168] S. R. Mansouri, A. Lowe, H. Gholamhosseini, and M. M. Baig, "Blood Pressure Estimation from Electrocardiogram and Photoplethysmography Signals Using Continuous Wavelet Transform and Convolutional Neural Network," in *CONF-IRM*, 2019, p. 28.

[169] A. E. Johnson *et al.*, "MIMIC-III, a freely accessible critical care database," *Scientific Data,* vol. 3, no. 1, pp. 1-9, 2016.

[170] A. L. Goldberger *et al.*, "PhysioBank, PhysioToolkit, and PhysioNet: components of a new research resource for complex physiologic signals," *Circulation,* vol. 101, no. 23, pp. e215-e220, 2000.

[171] L. A. Wong and J. C. Chen, "Nonlinear and chaotic behavior of structural system investigated by wavelet transform techniques," *International Journal of Non-linear Mechanics,* vol. 36, no. 2, pp. 221-235, 2001.

[172] O. Tsinalis, P. M. Matthews, Y. Guo, and S. Zafeiriou, "Automatic sleep stage scoring with single-channel EEG using convolutional neural networks," *Cornell University,* 2016.

[173] A. M. Badshah, J. Ahmad, N. Rahim, and S. W. Baik, "Speech emotion recognition from spectrograms with deep convolutional neural network," in *2017 International Conference on Platform Technology and Service (PlatCon)*, 2017: IEEE, pp. 1-5.

[174] Q. Mao, M. Dong, Z. Huang, and Y. Zhan, "Learning salient features for speech emotion recognition using convolutional neural networks," *IEEE Transactions on Multimedia,* vol. 16, no. 8, pp. 2203-2213, 2014.

[175] K. He, X. Zhang, S. Ren, and J. Sun, "Deep residual learning for image recognition," in *Proceedings of the IEEE conference on computer vision and pattern recognition*, 2016, pp. 770-778.

[176] L. Yuan and J. Cao, "Patients' EEG data analysis via spectrogram image with a convolution neural network," in *International Conference on Intelligent Decision Technologies*, 2017: Springer, pp. 13-21.

[177] P. Xia, J. Hu, and Y. Peng, "EMG-based estimation of limb movement using deep learning with recurrent convolutional neural networks," *Artificial Organs,* vol. 42, no. 5, pp. E67-E77, 2018.

[178] A. Vilamala, K. H. Madsen, and L. K. Hansen, "Deep convolutional neural networks for interpretable analysis of EEG sleep stage scoring," in *IEEE 27th International Workshop on Machine Learning for Signal Processing (MLSP)*, 2017: IEEE, pp. 1-6.

[179] K. Asai and N. Takase, "Finger motion estimation based on frequency conversion of EMG signals and image recognition using convolutional neural network," in *17th International Conference on Control, Automation and Systems (ICCAS)*, 2017: IEEE, pp. 1366-1371.

[180] J. Kilby and K. Prasad, "Continuous wavelet analysis and classification of surface electromyography signals," *International Journal of Computer and Electrical Engineering,* vol. 5, no. 1, p. 30, 2013.

[181] I. Goodfellow, Y. Bengio, and A. Courville, *Deep Learning*. MIT press, 2016.

[182] A. Krizhevsky, I. Sutskever, and G. E. Hinton, "Imagenet classification with deep convolutional neural networks," *Advances in Neural Information Processing Systems,* vol. 25, pp. 1097-1105, 2012.

[183] P. Luo, X. Wang, W. Shao, and Z. Peng, "Towards understanding regularization in batch normalization," *arXiv preprint arXiv:1809.00846,* 2018.

[184] S. Ioffe and C. Szegedy, "Batch normalization: Accelerating deep network training by reducing internal covariate shift," in *International Conference on Machine Learning*, 2015: PMLR, pp. 448-456.

[185] T. DeVries and G. W. Taylor, "Improved regularization of convolutional neural networks with cutout," *arXiv preprint arXiv:1708.04552,* 2017.

[186] N. Kalchbrenner, E. Grefenstette, and P. Blunsom, "A convolutional neural network for modelling sentences," *ArXiv Preprint ArXiv:1404.2188,* 2014.

[187] N. Qian, "On the momentum term in gradient descent learning algorithms," *Neural Networks,* vol. 12, no. 1, pp. 145-151, 1999.

[188] B. Mishra and N. Thakkar, "Cuffless Blood Pressure Monitoring Using PTT and PWV Methods," in *International Conference on Recent Innovations in Signal processing and Embedded Systems (RISE)* 2017, pp. 395-401.

[189] Y.-Z. Yoon *et al.*, "Cuff-less blood pressure estimation using pulse waveform analysis and pulse arrival time," *IEEE Journal of Biomedical and Health Informatics,* vol. 22, no. 4, pp. 1068-1074, 2018.

[190] G. R. Nidigattu, G. Mattela, and S. Jana, "Non-invasive modeling of heart rate and blood pressure from a photoplethysmography by using machine learning techniques," in *International Conference on COMmunication Systems & NETworkS (COMSNETS)*, 2020, pp. 7-12.

[191] P. Su, X.-R. Ding, Y.-T. Zhang, J. Liu, F. Miao, and N. Zhao, "Long-term blood pressure prediction with deep recurrent neural networks," in *IEEE EMBS International Conference on Biomedical & Health Informatics (BHI)*, 2018, pp. 323-328.

[192] S. Rastegar, H. Gholamhosseini, and A. Lowe, "A Novel Convolutional Neural Network for Continuous Blood Pressure Estimation," *EMBEC Conference* 2020.

[193] A. Arza, J. Lázaro, E. Gil, P. Laguna, J. Aguiló, and R. Bailon, "Pulse transit time and pulse width as potential measure for estimating beat-to-beat systolic and diastolic blood pressure," in *Computing in Cardiology 2013*, 2013, pp. 887-890.

[194] S. Goli and T. Jayanthi, "Cuff less continuous non-invasive blood pressure measurement using pulse transit time measurement," *Int. J. Recent Dev. Eng. Technol,* vol. 2, no. 1, pp. 16-86, 2014.

[195] J. Padilla, E. Berjano, J. Saiz, L. Facila, P. Diaz, and S. Merce, "Assessment of relationships between blood pressure, pulse wave velocity and digital volume pulse," in *2006 Computers in Cardiology*, 2006, pp. 893-896.

[196] M. Y.-M. Wong, C. C.-Y. Poon, and Y.-T. Zhang, "An evaluation of the cuffless blood pressure estimation based on pulse transit time technique: a half year study on normotensive subjects," *Cardiovascular Engineering,* vol. 9, no. 1, pp. 32-38, 2009.

[197] V. Chandrasekaran, R. Dantu, S. Jonnada, S. Thiyagaraja, and K. P. Subbu, "Cuffless differential blood pressure estimation using smart phones," *IEEE Transactions on Biomedical Engineering,* vol. 60, no. 4, pp. 1080-1089, 2012.

[198] A. Jadooei, O. Zaderykhin, and V. Shulgin, "Adaptive algorithm for continuous monitoring of blood pressure using a pulse transit time," in *2013 IEEE XXXIII International Scientific Conference Electronics and Nanotechnology (ELNANO)*, 2013, pp. 297-301.

[199] D. Hughes, C. F. Babbs, L. Geddes, and J. Bourland, "Measurements of Young's modulus of elasticity of the canine aorta with ultrasound," *Ultrasonic Imaging,* vol. 1, no. 4, pp. 356-367, 1979.

[200] H. M. Rai, A. Trivedi, and S. Shukla, "ECG signal processing for abnormalities detection using multi-resolution wavelet transform and Artificial Neural Network classifier," *Measurement,* vol. 46, no. 9, pp. 3238-3246, 2013.

[201] M. AlMahamdy and H. B. Riley, "Performance study of different denoising methods for ECG signals," *Procedia Computer Science,* vol. 37, pp. 325-332, 2014.

[202] B. Arvinti, M. Costache, D. Toader, M. Oltean, and A. Isar, "ECG statistical denoising in the wavelet domain," in *9th International Symposium on Electronics and Telecommunications*, 2010, pp. 307-310.

[203] A. Al-Qawasmi and K. Daqrouq, "ECG signal enhancement using wavelet transform," *WSEAS Trans on Biology and Biomedecine,* vol. 7, no. 2, pp. 62-72, 2010.

[204] V. Prasad, T. S. Latha, and M. Suresh, "Denoising of biological signals using wavelets," *Int. J. Curr. Eng. Technol,* vol. 3, no. 3, pp. 863-866, 2013.

[205] M. Kania, M. Fereniec, and R. Maniewski, "Wavelet denoising for multi-lead high resolution ECG signals," *Measurement Science Review,* vol. 7, no. 4, pp. 30-33, 2007.

[206] M. A. Awal, S. S. Mostafa, and M. Ahmad, "Performance analysis of Savitzky-Golay smoothing filter using ECG signal," *International Journal of Computer and Information Technology,* vol. 1, no. 02, p. 24, 2011.

[207] S. Hargittai, "Savitzky-Golay least-squares polynomial filters in ECG signal processing," in *Computers in Cardiology*, 2005, pp. 763-766.

[208] C. Chandrakar and M. Kowar, "Denoising ECG signals using adaptive filter algorithm," *International Journal of Soft Computing and Engineering (IJSCE),* vol. 2, no. 1, pp. 120-123, 2012.

[209] A. Savitzky and M. J. Golay, "Smoothing and differentiation of data by simplified least squares procedures," *Analytical Chemistry,* vol. 36, no. 8, pp. 1627-1639, 1964.

[210] S. Chauhan and L. Vig, "Anomaly detection in ECG time signals via deep long short-term memory networks," in *IEEE International Conference on Data Science and Advanced Analytics (DSAA)*, 2015, pp. 1-7.

[211] J. H. Tan *et al.*, "Application of stacked convolutional and long short-term memory network for accurate identification of CAD ECG signals," *Computers in Biology and Medicine,* vol. 94, pp. 19-26, 2018.

[212] F. P.-W. Lo, C. X.-T. Li, J. Wang, J. Cheng, and M. Q.-H. Meng, "Continuous systolic and diastolic blood pressure estimation utilizing long short-term memory network," in *39th Annual International Conference of the IEEE Engineering in Medicine and Biology Society (EMBC)*, 2017, pp. 1853-1856.

[213] Q. Zhao, X. Hu, J. Lin, X. Deng, and H. Li, "A novel short-term blood pressure prediction model based on LSTM," in *AIP Conference Proceedings*, 2019, vol. 2058, no. 1: AIP Publishing LLC, p. 020003.

[214] M. S. Tanveer and M. K. Hasan, "Cuffless blood pressure estimation from electrocardiogram and photoplethysmogram using waveform based ANN-LSTM network," *Biomedical Signal Processing and Control,* vol. 51, pp. 382-392, 2019.

[215] S. Hochreiter and J. Schmidhuber, "Long short-term memory," *Neural Computation,* vol. 9, no. 8, pp. 1735-1780, 1997.

[216] X. Tao and Z. Yun, "Fall prediction based on biomechanics equilibrium using Kinect," *International Journal of Distributed Sensor Networks,* vol. 13, no. 4, p. 1550147717703257, 2017.

[217] A. S. Zadi, R. Alex, R. Zhang, D. E. Watenpaugh, and K. Behbehani, "Arterial blood pressure feature estimation using photoplethysmography," *Computers in Biology and Medicine,* vol. 102, pp. 104-111, 2018.

[218] F. Miao *et al.*, "A Novel Continuous Blood Pressure Estimation Approach Based on Data Mining Techniques," *IEEE Journal of Biomedical and Health Informatics,* 2017.

[219] M. Elgendi, "On the analysis of fingertip photoplethysmogram signals," *Current cardiology reviews,* vol. 8, no. 1, pp. 14-25, 2012.

[220] M. Kachuee, M. M. Kiani, H. Mohammadzade, and M. Shabany, "Cuff-less high-accuracy calibration-free blood pressure estimation using pulse transit time," in *2015 IEEE International Symposium on Circuits and Systems (ISCAS)*, 2015: IEEE, pp. 1006-1009.

[221] A. J. Smola and B. Schölkopf, "A tutorial on support vector regression," *Statistics and Computing,* vol. 14, no. 3, pp. 199-222, 2004.

[222] Y. Liu and Y. F. Zheng, "FS_SFS: A novel feature selection method for support vector machines," *Pattern recognition,* vol. 39, no. 7, pp. 1333-1345, 2006.

[223] B. Zhang, H. Ren, G. Huang, Y. Cheng, and C. Hu, "Predicting blood pressure from physiological index data using the SVR algorithm," *BMC bioinformatics,* vol. 20, no. 1, p. 109, 2019.

[224] M. Kachuee, M. M. Kiani, H. Mohammadzade, and M. Shabany, "Cuffless blood pressure estimation algorithms for continuous health-care monitoring," *IEEE Transactions on Biomedical Engineering,* vol. 64, no. 4, pp. 859-869, 2016.

[225] G. Slapničar, N. Mlakar, and M. Luštrek, "Blood pressure estimation from photoplethysmogram using a spectro-temporal deep neural network," *Sensors,* vol. 19, no. 15, p. 3420, 2019.

[226] S. G. Khalid, J. Zhang, F. Chen, and D. Zheng, "Blood pressure estimation using photoplethysmography only: comparison between different machine learning approaches," *Journal of Healthcare Engineering,* vol. 2018, 2018.

[227] Ö. F. Ertuğrul and N. Sezgin, "A noninvasive time-frequency-based approach to estimate cuffless arterial blood pressure," *Turkish Journal of Electrical Engineering & Computer Sciences,* vol. 26, no. 5, pp. 2260-2274, 2018.

[228] L. Wang, W. Zhou, Y. Xing, and X. Zhou, "A novel neural network model for blood pressure estimation using photoplethesmography without electrocardiogram," *Journal of Healthcare Engineering,* vol. 2018, 2018.

[229] J. Zhang, D. Wu, and Y. Li, "Cuff-less and Calibration-free Blood Pressure Estimation Using Convolutional Autoencoder with Unsupervised Feature Extraction," in *41st Annual International*

Conference of the IEEE Engineering in Medicine and Biology Society (EMBC), 2019: IEEE, pp. 3323-3326.

[230] S. Baek, J. Jang, and S. Yoon, "End-to-End Blood Pressure Prediction via Fully Convolutional Networks," *IEEE Access,* vol. 7, pp. 185458-185468, 2019.

[231] Y. Hellman *et al.*, "Pulse oximeter derived blood pressure measurement in patients with a continuous flow left ventricular assist device," *Artificial Organs,* vol. 41, no. 5, pp. 424-430, 2017.

[232] S. Marathe, D. Zeeshan, T. Thomas, and S. Vidhya, "A Wireless Patient Monitoring System using Integrated ECG module, Pulse Oximeter, Blood Pressure and Temperature Sensor," in *2019 International Conference on Vision Towards Emerging Trends in Communication and Networking (ViTECoN)*, 2019: IEEE, pp. 1-4.

[233] S. Rastegar, H. GholamHosseini, and A. Lowe, "Non-invasive continuous blood pressure monitoring systems: current and proposed technology issues and challenges," *Australasian Physical & Engineering Sciences in Medicine,* pp. 1-18, 2019.

[234] S. Rastegar, H. Gholamhosseini, A. Lowe, F. Mehdipour, and M. Lindén, "Estimating Systolic Blood Pressure Using Convolutional Neural Networks," in *pHealth*, 2019, pp. 143-149.

[235] S. Rastegar Moghaddam Mansouri, H. Gholamhosseini, A. Lowe, and M. Lindén, "A Novel Convolutional Neural Network for Continuous Blood Pressure Estimation " *EMBEC2020 Conference,* 2020.